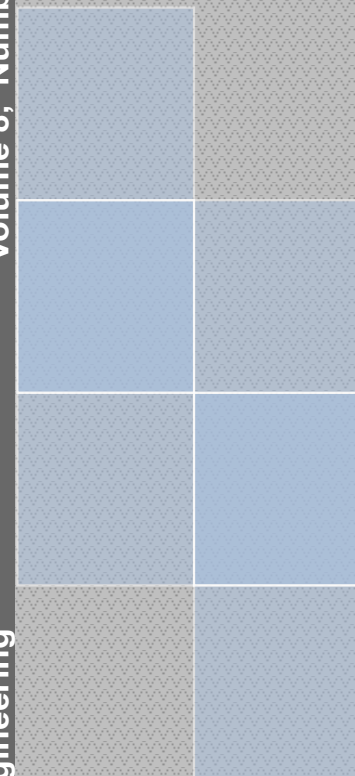


Volume 8, Number 1, 2014

Technical University of Cluj-Napoca
North University Centre of Baia Mare
Faculty of Engineering
Electrical. Electronic and Computer Engineering Department

Volume 8, Number 1, 2014

Carpathian Journal of Electrical Engineering



Carpathian Journal of Electrical Engineering

ISSN 1843 - 7583

NORDTECH PUBLISHER 

Carpathian Journal of Electrical Engineering

Volume 8, Number 1, 2014
ISSN 1843 – 7583

<http://cee.ubm.ro/cjee.html>

EDITOR-IN-CHIEF

Liviu NEAMȚ **Technical University of Cluj-Napoca, Romania**

ASSOCIATE EDITOR

Mircea HORGOS **Technical University of Cluj-Napoca, Romania**

EDITORIAL SECRETARY

Olivian CHIVER **Technical University of Cluj-Napoca, Romania**

SCIENTIFIC BOARD

Theodoros D. TSIBOUKIS	Aristotle University of Thessaloniki, Greece
Florin BREABĂN	University Artois, France
Luis Adriano DOMINGUES	Brazilian Electrical Energy Research Center, Brazil
Andrei VLADIMIRESCU	University of California at Berkeley, USA
Tom O'DWYER	Analog Devices, Ireland
Ștefan MARINCA	Analog Devices, Ireland
Adam TIHMER	University of Miskolc, Hungary
Jozsef VASARHELYI	University of Miskolc, Hungary
Clint COLE	Washington State University, SUA
Gene APPERSON	Digilent Inc. SUA
Jan TURAN	Technical University of Kosice, Slovakia
Andrei MARINESCU	Research and Testing Institute ICMET, Romania
Emil SIMION	Technical University of Cluj-Napoca, Romania
Iuliu DELESEGA	Politehnica University of Timișoara, Romania
Alexandru SIMION	Gheorghe Asachi Technical University of Iasi, Romania
Dan Călin PETER	Technical University of Cluj-Napoca, Romania
Constantin OPREA	Technical University of Cluj-Napoca, Romania

CONTENTS

Oliviu **MATEI**

PRELIMINARY RESULTS OF THE ANALYSIS OF FIELD DATA FROM OVENS..... 7

Denisa **STET**, Dan D. **MICU**, Levente **CZUMBIL**, Emil **SIMION**

*NUMERICAL EVALUATION OF SELF AND MUTUAL EARTH RETURN
IMPEDANCES* 13

Eleonora **POP**, Gherasim **DOMIDE**

*ON THE COMPUTATION OF ELECTRICAL RESISTANCE OF HYDRODYNAMIC
JOURNAL BEARING* 26

Olivian **CHIVER**, Liviu **NEAMT**, Eleonora **POP**

*INCREASING INDUCTION MOTORS EFFICIENCY BY REDUCING ELECTROMAGNETIC
LOADS*..... 35

Mircea **HORGOS**, Zoltan **ERDEI**, Cristian **BARZ**

MANAGEMENT OF ELECTRICITY TO A COUNTY LIBRARY..... 44

Liviu **NEAMT**, Olivian **CHIVER**, Eleonora **POP**

*CONSIDERATIONS ABOUT SHIELDING MATERIALS IN LOW FREQUENCY MAGNETIC
FIELDS*..... 54

Ioan **BERINDE**, Horia **BĂLAN**, Teodora **OROS(POP)**

REACTIVE POWER ON A POWER LINE CONNECTED FROM ONE END..... 63

Cristian **BARZ**, Tihomir **LATINOVIC**, Zoltan **ERDEI**, Gherasim **DOMIDE**, Alina
BALAN

PRACTICAL APPLICATION WITH PLC IN MANIPULATION OF A ROBOTIC ARM 78

Teodora Susana **OROS (POP)**, Ioan **BERINDE**

*THE STUDY, DESIGN AND SIMULATION OF A FREE PISTON STIRLING ENGINE
LINEAR ALTERNATOR 87*

Radu **JOIAN**, Mircea **HORGOS**, Alin **GRAMA**, Niculaie **PALAGHIȚĂ**

*CONTRIBUTIONS TO THE MANAGEMENT OF WIND POWER IN ROMANIA. THE
ABSORPTION SEN WIND ENERGY 2013. ELECTROMAGNETIC INTERFACE 96*

INSTRUCTIONS FOR AUTHORS 106

PRELIMINARY RESULTS OF THE ANALYSIS OF FIELD DATA FROM OVENS

Oliviu MATEI

Technical University of Cluj-Napoca, North University Centre of Baia Mare
oliviu.matei@cunbm.utcluj.ro

Keywords: ovens, statistics

Abstract: *The paper presents the preliminary results after analyzing the field data from 85 ovens deployed in the United States. We research especially the behavioral pattern of the user regarding the openings of the door and we prove that there are obvious relations between the pattern and some specific features, such as day of the week and hours of the day.*

1. INTRODUCTION

This paper presents the preliminary results after analyzing the data field collected from 85 ovens deployed in the United States.

We research a database of more than 1,000,000 records for several electrical appliances installed in real test field, containing data from ovens as well as from refrigerators. However our focus is on the behavioral pattern regarding the openings of the oven doors because there was no availability for refrigerator openings. For our specific purpose, we took into account a specific model of oven, namely Kenmore Elite 97102, having the serial number E02A82C5BEC0.

Of course, this is not the first attempt to analyze field data. This is crucial for any serious research and has been done in several domains, such as education [1], seismology [2], wildlife [3] and ecology [4].

On the other hand, ovens are part of our daily life, therefore a significant amount of scientific literature has been dedicated to them, especially with respect to temperature, home

and related aspects by Darigny et. al. [5], Omura et. al. [6], Li et. al. [7] and Boulet et. al. [8] and energy consumption [9].

2. METHODOLOGY

The data covers roughly 7 weeks: 15.11.2013 – 25.12.2013 and consists of 305 records. The data looks like in table 1.

Table 1. A snapshot of the database containing the data to be analysed

Timestamp	DW	Date	Hour	Door_Close	
15.11.2013 00:28	6	15.11.2013	0	TRUE	
15.11.2013 00:28	6	15.11.2013	0	FALSE	
15.11.2013 01:11	6	15.11.2013	1	TRUE	
15.11.2013 01:11	6	15.11.2013	1	FALSE	
15.11.2013 01:40	6	15.11.2013	1	TRUE	
15.11.2013 01:41	6	15.11.2013	1	FALSE	
15.11.2013 01:44	6	15.11.2013	1	TRUE	

The *Timestamp* and *Door_Close* are from the database. The day of the week (*DW*), *Date* and *Hour* fields have been drawn from the timestamp. A preliminary inspection of the data shows that the values are consistent (e.g. the number of records with *Door_Close* = *TRUE* is equal with the number of records with *Door_Close* = *FALSE*).

We research the correlations:

- Day of the week vs. number of openings of the door of the oven;
- Hours of the day vs. number of openings;
- Days of the week vs. hours when the door was opened.

3. RESULTS

3. 1. Day of the week vs. number of openings of the door of the oven

The scatter plot derived from the data depicted in Fig. 1. The *X* axis represents the days of the week (1 = Monday... 7 = Sunday). The *Y* axis shows the number of openings.

The statistical correlation factor (as defined by Hedges [10] or Hotelling [11]) between the days of the week and the number of openings is 0.1097, which shows that there is no statistical correlation between the two. But that does not mean that the two data sets are not related. For instance, it is obvious that on Tuesday the oven is not used at all.

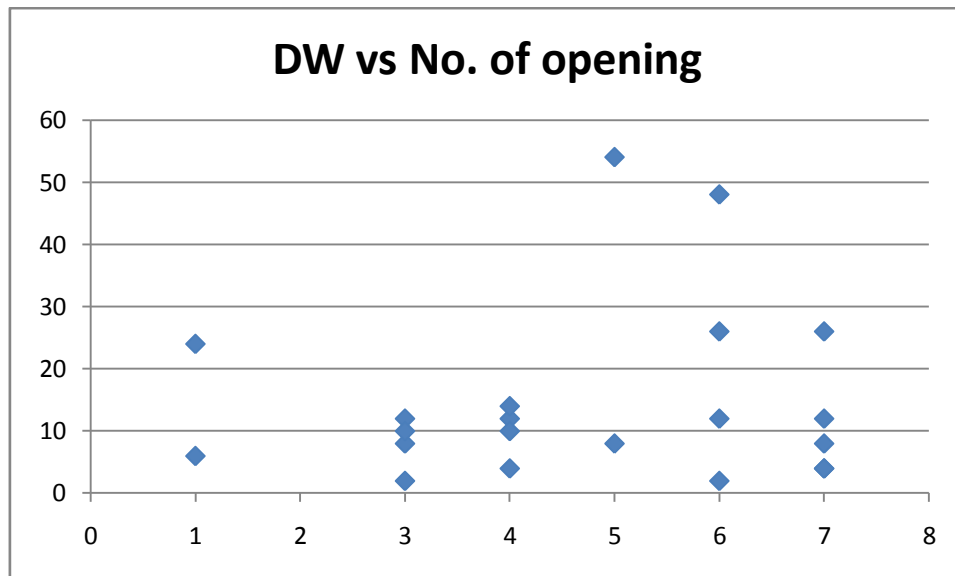


Fig. 1 – Day of the week vs. number of openings

3.2. Hours of the day vs. number of openings

The scatter plot is depicted in Fig. 2.

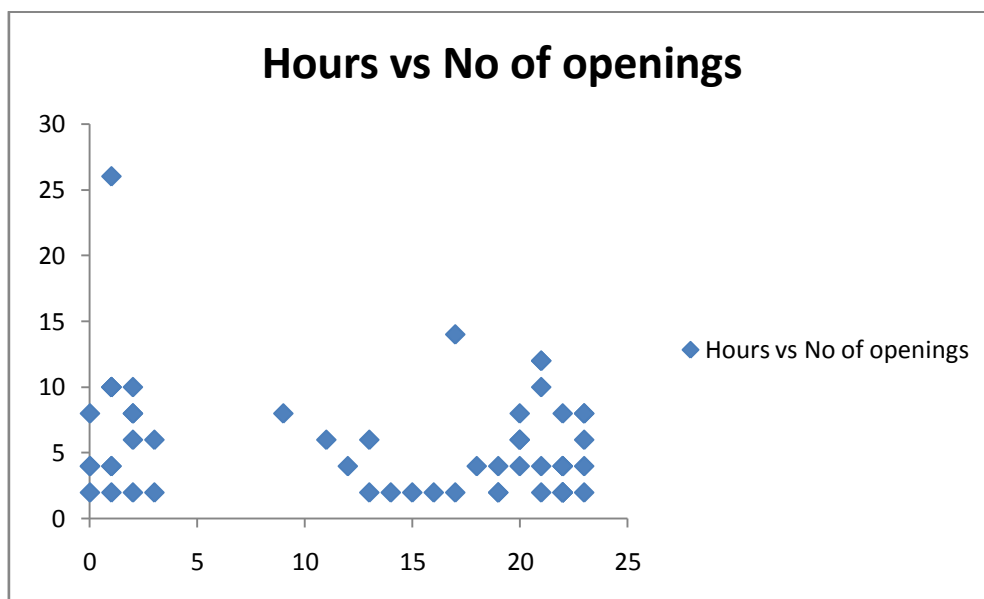


Fig. 2 – Hours of the day vs. number of openings

The X axis shows the hours (0..24) and the Y axis represents the number of openings. For relevance of the data, the time consists only of hours, not of minutes.

The correlation factor is -0.202 which says that there is no significant statistical correlation (although more than in the previous case – DW vs. number of openings). However, some conclusions can be drawn, such as that the oven is used over the night and is idle from 4:00 to 9:00.

3.3. Days of the week vs. hours when the door was opened

The scatter plot is shown in Fig. 3. The X axis represents the days of the week (1 – Monday,.. 7 = Sunday) and Y axis shows the hours when the door was opened. For relevance, the time contains only the hours, not the minutes. The correlation factor is 0.0247, which means that there is no statistical relation between the two data sets.

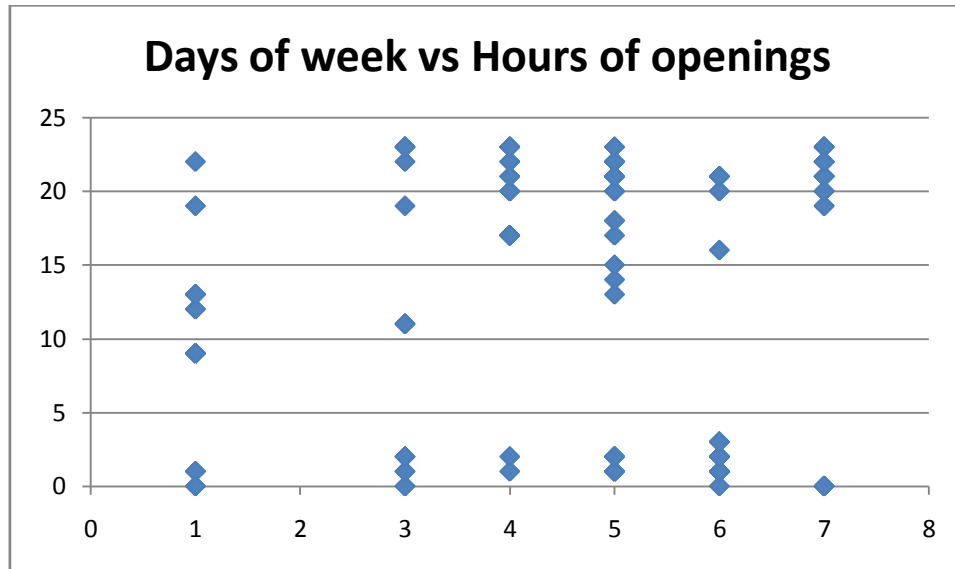


Fig. 3 – Days of the week vs. hours of the day when the door was opened

However, a close look at the plot shows that:

- The oven is not used on Tuesdays (the conclusion was drawn also previously – see section 3.a));
- The oven is not used from 4:00 – to 9:00 (see section 3.b));
- The time when the oven starts being used goes later over the week:
 - on Mondays, the oven starts working around 9:00;
 - on Tuesdays: off;
 - on Wednesdays: starts around 11:00;
 - on Thursdays: starts around 17:00;
 - on Fridays: starts around 13:00;
 - on Saturdays: starts around 16:00;
 - on Sundays: starts around 19:00.

4. CONCLUSIONS

In this research we analyzed only raw data, with no preprocessing (e.g. using only relevant data, by removing exceptions). However, the preliminary results are good and promising.

The first conclusion is that the data is consistent and relevant. Although there is no statistical correlation between the datasets compared, we could draw some interesting observations:

- The oven is not used on Tuesdays;
- The oven is not used at all from 4:00 – to 9:00;
- The time when the oven starts being used goes later over the week.

The data processed covers only seven weeks, which is a reasonable interval, but to make sure that the observations are correct, they should be applied on larger intervals, at least at this research stage.

5. FURTHER RESEARCH

We used all the data, but we can remove some exceptional situations, which will make the observations more relevant:

- In section 3.a), Mondays and Thursdays have less probability of using the oven as well as the number of openings above 40;
- In section 3.b), it is obvious that the case with more than 25 openings is not common and could be dropped.

In other words, we could discard observations with probability less than a specific threshold (which needs to be determined experimentally). Moreover, we can try predictions based on the existing data.

An attractive research direction is distributed data stream mining [12] in the home environment to extract patterns from data provided by multiple household appliances (stove, refrigerator, central heating), based on mobile agents technology [13] that can improve the usage of Big Data volumes.

ACKNOWLEDGEMENT. The research leading to these results has received funding from the European Community's Seventh Framework Programme under grant agreement No609143 Project ProSEco.

REFERENCES

1. Merriam, Sharan B., *Qualitative Research and Case Study Applications in Education. Revised and Expanded from "Case Study Research in Education."*. Jossey-Bass Publishers, 350 Sansome St, San Francisco, CA 94104, 1998.
2. Yilmaz, Özdoğan. *Seismic data analysis. Vol. 1*. Tulsa: Society of Exploration Geophysicists, 2001.

3. **Kenward, Robert.** *Wildlife radio tagging: equipment, field techniques and data analysis*. London: Academic Press, 1987.
4. **Jongman, Robert HG, Cajo JF Ter Braak, and Onno FR Van Tongeren,** eds. *Data analysis in community and landscape ecology*. Cambridge university press, 1995.
5. **Darigny, Franck, Jacky Guerin, and Paul Muller.** "Electronic control device for automatic cooking, including learning for home electric oven." U.S. Patent No. 4,914,277. 3 Apr. 1990.
6. **Omura, Y., and M. Losco.** "Electro-magnetic fields in the home environment (color TV, computer monitor, microwave oven, cellular phone, etc) as potential contributing factors for the induction of oncogen C-fos Ab1, oncogen C-fos Ab2, integrin alpha 5 beta 1 and development of cancer, as well as effects of microwave on amino acid composition of food and living human brain." *Acupuncture & electro-therapeutics research* 18.1 pp. 33-73, 1992.
7. **Li, Bojun, Piyanuch Hathaipontaluk, and Suhuai Luo.** "Intelligent oven in smart home environment." *Research Challenges in Computer Science, 2009. ICRCCS'09. International Conference on.* IEEE, 2009.
8. **Boulet, Micael, et al.** "CFD modeling of heat transfer and flow field in a bakery pilot oven." *Journal of food engineering* 97.3 pp. 393-402, 2010.
9. **Neamt Liviu,** "Energy audit for domestic customers", *Energetica*, year 62. no. 7, pp. 278-281, 2014.
10. **Hedges, Larry V.** "Statistical Methodology in Meta-Analysis", 1982.
11. **Hotelling, Harold.** "Analysis of a complex of statistical variables into principal components." *Journal of educational psychology* 24.6, 1993,.
12. **Costea, C. and Cola, C.** "A Practical Model for Distributed Sensing and Analysis using RPi", *Proceedings of the International Conference of the Carpathian Euro-Region's Specialists in Industrial Systems, CEurSIS* pp.180-183, 2014.
13. **Costea, C.** "Applications and Trends in Mobile Cloud Computing." *Carpathian Journal of Electronic and Computer Engineering*, vol 5, pp. 57-60., 2012.

NUMERICAL EVALUATION OF SELF AND MUTUAL EARTH RETURN IMPEDANCES

Denisa STET, Dan D. MICU, Levente CZUMBIL, Emil SIMION

Electrical Engineering and Measurement Department, Technical University of Cluj-Napoca, Romania

Denisa.Stet@ethm.utcluj.ro, Dan.Micu@ethm.utcluj.ro, Levente.Czumbil@ethm.utcluj.ro,

Emil.Simion@ethm.utcluj.ro

Keywords: electromagnetic interference, impedance, algorithms

Abstract: *The paper presents an evaluation of analytical self and mutual impedances formulas of lines with earth return, taking into account the ground correction terms. The determined formulas contain semi-infinite integral terms which are calculated by a novel stable and efficient numerical integration scheme in order to overcome the involved oscillation problems. It might seek approximations of the semi-infinite integrals by replacing an exponential or algebraic function, the objective being to permit analytic integration. Since there is no good systematic method for making these replacements, their success depends directly on the intuition and ingenuity, taking into account that in practice the integrand has limited accuracy.*

1. INTRODUCTION

The problem of environmental effects and electromagnetic interferences produced by time varying electric and magnetic fields due to A.C. currents flowing through high voltage or medium voltage power lines have been the topic of numerous research papers over the last decades [1-3]. Therefore, it is well known that due to inductive and capacitive couplings, dangerous eddy currents could be induced in any metallic structure placed nearby overhead or underground power lines. These dangerous situations could be also detected in case of underground electrical cables or cable screens, designed to attenuate the electric and magnetic field distributions in the surrounding zone. The result consists in insulation overheating which leads to structural integrity of these cables [4, 5].

There are generally two ways to analyze the electromagnetic interference between transmission lines and nearby parallel metallic structures: (1) using the conventional circuit method along with grounding analysis or (2) using the electromagnetic field method. Regardless of the method used, an essential step during the numerical algorithm is the computational of the self and mutual impedances of the underground/aerial conductors.

There are many efforts to solve the problem in the reference materials, but usually the authors made the approximations derived from the circuit's theory. Many physical events cannot be taken into account using the elements with concentrated parameters, i.e. grounding resistors, capacitors and inductances to describe the behavior into the soil. To avoid mathematical difficulties, it is introduced some simplifications, which conceal the physical picture of the problem. Skin effect in the soil, especially for different earth's resistivity, is hidden in empiric formulas, diagrams and nomograms, usually applied in power engineering. For this reason, it has been decided to take the physical base as an essential electromagnetic starting-point and the applied mathematical methods used to compute the self and mutual impedances, will be only the consequence of such a treatment [6].

2. EARTH RETURN IMPEDANCE EVALUATION USING CARSON FORMULAS

J. R. Carson published a theory [7] suitable to calculate the electromagnetic fields due to a horizontal current carrying conductor, which is above a lossy earth. The integral found by Carson is usually applied for the calculation of self and mutual impedance of lines with earth return. He was one of the firsts who evaluated transmission line parameters and found expressions for the elements of the impedance matrix Z that nowadays serve as a good reference under the name "Carson's equations". Accordingly to this theory, the calculation of line impedance (self and mutual impedance of lines with earth return) is based on equations that contain semi-infinite integrals with complex arguments. For evaluation of these integrals, infinite series and also some convenient approximations for low frequencies have been proposed.

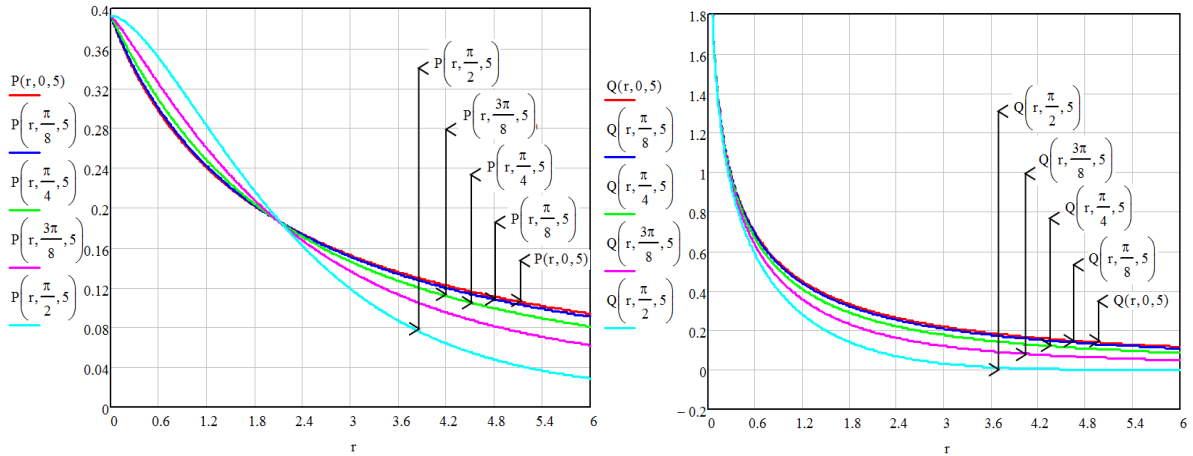
In the mutual impedance equation (1) could be identified a Sommerfeld integral [6, 8], highlighted in equation (2),

$$\underline{Z}_{12} = j2\omega \ln\left(\frac{\rho''}{\rho'}\right) + 4\omega \int_0^{\infty} \left(\sqrt{\mu^2 + j} - \mu\right) e^{-(h_k + h_l)\mu} \cos(x'\mu) d\mu \quad (1)$$

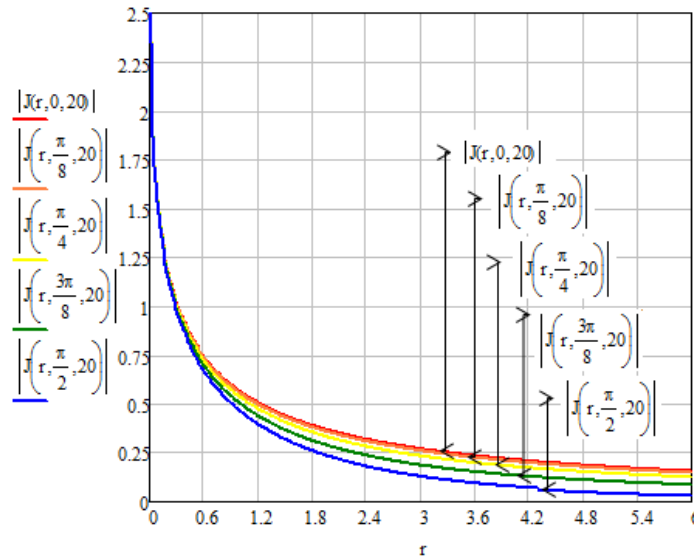
$$J(p, q) = \int_0^{\infty} \left(\sqrt{\mu^2 + j} - \mu\right) \cdot e^{-p\mu} \cdot \cos(q\mu) \cdot d\mu \quad (2)$$

which formulates a solution $J = P + jQ$ in the form of a sum of eight infinite series (*figure 1*):

$$\begin{cases} P = \frac{\pi}{8}(1-s_4) + \frac{1}{2} \ln\left(\frac{2}{\gamma r}\right) \cdot s_2 + \frac{1}{2} \theta \cdot s'_2 - \frac{1}{\sqrt{2}} \sigma_1 + \frac{1}{2} \sigma_2 \frac{1}{\sqrt{2}} \sigma_3 \\ Q = \frac{1}{4} + \frac{1}{2} \ln\left(\frac{2}{\gamma r}\right) \cdot (1-s_4) - \frac{1}{2} \theta \cdot s'_4 + \frac{1}{\sqrt{2}} \sigma_1 - \frac{\pi}{8} s_2 + \frac{1}{\sqrt{2}} \sigma_3 - \frac{1}{2} \sigma_4 \end{cases} \quad (3)$$


 Fig. 1 – Representation of the P and Q functions

The infinite series are rapidly convergent and an implementation in a numerical computation software lead to the function J , plotted against r and θ and using $n = 5$ as the number of considered factors [9].


 Fig. 2 - Function J plotted against r and θ

Introducing in inductances relations the (concept of) skin depth these parameters becomes a complex numbers with terms which represent the energy dissipation in the ground. This principle is available for conductor's self and mutual inductance calculations [10].

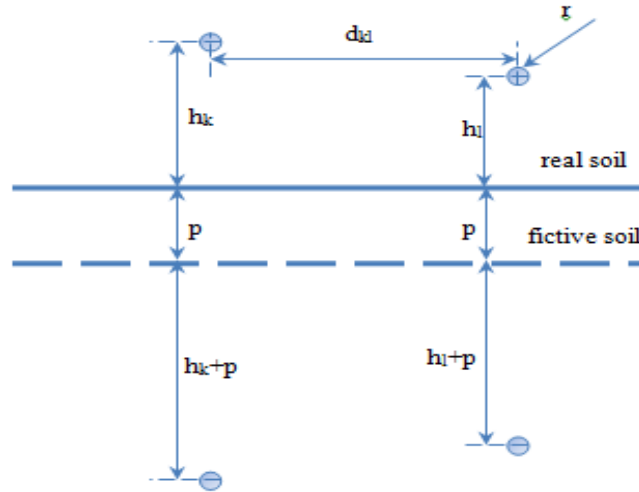


Fig. 3 – Geometrical configuration using a fictive ground return plane

The complex ground return plane could be explained using some fundamental equations for self and mutual impedances of the ideal conductor (complex plane). It starts with the ideal conductor/ground return (self and mutual) impedances:

$$\begin{cases} \underline{Z}_m = j\omega \frac{\mu_0}{2\pi} \ln \frac{\sqrt{(h_k + h_l)^2 + d_{kl}^2}}{\sqrt{(h_k - h_l)^2 + d_{kl}^2}} + \underline{Z}_{mg} \\ \underline{Z}_s = j\omega \frac{\mu_0}{2\pi} \ln \frac{2h}{r} + \underline{Z}_{sg} \end{cases} \quad (4)$$

The impedances \underline{Z}_{mg} , \underline{Z}_{sg} are the Carson's ground correction terms of the mutual and self-impedance per unit length that introduce the skin depth effect in the ground.

Could be recognizing in the first term of the equations (4), with the effect hypothesis (the alternative current is concentrating on the conductor exterior surface) [10]. The ground correction term of the impedances per unit length is:

$$\underline{Z}_{mg} = j\omega \frac{\mu_0}{2\pi} \int_0^\infty \frac{2e^{-(h_k + h_l)\lambda}}{\lambda + \sqrt{\lambda^2 + j\omega\mu_0\sigma}} \cdot \cos(\lambda d_{kl}) \cdot d\lambda \quad (5)$$

$$\underline{Z}_{sg} = j\omega \frac{\mu_0}{2\pi} \cdot \int_0^\infty \frac{2e^{-2h\lambda}}{\lambda + \sqrt{\lambda^2 + j\omega\mu_0\sigma}} \cdot d\lambda \quad (6)$$

After evaluating the semi-infinite integrals using series expansion it is obtained the following expressions of impedances, using the complex earth return plane:

$$\begin{cases} \underline{Z}_s = j\omega \frac{\mu_0}{2\pi} \cdot \ln \left(\frac{2(h + p)}{r} \right) \\ \underline{Z}_m = j\omega \frac{\mu_0}{2\pi} \cdot \ln \left(\frac{\sqrt{(h_k + h_l + 2p)^2 + d_{kl}^2}}{\sqrt{(h_k - h_l)^2 + d_{kl}^2}} \right) \end{cases} \quad (7)$$

These equations provide simple and also remarkably accurate substitutes to Carson's equations (electronic handheld calculators can evaluate them instead of computers) over the whole range of frequencies.

The authors developed an algorithm which can compute the error between the formulas for self and mutual impedances, for arbitrary geometries (see the results in *figure 4*) with the following steps (*figure 3*):

<p>STEP 1:</p> $J_{\text{Carson}}(f, k, 1) := \begin{cases} \int_0^{\infty} \frac{j \cdot e^{-2h_k \cdot \lambda}}{\lambda + \sqrt{\lambda^2 + j \cdot \omega(f) \cdot \mu_0 \cdot \sigma}} d\lambda & \text{if } k = 1 \\ \int_0^{\infty} \frac{j \cdot e^{-2(h_k + h_1) \cdot \lambda}}{\lambda + \sqrt{\lambda^2 + j \cdot \omega(f) \cdot \mu_0 \cdot \sigma}} \cdot \cos(\lambda \cdot d_{k,1}) d\lambda & \text{otherwise} \end{cases}$	$Z_{\text{Carson}}(f, k, 1) := \begin{cases} j \cdot \omega(f) \cdot \frac{\mu_0}{2\pi} \cdot \ln\left(\frac{2h_k}{r}\right) + \omega(f) \cdot \frac{\mu}{\pi} \cdot J_{\text{Carson}}(f, k, 1) & \text{if } k = 1 \\ j \cdot \omega(f) \cdot \frac{\mu_0}{2\pi} \cdot \ln\left[\frac{\sqrt{(h_k + h_1)^2 + (d_{k,1})^2}}{\sqrt{(h_k - h_1)^2 + (d_{k,1})^2}}\right] + \omega(f) \cdot \frac{\mu}{\pi} \cdot J_{\text{Carson}}(f, k, 1) & \text{otherwise} \end{cases}$ $R_{\text{Carson}}(f, k, 1) := \text{Re}(Z_{\text{Carson}}(f, k, 1))$ $X_{\text{Carson}}(f, k, 1) := \text{Im}(Z_{\text{Carson}}(f, k, 1))$
<p>STEP 2:</p> $Z_{\text{prop}}(f, k, 1) := \begin{cases} j \cdot \omega(f) \cdot \frac{\mu_0}{2\pi} \cdot \ln\left(\frac{2h_k + p(f)}{r}\right) & \text{if } k = 1 \\ j \cdot \omega(f) \cdot \frac{\mu_0}{2\pi} \cdot \ln\left[\frac{\sqrt{(h_k + h_1 + 2p(f))^2 + (d_{k,1})^2}}{\sqrt{(h_k - h_1)^2 + (d_{k,1})^2}}\right] & \text{otherwise} \end{cases}$	$R_{\text{prop}}(f, k, 1) := \text{Re}(Z_{\text{prop}}(f, k, 1))$ $X_{\text{prop}}(f, k, 1) := \text{Im}(Z_{\text{prop}}(f, k, 1))$ $D(k, 1) := \sqrt{(d_{k,1})^2 + (h_k + h_1)^2}$ $a(f, k, 1) := \frac{\sqrt{2}}{ p(f) } \cdot D(k, 1)$
<p>STEP 3:</p> $\varepsilon_R(f, k, 1) := \frac{R_{\text{Carson}}(f, k, 1) - R_{\text{prop}}(f, k, 1)}{ Z_{\text{Carson}}(f, k, 1) }$ $\varepsilon_X(f, k, 1) := \frac{X_{\text{Carson}}(f, k, 1) - X_{\text{prop}}(f, k, 1)}{ Z_{\text{Carson}}(f, k, 1) }$	$\varepsilon_X(f, k, 1) := \frac{X_{\text{Carson}}(f, k, 1) - X_{\text{prop}}(f, k, 1)}{ Z_{\text{Carson}}(f, k, 1) }$ $\varepsilon_Z(f, k, 1) := \frac{ Z_{\text{Carson}}(f, k, 1) - Z_{\text{prop}}(f, k, 1) }{ Z_{\text{Carson}}(f, k, 1) }$

Fig. 4 – Error computation using a Mathcad algorithm

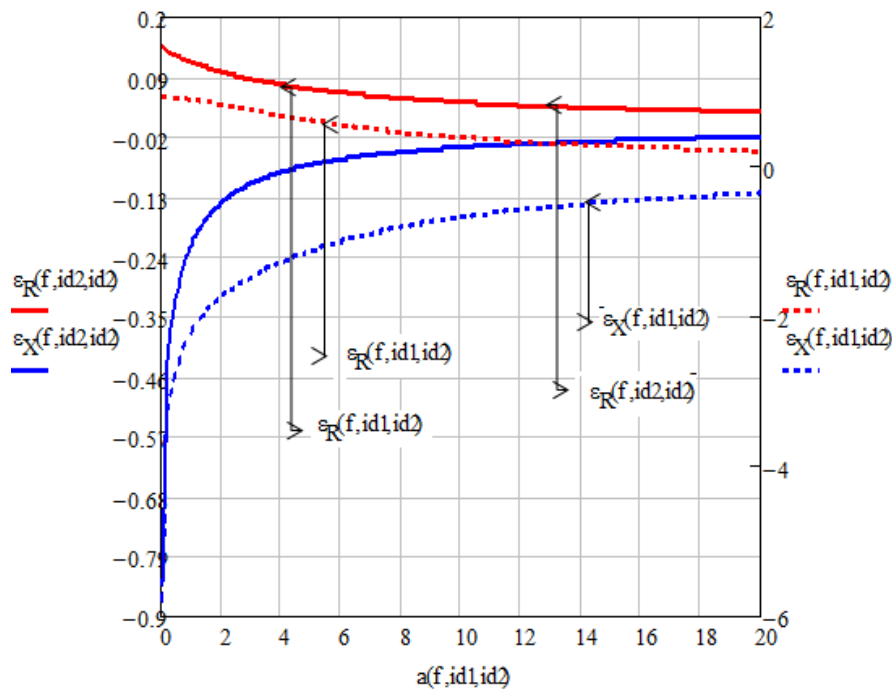


Fig. 5 - Relative error between the formulas for self and mutual impedances, for arbitrary geometries

3. EARTH RETURN IMPEDANCE EVALUATION USING POLLACZEK FORMULAE

Pollaczek [11] derives a solution for the electromagnetic coupling problem by following roughly the same path as Carson. His solution is also formulated in an integral form, however this integral is a doubly infinite one compared to Carson's semi-infinite one. To calculate buried cable earth impedances, one has to solve Pollaczek's integral, which, as the one by Carson, does not have a closed form solution.

But, whilst Carson's integral can be solved numerically with relative easiness (using the infinite series expansion), Pollaczek's integrand is highly oscillatory and irregular. For this reason, its integration by series or by general purpose algorithms presents convergence problems. Wedepohl [12] has proposed a series solution to Pollaczek's integral, but this series is very difficult to handle and has slow convergence rate at certain application ranges [13].

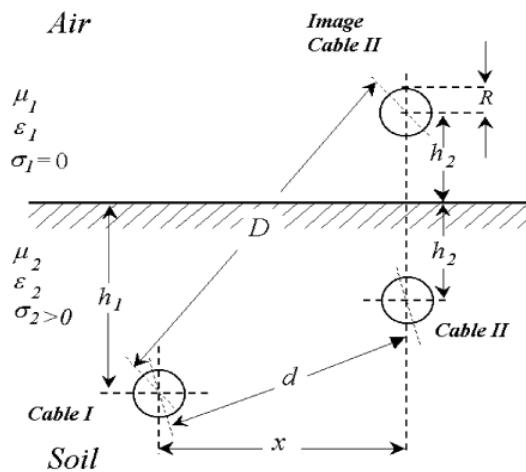


Fig. 6 - Underground transmission network

For a system of two underground cables, presented in figure 6, the self and mutual impedances can be calculated with equation (8)

$$\underline{Z}_P = \frac{j\omega\mu_0}{2\pi} \left[K_0\left(\frac{d}{p}\right) - K_0\left(\frac{D}{p}\right) + J \right] \quad (8)$$

where J is the infinite integral and has the form emphasized in equation (9):

$$J = \int_{-\infty}^{+\infty} \frac{\exp\left[-2 \cdot h \sqrt{\beta^2 + \frac{1}{p^2}}\right]}{|\beta| + \sqrt{\beta^2 + \frac{1}{p^2}}} \cdot \exp(j\beta x) \cdot d\beta \quad (9)$$

By introducing in equation (8) the variable change: $\beta = u/|p|$ respectively considering that $\sqrt{u^2 + j} + u = \frac{j}{\sqrt{u^2 + j - u}}$, a new formula for J is obtained:

$$J = -2j \cdot \int_0^{\infty} \left(\sqrt{u^2 + j} - u \right) \cdot \exp \left[- \left(\frac{2h}{|p|} \right) \sqrt{u^2 + j} \right] \cdot \cos \left(u \frac{x}{|p|} \right) \cdot du \quad (10)$$

It should be noted that h and x are always divided by $|p|$, which is interpreted as normalizations of distances h and x with respect to the penetration depth $|p|$. Thus, the following reduced dimensions parameters are introduced in equation (10): $\xi = \frac{2h}{|p|}$, $\eta = \frac{x}{2h}$, alongside the notation:

$$\sqrt{u^2 + j} = \frac{\sqrt{u^2 + \sqrt{u^4 + 1}}}{\sqrt{2}} + j \cdot \frac{\sqrt{-u^2 + \sqrt{u^4 + 1}}}{\sqrt{2}} = F(u) + j \cdot G(u) \quad (11)$$

in order to obtain a final formula for J , that highlights the fact that this integral is a function of dimensionless variables ξ and η only:

$$J = -2j \cdot \int_0^{\infty} [F(u) - u + j \cdot G(u)] \cdot \exp \{ - \xi [F(u) + jG(u)] \} \cdot \cos(\xi \eta u) \cdot du \quad (12)$$

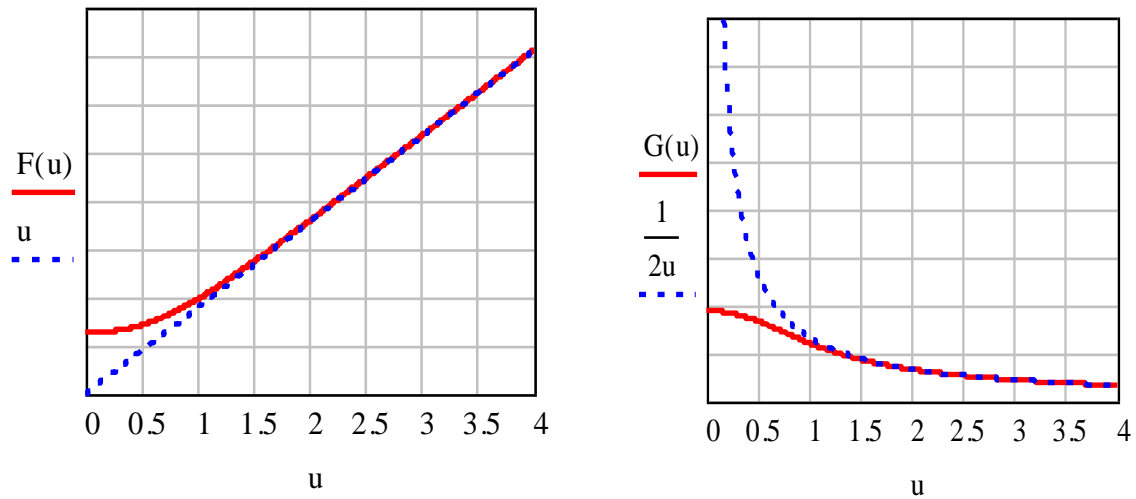


Fig. 7 - Graphical representation of $F(u)$ and $G(u)$

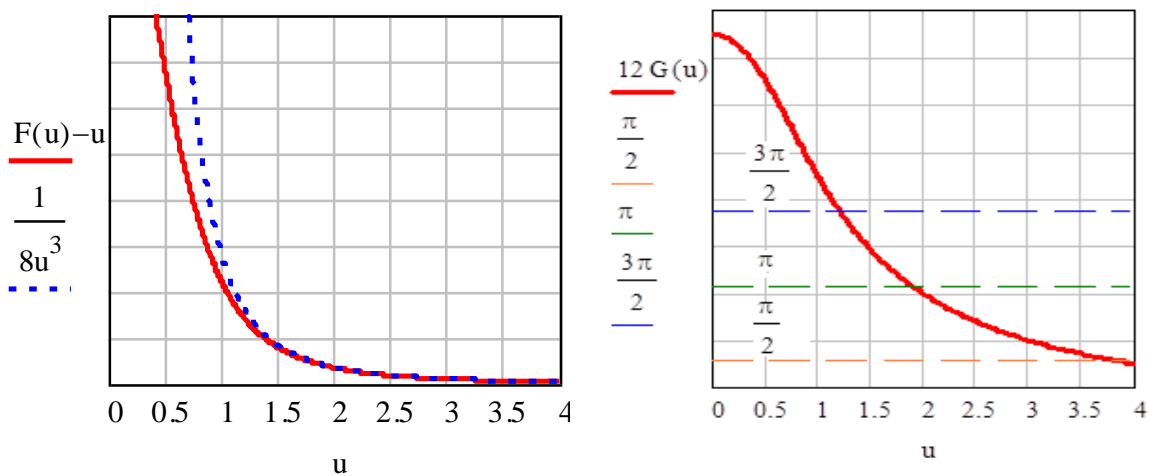


Fig. 8 - Graphical representation of $F(u)-u$ and $12 \cdot G(u)$

Based on *figures 7 and 8* an asymptotic approximations could be considered, used to formulate approximation criteria of the integral:

$$F(u) \rightarrow u, G(u) \rightarrow \frac{1}{2u}, F(u) - u \rightarrow \frac{1}{(2u)^3}; \text{ for } u > 1 \quad (13)$$

The first term from equation (11) is a complex function, with real and imaginary components that are decreasing dependent on the physical parameters of the cable system. As opposed to the first mentioned term, the other three terms are depending on the cable system physical properties. Based solely on the second term, a truncation criterion for integral is proposed. By replacing the semi-infinite integral with a finite one:

$$\int_0^{\infty} \exp(-\xi u) du \cong \int_0^{u_{\max}} \exp(-\xi u) du \quad (14)$$

which leads to the relative error of the approximation:

$$\varepsilon_r = \exp(-\xi \cdot u_{\max}) \Rightarrow u_{\max} = \frac{-\ln(\varepsilon_r)}{\xi} \quad (15)$$

Using empirical methods [14] it is possible to establish the value of ξ to provide $u_{\max} > 2$. The third term from equation (12) is a complex one, with irregular oscillations

$$\exp[-j\xi G(u)] = \cos[\xi G(u)] - j \sin[\xi G(u)] \quad (16)$$

If the condition from equation (17) is fulfilled, the last term does not oscillate:

$$\xi G(u) < \frac{\pi}{2} \Rightarrow \xi > \frac{\sqrt{2}}{2} \pi \cong 2.221 \quad (17)$$

The graphical representation of $12 \cdot G(u)$ from *figure 8*, is made for a value of ξ parameter higher than the value indicated in equation (17).

Each value which is an odd multiple of $\pi/2$, corresponds to a zero crossing of the cosine term in (16), while even multiples of $\pi/2$ correspond to the zeros of the sine term. The

total number of zeros is $n = \left\lceil \frac{\sqrt{2}\xi}{\pi} \right\rceil$ and the values of u corresponding to these zeros are

obtained by the relation:

$$u_k = G^{-1}\left(\frac{k\pi}{\xi\sqrt{2}}\right) = \frac{\sqrt{\xi^4 - \frac{k^4\pi^4}{4}}}{\xi k \pi}, \quad k = n, \dots, 2, 1 \quad (18)$$

Figure 9 shows the irregular oscillations of the third term by a set plot for $\cos[\xi G(u)]$ and $\sin[\xi G(u)]$ for different values of ξ .

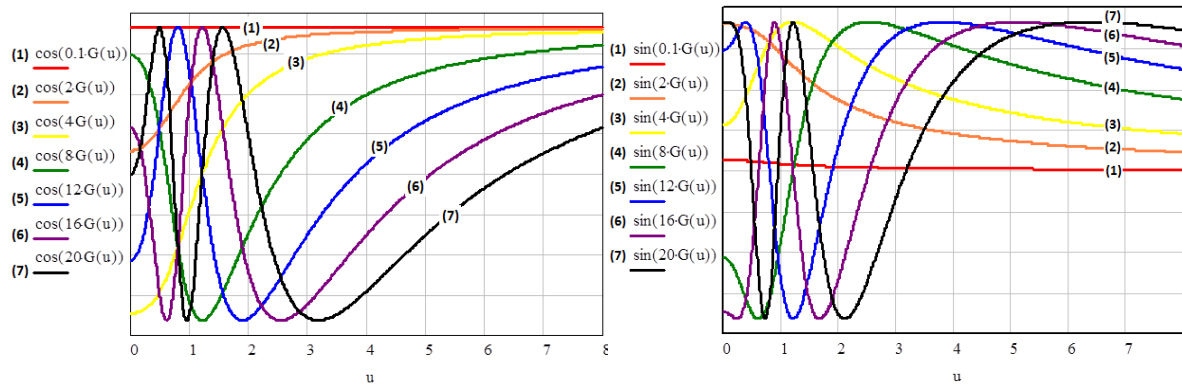


Fig. 9 - Graphical representation of $\cos[\xi G(u)]$ and $\sin[\xi G(u)]$

The fourth term from equation (12) is a cosine function, so it is an oscillatory regular term. The number of zeros within the truncated interval of u (that is $[0, u_{\max}]$) is:

$$z = \left\lceil \frac{\xi \eta u_{\max}}{\pi} + \frac{1}{2} \right\rceil \quad (19)$$

This doesn't present oscillations in the truncated interval if: $\eta < \frac{\pi}{2\xi u_{\max}}$.

Uribe [14] does a comprehensive study of Pollaczek's integral and points out the difficulties encountered when attempting its numerical solution. His analysis provides a strategy to avoid these difficulties. Furthermore, he provided solutions to Pollaczek's integral in graphic form for a broad range of applications besides normalized impedances for underground cables within the same broad application range. Finally, he compares the normalized impedances against those from a widely used approximation. His studies focus mainly on underground cables.

4. PROPOSED NUMERICAL INTEGRATION PROCEDURES

New analytical formulas for ground correction terms for self and mutual impedances are derived [6, 15, 16]. The determined formulas contain semi-infinite integral terms which are calculated by a novel stable and efficient numerical integration scheme in order to overcome the problems arising from the oscillate form of the infinite integrals.

In the solution of larger electromagnetic interference problems, it is often needed the evaluation of an integral that is function of a parameter. A choice of numerical integration may be given by the use of a family of orthogonal polynomials. These polynomials generate a Gaussian quadratic rule, according to the following theorem: assume a weight function on the interval $[a; b]$, respectively a family of orthogonal polynomials $\{\varphi_k(x)\}$ with respect to this weight function and this interval [6, 16].

The quadratic rule is defined by:

$$G_n(x) = \sum_{i=1}^n w_i^{(n)} \cdot f(x_i^{(n)}) \quad (20)$$

For $x_i^{(n)}$ the roots of φ_n and $w_i^{(n)}$ is given by relation above:

$$w_i^{(n)} = \int_a^b w(x) \cdot \left(\prod_{k=1, k \neq i}^n \frac{x - x_k^{(n)}}{x_i^{(n)} - x_k^{(n)}} \right) dx \quad (21)$$

Then $G_n(p)$ is exact for all polynomials $p \in P_{2n-1}$, and there exists $\xi \in [a; b]$ such that

$$\int_a^b w(x) \cdot f(x) dx - G_n(f) = \frac{1}{(2 \cdot n)!} \cdot \left(\int_a^b \Psi(x) dx \right) f^{(2 \cdot n)}(\xi_n) \quad (22)$$

For all $f \in C^{2 \cdot n}([a; b])$, where:

$$\Psi_n(x) = \prod_{k=1}^n (x - x_k^{(n)})^2 \quad (23)$$

Applying this theorem to construct a Gaussian quadratic rule for semi-infinite integrals of the form leads to:

$$I(f) = \int_0^\infty e^{-x} \cdot f(x) dx \quad (24)$$

For our case, the weight function is the reduced decaying exponential $w(x) = e^{-x}$, so the orthogonal polynomial family that we need to use is the Laguerre family. We choose the solutions of the fourth-order Laguerre polynomial:

$$L_4(x) = \frac{1}{24} \cdot (x^4 - 16 \cdot x^3 + 72 \cdot x^2 - 96 \cdot x + 24) \quad (25)$$

Then the weights are correspondingly evaluated, by the particular form of relation above:

$$w_1^{(4)}(h) = \int_0^\infty e^{-x \cdot h} \cdot \prod_{k=1, k \neq i}^4 \frac{(x - x_k^{(4)})}{(x_i^{(4)} - x_k^{(4)})} \quad (26)$$

The parameter h provides an extension in the numerical evaluation of the semi-infinite integral. These weight integrals are computed using some kind of numerical integration routine, such as the trapezoid of Simpson rule. Their values, according to the imposed parameter are exposed in the following *Table 1*:

Table 1. Numerical values of the weight integrals

h [m]	1	2	3
w ₁	0.693	0.441	0.339
w ₂	0.357	0.056	-0.011
w ₃	0.039	0.0024	0.0055
w ₄	0.0005	-0.00019	-0.00047

On these conditions, we may apply the explained solving procedure to the case of a semi-infinite integral involving the evaluation of a pipeline to ground impedance [15], and indirectly the induced potential or current density on the metallic pipeline due to the coexistence with a high voltage power grid, above the ground. The explicit integral is:

$$I = \int_0^{\infty} e^{y \cdot \sqrt{x^2 + m^2} - x \cdot h} \cdot \frac{\cos(u \cdot x)}{x + \sqrt{x^2 + m^2}} dx \quad (27)$$

Considering the evaluation of this integral at the surface level of the earth $y=0$ and the m coefficient depends on the value of the working frequency of the power grid, as this relation shows:

$$m = \sqrt{\frac{j \cdot 2 \cdot \pi \cdot f \cdot 4 \cdot \pi \cdot 10^{-7}}{50}} \quad (28)$$

the involved function is:

$$f(x, u) = \frac{\cos(u, x)}{x + \sqrt{x^2 + m^2}} \quad (29)$$

and it remains only to apply and evaluate the quadratic rule:

$$I(u, h) = \sum_{i=1}^4 w_i(h) \cdot f(x_i, u) \quad (30)$$

For an imposed test parameter $u=1,2,3$, in the conditions presented above, regarding the weight integrals and the parameter h , a matrix of results it is achieved.

Table2. Numerical values of the semi-infinite integral – test case

$\begin{matrix} u \\ h \end{matrix}$	1	2	3	
1	0.868-1.681j	0.646-1.231j	0.049-0.946j	$\cdot 10^{-5}$
2	0.647-1.411j	0.531-1.036j	0.042-0.797j	
3	0.584-1.01j	0.039-0.736j	0.029-0.565j	

It is worthwhile to notice that the results are complex values, and their physical significance relates to mutual impedance, with the real part – the resistance and the imaginary part – the reactance.

It is observed that most of the area under integrand occurs for small values of x , especially when y is large. This fact suggests that we might seek approximations of integral by replacing an exponential or algebraic function, the objective being to permit analytic integration.

Since there is no good systematic method for making these replacements, their success depends directly on the intuition and ingenuity, taking into account that in practice the integrand has limited accuracy.

4. CONCLUSIONS

The paper presents a numerical evaluation of the self and mutual impedance formulas for lines with earth return, formulas which contain semi-infinite integrals with high oscillation integrand. New analytical formulas for these terms are presented in the paper. We might seek approximations of the semi-infinite integrals by replacing an exponential or algebraic function, the objective being to permit analytic integration. Since there is no good systematic method for making these replacements, their success depends directly on the intuition and ingenuity, taking into account that in practice the integrand has limited accuracy.

It can be observed that the integrand of Pollaczek infinite integral has negative real part and positive imaginary part at high frequencies, which result in negative resistance and inductance. The incorrect integrand in a high frequencies region causes the numerical instability of the infinite integral. So, it is necessary to find an applicable analytically limit for this infinite integral.

However, it is very hard to calculate the earth-return impedance, but a very promising solution to the problem might be a numerical electromagnetic analysis which not requires any impedance and admittance formulas, which are compulsory to use in circuit theory approach.

ACKNOWLEDGMENT

This paper was supported by the Post-Doctoral Programme POSDRU/159/1.5/S/137516, project co-funded from European Social Fund through the Human Resources Sectorial Operational Program 2007-2013.

REFERENCES

1. **H.M. Ismail**, *Characteristics of the Magnetic Field Under Hybrid AC/DC High Voltage Transmission Lines*, Electr. Power Syst. Res., vol. 79, no. 1, p. 1-7, 2009.
2. **K.E. Holbert, G.G. Karady, S.G. Adhikari, and M.L. Dyer**, *Magnetic Fields Produced by Underground Residential Distribution System*, IEEE Transaction on Power Delivery, vol. 24, no. 3, p. 1616-1622, 2009.
3. **D. Andreuccetti, N. Zoppetti, R. Conti, N. Fanelli, A. Giorgi, and R. Rendina**: *Magnetic fields from overhead power lines: advanced prediction techniques for environmental impact assessment and support to design*, IEEE Bologna Power Tech Conference, Bologna, Italy, June 23-26, 2003.
4. **M. Rachek, and S. Nait Larbi**, *Magnetic Eddy-Current and Thermal Coupled Models for the Finite-Element Behavior Analysis of Underground Power Cables*, IEEE Trans. on Magnetics, vol. 44, no. 12, p. 4739-4746, 2008.

5. **O.E Gouda, A.Z. El Dein, G.M. Amer**, *Effect of dry zone formation around underground power cables on their ratings*, International Journal of Emerging Electric Power Systems, vol. 10, no. 3, 2009.
6. **D.D. Micu, L. Czumbil, G.C. Christoforidis**, *Semi-infinite Integral Implementation in the Development Steps of InterfStud Electromagnetic Interference Software*, 47th International Universities' Power Engineering Conference, London, September 4-7, 2012.
7. **J. R. Carson**, *Wave propagation in Overhead Wires with Earth Return*, Bell System Technical Journal, pp. 539-554, 1926.
8. **A. Gupta, M. J. Thomas**, *Coupling of High Voltage AC Power Lines Fields to Metallic Pipelines*, International Conference on Electromagnetic Interference and Compatibility, INCEMIC, Bangalore, India, February 23-24, 2006.
9. **A. Ametani, T. Yoneda, Y. Baba, N. Nagaoka**, *An investigation of the earth return impedance between overhead and underground conductors and its approximation*, IEEE Transaction on Electromagnetic Compatibility, Vol 51, p.860-867, 2009.
10. **A. Deri, G. Tevan, A. Semlyen, A. Castanheira**, *The complex ground return plane. A simplified model for homogeneous and multi-layer earth return*, PAS-100, No. 9, 1988, p. 3686-3693.
11. **F. Pollaczek**, *On the Field produced by an infinitely long wire carrying alternating current*, Elektrische Nachrichten Technik, vol. 3, 1929.
12. **M. Wedepohl**, *Propagation Characteristics of an Infinitely Long Single Conductor*, IEE, vol. 125, 1984.
13. **H. W. Dommel**, *Electromagnetic Transients Program - Reference Manual*. Portland, OR: EMTP Theory Book, 1986.
14. **F. A. Uribe, J. L. Naredo, P. Moreno, and L. Guardado**, *Algorithmic Evaluation of Underground Cable Earth Impedances*, IEEE Transactions on Power Delivery, vol. 19, no. 1, p. 316-318, 2004.
15. **G.K. Papagiannis, D.A. Tsiamitros, D.P. Labridis, P.S. Dokopoulos**, *Direct numerical evaluation of earth return path impedances of underground cables*, IEE Proc. Generation Transmission Distribution, vol. 152, No.3, p. 321-327, 2005.
16. **G. Christoforidis, D. Labridis**, *Inductive interference on pipelines buried in multilayer soil due to magnetic fields from nearby faulted power lines*, IEEE Transaction on Electromagnetic Compatibility, Vol. 47, No. 2, p. 254-262, 2005.

ON THE COMPUTATION OF ELECTRICAL RESISTANCE OF HYDRODYNAMIC JOURNAL BEARING

Eleonora POP, Gherasim DOMIDE

*Department of Electrical Electronic and Computers Engineering, North University Center, Technical
University of Cluj Napoca*

eleonora.pop@cunbm.utcluj.ro , gherasim.domide@cunbm.utcluj.ro

Keywords: Hydrodynamic, journal, bearing, electrical resistance.

Abstract: *The paper approaches the mathematical model of electrical resistance of hydrodynamic journal bearing under different parameters of operation so as to predict bearing performance and safe load carrying capacity. The currents circulating in the journal bearing of electrical machine causes reducing of lifespan by appearance of pitting on their surface and the degradation of the lubricant. In a hydrodynamic journal bearing, the zone of minimum film thickness, load-carrying oil film varies along the circumference of a bearing through its length. This has been found to form a capacitor of varying capacitance between the journal and the bearings dependent on permittivity of the lubricant used, the bearing length, the eccentricity ratio and the clearance ratio. Besides this, load-carrying on oil film offers resistance that depends on operating parameters and resistivity of the lubricant.*

1. INTRODUCTION

On the metallic surfaces of the lining and shaft of the hydrodynamic journal bearing found in dynamic functioning mode, free electric charges appear, producing an electric field in the lubricant film. This electric field causes current either by the resistance effect that occurs between the two plates and by the capacitive effect. Current through the bearings longer appears due to voltage induced in the machine shaft. The study of induced voltage in the electrical machine shaft was approached by the authors in [2] and the electric bearing

capacity calculation in [3]. In this paper only electrical resistance of the hydrodynamic journal bearing will be approached. This theme was initially approached by the authors in [4].

The induced currents circulating through the bearings increase the losses of the machine, besides reducing its lifespan. The losses in asynchronous machine and the theme of decreasing losses, was approached by authors in [5].

The majority of the electric charges are found in the area where the lubricant film is at the minimum, noted with h_0 . The oil used for the lubrication of the bearing has an electric resistivity that depends on its physical characteristics, especially on its viscosity and its consistency. The electric resistivity of the lubricant also depends on the number and nature of the impurities found in the lubricant and on some other products, such as additives, which are used in the oil from the lubricating circuit. As a result of the fact that the metallic surfaces of the lining and of the shaft are electrically charged, and the oil used for the lubrication of the bearing has a low electric conductivity, an electric resistance appears in the bearing. The journal bearing with hydrodynamic lubrication has a variable thickness of the lubricant film along the circumference, the minimum thickness being noted with h_0 . As a result of the fact that the electric charges are spread unevenly on the metallic surfaces of the shaft and of the lining and that the distance between the metallic surfaces is uneven, we can speak of a specific electrical resistance which exists in the electric field tube that appears between the shaft and the lining of the bearing.

2. DETERMINATION OF THE THEORETICAL ELECTRICAL RESISTANCE OF THE BEARING

The specific electrical resistance of the journal bearing depends on the resistivity of the lubricant ρ , on the area of the metallic surfaces of the shaft and lining, on the eccentricity ratio e and on the lap c that exists between the shaft and the lining of the bearing. The specific electrical resistance of the bearing is the lowest in the point where the lubricant film has the minimum thickness h_0 and it increases once with the increase of the lubricant film. In a journal bearing, the thinner the film is, the higher the electrical conductivity gets. This means that the electric charges accumulated on the metallic surfaces of the shaft and of the lining will be passing easier through the lubricant film in the area where the film is thinner. In this area the lubricant film is also subjected to very high pressure p , due to the charging of the bearing. These external forces affect the geometry of the oil molecules, which leads to the increase of the electric conductivity of the lubricant.

The uneven distribution of the electrical charges on the metallic surfaces of the shaft and lining and the uneven thickness of the lubricant film make the calculation of the electrical resistance of a hydrodynamic journal bearing a very difficult one. In order to calculate the equivalent electrical resistance, which appears in the electric field tube existing between the

metallic surfaces of the bearing shaft and lining, we started from the fact that the specific electrical resistance of the bearing is minimal in the area where the thickness of the lubricant film is minimum h_0 . The calculation of the electrical resistance has been done in the area where the majority of the electrical charges are found and where the thickness of the lubricant film is at its minimum, this means the area where the position angle takes values from $+\theta$ to $-\theta$ reported to h_0 . We named this value of the electrical resistance of the hydrodynamic journal bearing, the equivalent electrical capacitance of the field tube. The conducted theoretical and practical studies confirm the fact that the total electrical resistance of a hydrodynamic journal bearing is very close to the value of the equivalent electrical resistance, calculated in this mode.

The determination of the equivalent electrical resistance of the bearing is made starting from the schematic representation of the bearing illustrated in Figure 1.

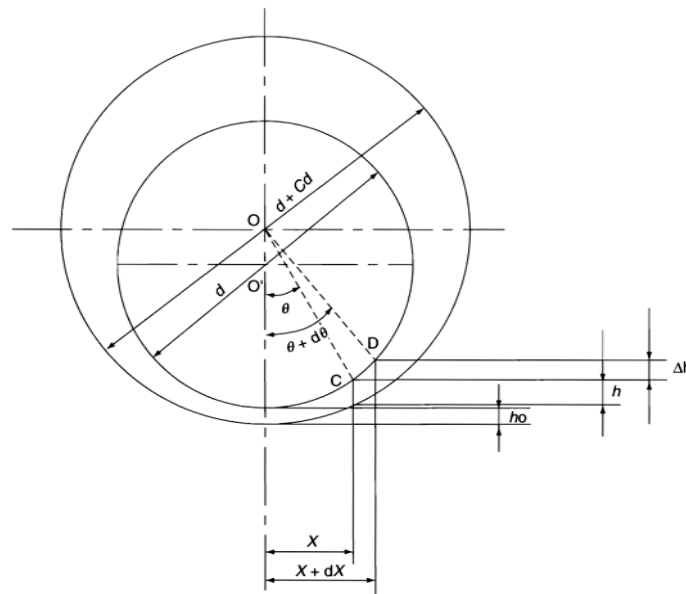


Fig. 1 - The configuration of the shaft in the hydrodynamic journal bearing [2]

The thickness h of the lubricant film in an arbitrary point C on the bearing surface, situated at an angle θ from position where the thickness of the lubricant film has the minimum value h_0 , is given by the following formula:

$$h = C_r [1 - \varepsilon \cos \theta] \quad (1)$$

where

ε is the eccentricity ratio;

θ is the angle from the vertical position of the bearing;

C_r is the distance from the bearing center, O , to the h_0 .

And the minimum film thickness is obtained when $\theta = 0$ and given as:

$$h_0 = C_r (1 - \varepsilon) \quad (2)$$

The change in conductance/resistance-1 (ΔF_b) between two rectangular plates of width dX situated between $(X + dX)$ and X along X-axis (along the bearing circumference) of bearing length L (along Y-axis) located at the attitude angles varying between $(\theta + d\theta)$ and θ and separated by a film thickness varying between $h + \Delta h$ and h (Fig. 1), is given as:

$$\Delta F_b = \frac{dX L}{\rho h} \quad (3)$$

From relation 3, we find that the variation of the conductance depends on the thickness of the lubricant film h and the thinner h is, the higher the conductance is. Along the circumference of the bearing, the thickness of the lubricant film is minimal in point h_0 . The further we get from this point and the higher the angle θ becomes, the thicker the lubricant film becomes, reason for which the conductance F decreases.

In order to find the highest value for the conductance of the lubricant film for a hydrodynamic journal bearing, we'll integrate between the position angle $+\theta$ and $-\theta$ reported to the minimum thickness of the lubricant film noted with h_0 . In point h_0 the position angle is zero, thus $\theta = 0$. From figure 1, it is evident that

$$dX = \frac{d\theta d}{2} \quad (4)$$

If we substitute relations 1 and 4 in relation 3, the variation of the electrical conductance for the hydrodynamic journal bearing, represented in figure 1, is given by relation

$$F_b = \frac{1}{R_b} = \int_{-\theta}^{\theta} \frac{(L/\psi \rho) d\theta}{(1 - \varepsilon \cos \theta)} \quad (5)$$

After the integration of this relation between the the position angle $+\theta$ and $-\theta$ reported to the minimum thickness of the lubricant film noted with h_0 , we obtained the following relation for the equivalent electrical resistance of the hydrodynamic journal bearing:

$$R_b = \frac{\left| \rho \psi (1 - \varepsilon^2)^{1/2} \right|}{4 L \tan^{-1} \tan 0.5\theta \left[\frac{(1 + \varepsilon)}{(1 - \varepsilon)} \right]^{1/2}} \quad (6)$$

The specialized publications in this field [4] confirm the fact that the variation of the specific electrical resistance of the hydrodynamic journal bearing is maximum between the limits in which the position angle takes the values $+\pi/4$ și $-\pi/4$, reported to the area where the thickness of the lubricant film is minimal, and the position angle θ takes the value zero.

Having these conditions for the integration interval, the equivalent electrical resistance of the hydrodynamic journal bearing is determined with relation

$$R_b = \frac{\left| \rho \psi (1 - \varepsilon^2)^{1/2} \right|}{4 \delta d \tan^{-1} 0.41 \left[\frac{(1 + \varepsilon)}{(1 - \varepsilon)} \right]^{1/2}} \quad (7)$$

Where:

ε is the eccentricity ratio;

δ is the bearing shaft length and diameter ratio ($\delta = L/d$);

ρ is resistivity of lubricant

To study the variation of the equivalent electrical resistance of the bearing, we used the hydrodynamic journal bearing, which in dynamic functioning mode has 360 or 600 revolutions and 3600 rotations/minute, and the lubricant used is an oil with additives for LA32 type bearings, which has the electrical resistivity $\rho=1014 \Omega \cdot \text{cm}$.

2.1 The influence of the ratio ψ over the equivalent electrical resistance R_b

The study of the variation of the equivalent electrical resistance R_b for the hydrodynamic journal bearing when ratio ψ modifies, has been conducted considering that the eccentricity ratio ε and the ratio δ between the length and the diameter of the shaft are constant. The study of the variation of the equivalent electrical resistance R_b for the bearing is conducted for the situation in which the same lubricant, the LA 32, STR 5152-89 type of oil is used for the hydrodynamic journal bearing. The electrical resistivity ρ of the lubricant used for the lubrication for the bearing has the value $1014 \Omega \cdot \text{cm}$. The hydrodynamic journal bearing considered to be the experimental bearing, has:

lap $c = 0,08 \text{ mm}$;

ratio $\psi = 0,0013$.

In order to determine the mode in which the variation of parameter ψ influences the variation of the equivalent electrical resistance R_b for the hydrodynamic journal bearing, we assumed that the lap c of the shaft modifies with $\pm 0,01 \text{ mm}$ reported to the value obtained through calculation, which for this bearing is of $0,08 \text{ mm}$. In this situation, the lap c between the shaft and the lining of the bearing, which the calculation showed to be $0,08$, modifies and is found in the interval $0,07 - 0,09$. For a variation of lap c of the bearing, in the interval $0,07 - 0,09$, ratio ψ will have a variation between $0,0011$ and $0,0015$. The variation of the equivalent electrical resistance for the hydrodynamic journal bearing, for the three values of ratio ψ : $0,0011$, $0,0013$ and $0,0015$ are presented in table 1.

Table 1. The variation of the equivalent electrical resistance with the ψ ratio

Ratio ψ [mm]	ε	0,0011	0,0013	0,0015
The bearing resistance [$10^9 \Omega$]	0,9	2.27	2.67	3.088
The bearing resistance [$10^9 \Omega$]	0,72	2.30	2.71	3.14
The bearing resistance [$10^9 \Omega$]	0.58	2.32	2.74	3.17

The next graphs show the variation of the equivalent electrical resistance of the bearing

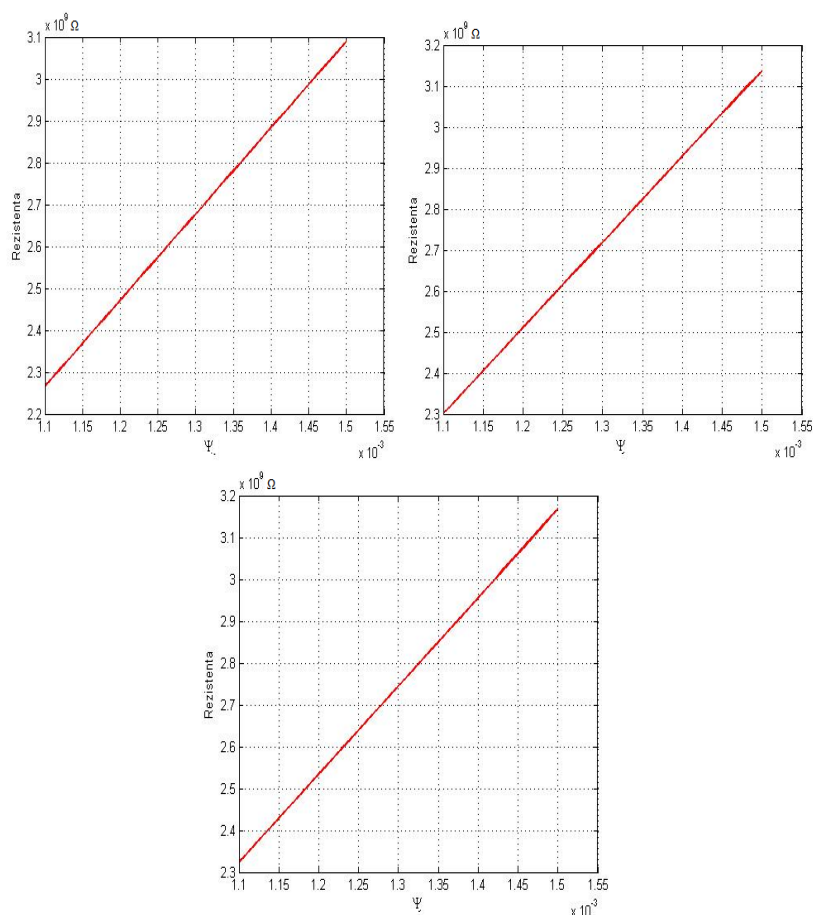


Fig. 2 - The variation of the equivalent electrical resistance of the bearing with ψ ratio

2.2 The influence of the eccentricity ratio ε over the equivalent electrical resistance

The study on the influence of the eccentricity ratio ε over the equivalent electrical resistance of the bearing, R_b , is made keeping constant the values of ψ ratio and δ ratio. The resulted values are presented in Table 2.

Table 2. The variation of the equivalent electrical resistance with the ε ratio.

The eccentricity ratio ε	ψ	0,58	0,72	0,9
The bearing resistance [$10^9 \Omega$]	0,0015	1,52	1,10	0,51
The bearing resistance [$10^9 \Omega$]	0.0013	1,31	0,94	0,44
The bearing resistance [$10^9 \Omega$]	0,0011	1,11	0,80	0,37

The next graphs show the variation of the equivalent electrical resistance of the bearing.

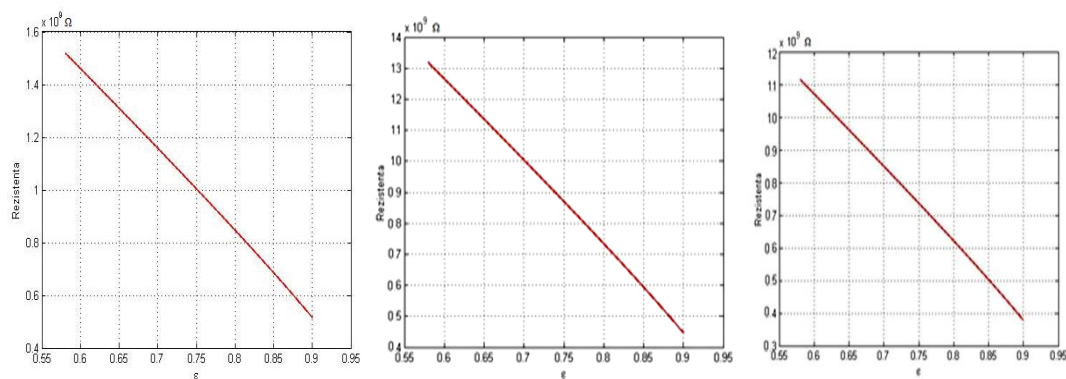


Fig. 3 - The variation of the equivalent electrical resistance of the bearing with ε ratio

Table 3 The variation of the equivalent electrical resistance with the ε ratio.

The eccentricity ratio ε	δ	0,58	0,72	0,9
The bearing resistance [$10^9 \Omega$]	1/2	1,31	0,95	0,44
The bearing resistance [$10^9 \Omega$]	1	0,65	0,47	0,22

The next graphs show the variation of the equivalent electrical resistance of the bearing.

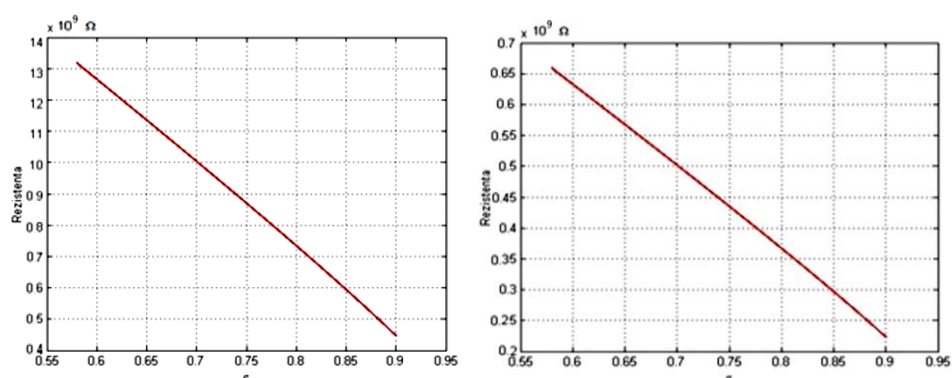
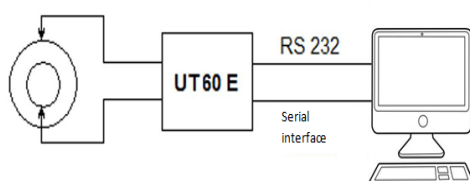
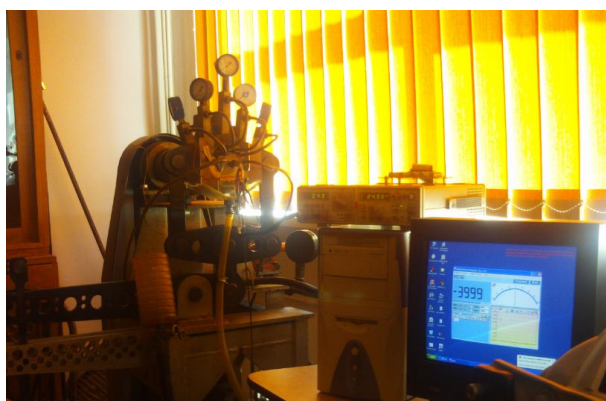


Fig. 4 - The variation of the equivalent electrical resistance of the bearing with δ ratio

Experimental study of electrical resistance of hydrodynamic journal bearings was carried out using the stand presented in fig. 5.



a) Stand scheme



b) Stand foto

Fig. 5 – Stand for determination electrical resistance

Data are acquired with a frequency of three samples per second and transmitted to a personal computer via the standard RS232 serial interface. Transfer rate is 2400 bps.

The studied radial bearing has a nominal diameter $D = 60$ mm and the width $L = 30$ mm, bronze material in the composition 88% Sn, 8% Sb, 4% Cu, and the journal material is 18MoCr10.

Effective diameters of the journal and liner are $d_e = 59.85$ mm, $D_e = 59.93$ mm and bearing width is $L = 30$ mm. Input speed variation is achieved by means of a gearbox, which provides speeds of 120, 360, 600 and 960 rev / min.

The measured value of the electrical resistance of the hydrodynamic journal bearings at the speed of 120 rev / min, after having been filtered through the sliding average method, are shown in Fig. 6.

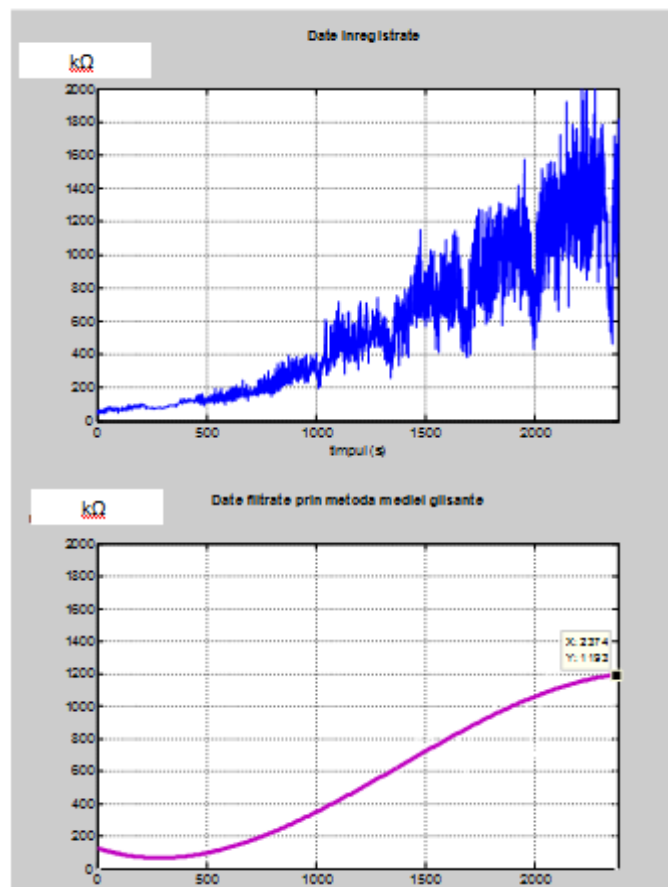


Fig. 6 – Electrical resistance variation with time(s)

3. CONCLUSIONS

The theoretical values of the equivalent electrical resistance R_b of the experimental bearing, presented in three tables and three figures, lead to the following conclusions:

The value of the equivalent electrical resistance R_b of the bearing increases if the ψ ratio increases. The increase of the value of the equivalent electrical resistance once with the increase of ratio ψ is justified, because the lubricant film thickens. Once with the increase of

the lubricant film thickness, the conductivity of the oil used to lubricate the bearing decreases, which leads to the increase of the equivalent electrical resistance of the bearing.

The value of the equivalent electrical resistance R_b of the bearing decreases if the eccentricity ratio ε increases. The increase of the eccentricity leads to the decrease of the lubricant film. The decrease of the lubricant film between the shaft and the lining results in the decrease of the equivalent electrical resistance of the bearing.

The value of the equivalent electrical resistance R_b of the bearing decreases if the bearing length and diameter ratio increases. The increase of ratio δ , between the length and the diameter of the tree shaft, from value $\frac{1}{2}$ to 1, is equivalent to the increase of the surface of the bearings shaft and liner. The increase of the metallic surfaces of the shaft and liner, which are electrically charged, leads to the increase of the lubricant film conductivity, which means the decrease of the electrical resistance of the bearing.

Experimentally it was observed that the electrical resistance is not constant over time. At the beginning of operation it grows and then tending to stabilize at a maximum value.

REFERENCES

1. **Gopinath K., Mayuram M.M.** *Hydrodynamic, Lubrication of Journal Bearings. Theory and Practice. Machine Design II*, Indian Institute of Technology Madras.
2. **Eleonora Pop, Olivian Chiver and Radu Cotetiu**, *Study of electrical voltages induced in the electrical machines shaft*, SCIENTIFIC BULLETIN, Serie C, Fascicle: Mechanics, Tribology, Machine Manufacturing Technology, ISSN 1224-3264, Vol. 2012, No. XXVI.
3. **Pop Eleonora, Buchman A., Chiver O., Horgoş M., Alexandrescu M.**, *Study of electrical capacitance of hydrodynamic journal bearing* – International Multidisciplinary Conference 9th Edition, 19-21 Mai 2011 North university of Baia Mare Romania, University College of Nyiregyhaza;
4. **Eleonora Pop, Marius Alexandrescu**, *Study of electrical resistance of hydrodynamic journal bearing*, Proceedings of the International Conference of the Carpathian Euro-region's Specialists in Industrial Systems - 10th edition – BAIA MARE, Sept., 11st – 13rd, ISBN 978-606-737-003-42014, Ed. U.T.PRESS, Cluj-Napoca, 2014.
5. **Olivian CHIVER, Liviu NEAMT, Eleonora POP**, *Study regarding solutions to increase the efficiency of induction motors*, Proceedings of the International Conference of the Carpathian Euro-region's Specialists in Industrial Systems - 10th edition – BAIA MARE, Sept., 11st – 13rd, ISBN 978-606-737-003-42014, Ed. U.T.PRESS, Cluj-Napoca, 2014.
6. **Prashad, H.**, *Tribology in electrical environments*. Oxford, UK, Elsevier Ltd., 2006.
7. **Prashad H. & K. N. Rao**, *Analysis of Capacitive Effect and Life Estimation of Hydrodynamic Journal Bearings on Repeated Starts and Stops of a Machine Operating Under the Influence of Shaft Voltages*, pp. 641-645, Published online 25 Mar 2008.

INCREASING INDUCTION MOTORS EFFICIENCY BY REDUCING ELECTROMAGNETIC LOADS

Olivian **CHIVER**, Liviu **NEAMT**, Eleonora **POP**

Department of Electrical Electronic and Computers Engineering, North University Center, Technical University of Cluj Napoca

olivian.chiver@cunbm.utcluj.ro, liviu.neamt@cunbm.utcluj.ro, eleonora.pop@cunbm.utcluj.ro

Keywords: Induction, motor, characteristics, efficiency;

Abstract: *The efficiency of any device is a major problem today. The design and construction of high efficiency motors is strongly required from the viewpoint of reducing energy consumption and protecting the environment. This paper deal with the problem of improving efficiency by reducing electrical and magnetic loads of these motors. Using the finite elements method (FEM), the authors will study the influence of these changes on the parameters and characteristics of the initial motor.*

1. INTRODUCTION

Increasing the efficiency of the electrical motors is a continuing and topical problem which is a provocation for designers and manufacturers of electric machines.

But how can it be increased the efficiency of the electric motors? It is possible to improve efficiency by using new materials and technologies, proposing some new constructive solutions (even for conventional motors), or increasing the volume of used active materials. In case of the rotor cage induction motors, in the last twenty years, the active materials have suffered only minor improvements and new design solutions are almost inexistent.

According to [1] all low voltage (<1000 V) rotor cage induction motors, with 2- 6 poles and with rated power between 7.5 - 375 kW must fulfill the minimum conditions

imposed by IE-3 standard since 2015, and from 2017, these minimum conditions must be fulfilled of all above electrical motors but with power ranging from 0.75 kW.

Electrical motors which fulfill only IE-2 standard efficiency will be allowed only if they are driven by frequency converters.

According to IE-2 and IE-3 standards, the minimum efficiency in terms of the rated power for rotor cage induction motors with 2-6 poles is shown in Fig. 1.

These measures have been taken because about 70% of electricity consumed in the industrial sector is the energy converted into mechanical energy by electric motors [1].

As an order of magnitude, in 2005, the electrical motors have had 1067 TWh consumption which corresponds to 427 Mt CO₂ emissions.

It is estimated that in 2020, the energy consumption of electric motors to reach 1252 TWh, such as a small improvement in the efficiency can lead to very significant reductions in CO₂ emissions, and also to the protection of the environment.

The efficiency of an electric motor depends on the quality of the used materials and technology. The problem that occurs is due to the fact that the materials used in the construction of a rotor cage induction motor (electrical circuits, magnetic and insulating materials) have not really been improved in the recent years.

For this reason, the problem of efficiency increasing must be solved not by using new materials, but possibly using new technologies or new constructive solutions, high efficiency motors (with permanent magnets) instead of conventional motors (as induction motor), but mainly by reducing the motor loads (electrical and magnetic), which involves increasing the size at the same rated power. Increasing the size of a motor involves also the increase of the price per power unit, but this is less important than the fact that losses are reduced and in consequence the efficiency is higher.

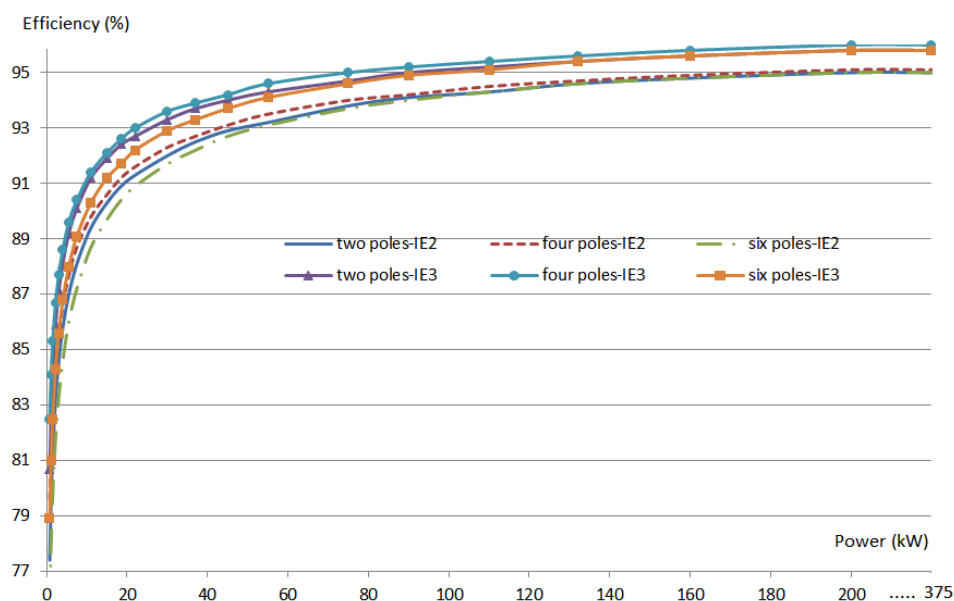


Fig. 1 - Minimum efficiency of rotor cage induction motors, according to IE-2 and IE-3

It is confirmed [2] that an electric motor consumes during its operating life, energy that is 100-200 times greater than its value, so it is more important that the motor be with higher efficiency than be cheaper. It is also important to mention that it is not enough to have a high efficiency motor; it is necessary that the electrical drive reach high efficiency, for this reason it is recommended to use controlled motors with frequency convertor that change proportionally the voltage as well.

Changing motor size on the same rated power implies the change of the motor parameters as inductances and windings resistance, and also the motor speed and torque. Some of these changes were analyzed in [3]. In addition, this paper calculates the resistive losses, considering the skin effect in the rotor.

The iron losses of the initial motor and of the motors with size increased will be analyzed comparatively.

The characteristics: torque-slip and current-slip will also be studied comparatively. Finite elements analysis will be used in order to determine these characteristics.

2. INDUCTION MOTOR EFFICIENCY

Like any other device, in case of squirrel cage induction motor, efficiency can be defined as the ratio of mechanical power output, P and electrical power input, P_1 ,

$$\eta = \frac{P}{P_1} \quad (1)$$

The difference between electrical power input and mechanical power output represents the total motor losses, P_t , and efficiency can be written as:

$$\eta = \frac{P}{P + P_t} \quad (2)$$

The total motor losses include: resistive losses in the motor windings, P_{Cu} , iron losses in the magnetic circuit, P_{Fe} , additional losses, P_{add} and friction and ventilation losses, P_{fv} ,

$$P_t = P_{Cu} + P_{Fe} + P_{add} + P_{fv} \quad (3)$$

Resistive losses are due to the current flowing in the motor windings; they are proportional to the square of the rms stator phase current, I_1 , and to the windings resistance R_1 and R_2' .

$$P_{Cu} \sim (R_1 + R_2') I_1^2 \quad (4)$$

R_1 is the stator phase resistance and R_2' is the rotor phase resistance referred to the stator.

Iron losses include hysteresis and eddy current losses.

Hysteresis losses depend on frequency, f , the peak magnetic flux density, B , mass of the magnetic circuit, m_{fe} , and a constant material, $1 \leq \alpha \leq 2$,

$$P_h \sim m_{fe} f B^\alpha \quad (5)$$

Eddy current losses are proportional to the same quantities but the exponents differ,

$$P_{ec} \sim m_{fe} f^2 B^2 \quad (6)$$

Experimental determination of additional or stray load losses is described in [4], and they depend on the rotor current, I_2 , which at his turn is determined in terms of the stator current, I_1 (for which additional losses are computed) and no load current, I_0 ,

$$P_{add} \sim I_2^2, I_2 = \sqrt{I_1^2 - I_0^2} \quad (7)$$

If additional losses are not determined experimentally, they can be obtained in terms of the input power.

Friction losses depend on the rotor diameter, rotor mass, inner diameter of the bearing and of course depend on the speed and the type of bearing. Ventilation losses depend on the ventilator efficiency for a given power.

In order to improve motor efficiency, losses must be reduced.

Resistive losses can be reduced because the current remains the same (power remains the same) only by reducing the windings resistance.

If all the initial motor dimensions are multiplied by a factor k , it can be demonstrated that the cross section of the new motor will be k^2 times higher and the length will be k times higher. The conductors will also have cross section k^2 times higher and the length will be approximatively k times higher. In conclusion, the new motor will have windings resistance k times lower and resistive losses will be k times lower as well.

Because the surface through which the magnetic flux closes increases k^2 times, and the polar flux remains unchanged (as the supply voltage remains unchanged), the magnetic flux density will be reduced k^2 times.

Mass of the magnetic circuit will be increased k^3 times. Hysteresis losses of the new motor, P_{hn} , will be, in terms of the hysteresis losses of the initial motor, P_h ,

$$P_{hn} \sim m_{fen} f B_n^\alpha = k^3 m_{fe} f \left(\frac{B}{k^2}\right)^\alpha = k^{3-2\alpha} P_h \quad (8)$$

The above relation shows that for $\alpha > 1.5$, hysteresis losses of the new motor are reduced.

Eddy current losses of the new motor are:

$$P_{ecn} \sim m_{fen} f^2 B_n^2 = k^3 m_{fe} f^2 \left(\frac{B}{k^2}\right)^2 = \frac{P_{ec}}{k} \quad (9)$$

Friction and ventilation losses of the new motor will increase slightly because the rotor mass and diameter will be larger. But because these losses are much lower than the iron and resistive losses, the total motor losses will be lower.

If only the motor diameters are multiplied with k , and the initial length is kept, windings resistance will decrease approximately k^2 times (because the length of the end windings will increase) and also the resistive losses. In this case, the new hysteresis losses are:

$$P_{hn} \sim m_{fen} f B_n^\alpha = k^2 m_{fe} f \left(\frac{B}{k}\right)^\alpha = k^{2-\alpha} P_h \quad (10)$$

Eddy current losses will be:

$$P_{ecn} \sim m_{fen} f^2 B_n^2 = k^2 m_{fe} f^2 \left(\frac{B}{k}\right)^2 = P_{ec} \quad (11)$$

If resistive losses are higher than iron losses, this solution needs to be analyzed.

As conclusion, increasing the size of a motor (at the same rated power), its efficiency increases as well.

The drawback is that the motor characteristics will also be changed.

In the following, the characteristics of the initial motor will be showed comparatively with the characteristics of the increased motors.

It is important to mention that in the design phase the losses require to be determined with high accuracy, this involving a high accuracy for the efficiency determination. Many papers deal with this topic, this paper refer to some of them [5]-[10].

3. CASE STUDY

This study was carried out using an electromagnetic field computation program based on the finite elements method (FEM).

Resistive losses in stator can be calculated analytically with high accuracy (for any current).

Rotor resistive losses can be calculated analytically also with high accuracy, but ignoring skin effect. If skin effect is to be taken in consideration, the analytically calculation of the resistive losses in rotor has a fairly low accuracy. In this case it is preferable that the rotor resistive losses to be calculated by FEM simulations.

Iron losses are calculated by the used program based on the field values, the magnetic material having the losses curve, at 60 Hz, showed in Fig. 2. Iron losses will be recalculated at 50 Hz.

The studied three-phase rotor cage induction motor has the following main data: rated power 0.37 kW, nominal phase voltage 230 V, stator core length 75 mm, inner and outer diameter of the stator 70 mm and 106.5 mm respectively, two pole-pairs, stator slots number 36 and number of turns in a coil 133, the numerical model being shown in Fig. 3.

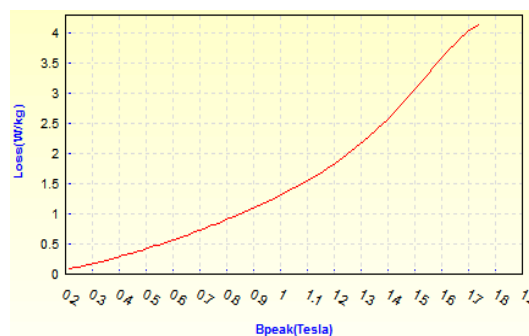


Fig. 2 - Losses curve at 60 Hz, for the magnetic material

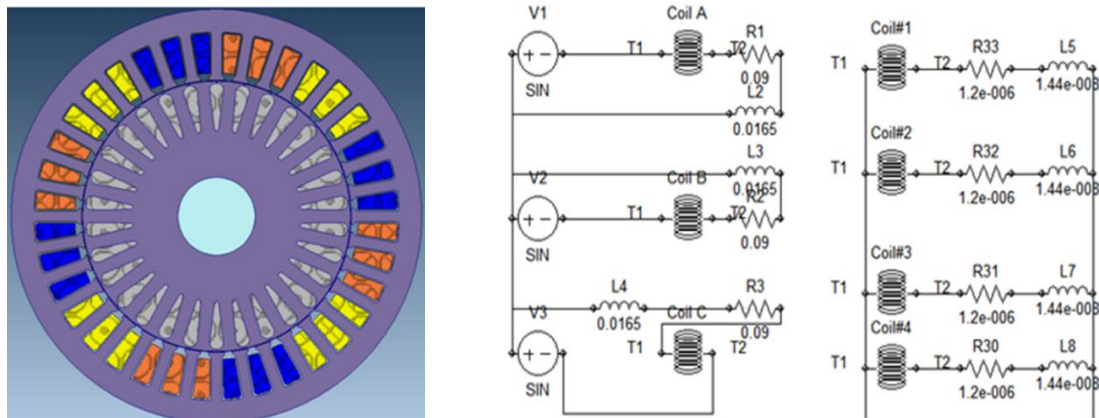


Fig. 3 - Studied motor: a) Numerical model; b) Motor windings

Based on the presented model (denoted initial), other two models were performed: one with size increased by $k = 1.5$ times (denoted with M1); the other where only the diameters were increased by $k = 1.5$ times, but the length being kept (denoted with M2).

Time-harmonic analysis was used, the frequency being in terms of the slip, $f = sf_n$. The procedure is described in [11].

Next, it will be presented comparatively (Fig. 3 - 10) the obtained results for the three models of rotor cage induction motors.

4. CONCLUSION

Noticing the manner of iron losses variation for the three motors, it can be concluded that, for slip values corresponding to the normal operation regime, the total iron losses are the lowest for motor M1 and the highest for motor M2. This is understandable because the hysteresis losses are much higher than the eddy current losses.

Regarding resistive losses must specify that they are determined according to the slip (load). But the motors do not have the same slip for the same load. For a fair comparison between resistive losses, the slip corresponding to the same nominal power must be determined for each motor. This will be done in a future work.

It can be also noticed that the size increasing involves the decrease of the starting torque. This is explained by the fact that the rotor resistance is reduced. The motor M2 has the highest maximum torque, followed by the initial motor and then by motor M1.

Motor M1 has the most convenient current-slip characteristic and then the initial and M2 motor.

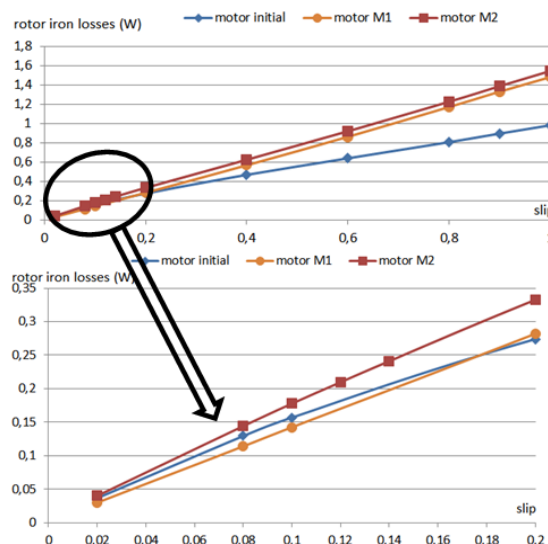


Fig. 3 - Rotor iron losses in terms of slip

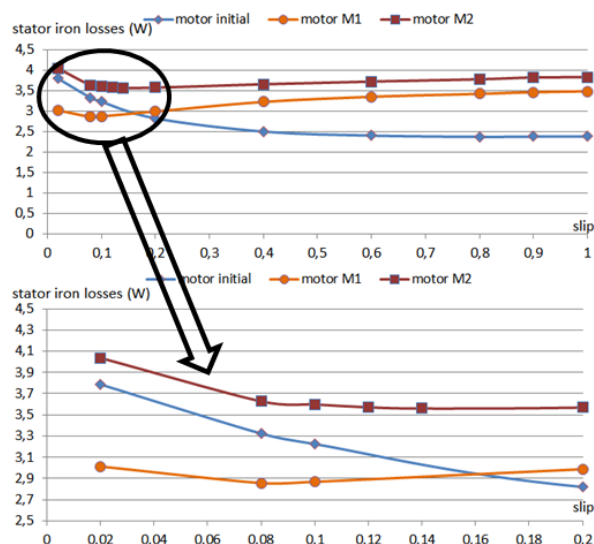


Fig. 4 - Stator iron losses in terms of slip

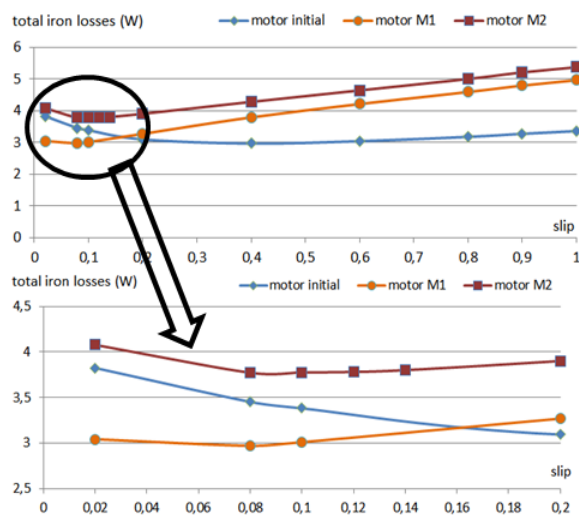


Fig. 5 - Total iron losses in terms of slip

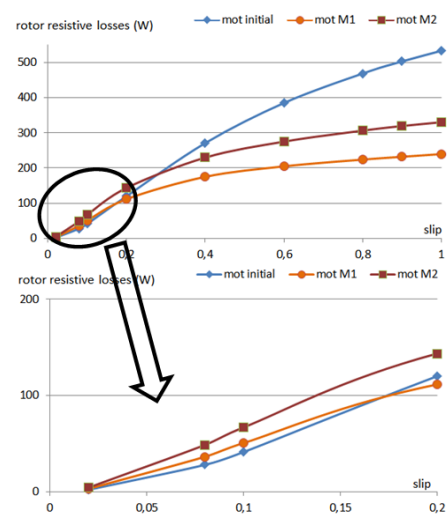


Fig. 6 - Rotor resistive losses

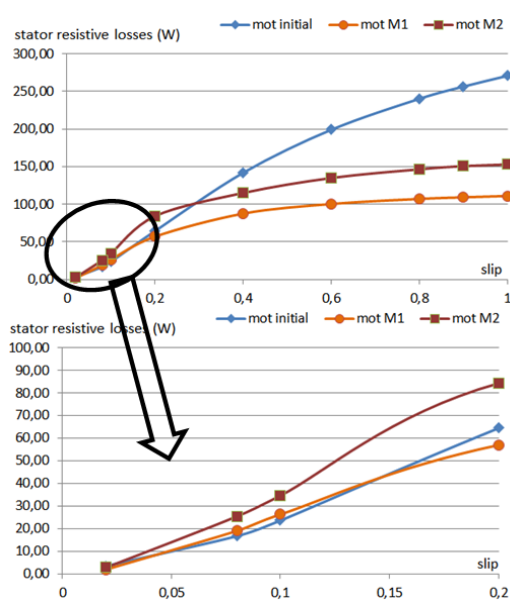


Fig. 7 - Stator resistive losses

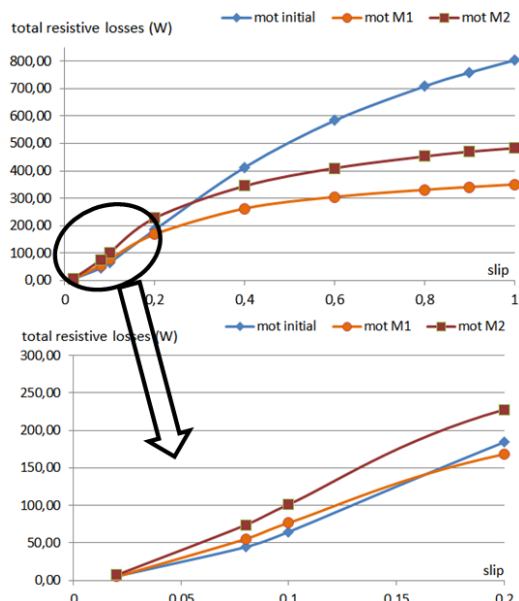


Fig. 8 - Total resistive losses

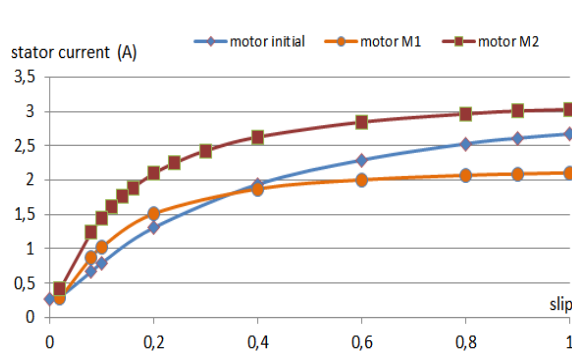


Fig. 9 - Current-slip curve (at rated voltage)

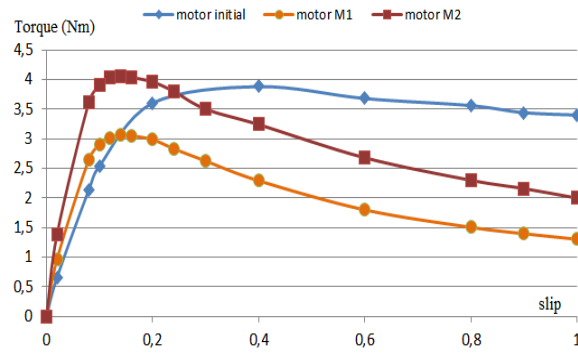


Fig. 10 - Torque-slip curve (at rated voltage)

REFERENCES

1. *** (2009), Commission Regulation (EC) No 640/2009 of 22 July 2009 implementing Directive 2005/32/EC of the European Parliament and of the Council with regard to ecodesign requirements for electric motors.
2. Ban D., Zharko D., and Mirchevski S., *The current state and trends of increasing the efficiency of electric machines*. Russian Electrical Engineering vol. 83 no. 1, p. 14-20, 2012.
3. Olivian CHIVER, Liviu NEAMT, Eleonora POP, *Study regarding solutions to increase the efficiency of induction motors*, Proceedings of the international conference of the carpathian euro-region's specialists in industrial systems - 10th edition – BAIA MARE, Sept., 11st – 13rd, 2014.
4. *** IEEE Std.112, (1991), *Standard test procedure for polyphase induction motors and generators*.
5. Auinger H., *Determination and designation of the efficiency of electrical machines*. Power Engineering Journal, February 1999, p. 15-23.
6. De Almeida Anibal T. and Ferreira Fernando, *Efficiency testing of electric induction motors*. ISR, Dep. Eng. Electrotecnica University of Coimbra, Polo II 3030 Coimbra, Portugal Retrieved on 02.08.2014 from ftp://ftp.unicauca.edu.co/Facultades/FIET/DEIC/Materias/Control%20de%20maquinas/bibliografia/estimacion%20parametros/Almeida_paper.pdf
7. Groza V., Pitis C D., Merabet A., Giurgiu V D., *Novel method of pre-determining induction machine parameters and energetic efficiency*. Proceedings of IEEE Electrical Power & Energy Conference (EPEC), Halifax, Canada, 21-23.08.2013.
8. Nakamura Kenji, Fujita Kentaro, and Ichinokura Osamu, *Magnetic-circuit-based iron loss estimation under square wave excitation with various duty ratios*. IEEE Trans. Magnetics, vol. 49, no.7, July 2013, p 3997-4000.
9. Reljic Dejan D., Matic Dragan Z., Jerkan Dejan G., Oros Djura V., Vasic Veran V., *The estimation of iron losses in a non-oriented electrical steel sheet based on the artificial neural network and the genetic algorithm approaches*. Proceedings of IEEE International Energy Conference (ENERGYCON), Dubrovnik, Croatia, 13-16.05.2014, p. 51-57.
10. Stermecki Andrej, Bíró Oszkár, Preis Kurt, Rainer Siegfried, Krischan Klaus, Ofner Georg, *Calculation of load-dependent equivalent circuit parameters of squirrel cage induction motors using*

time-harmonic FEM. Proceedings of the 2008 International Conference on Electrical Machines, Vilamoura, Portugal, 6-9.09.2008, p. 1736-1741.

11. Olivian Chiver, Liviu Neamt, Cristian Barz and Cristinel Costea, *Frequency domain numerical analysis of rotor cage induction motor*, Proceedings of the International Conference and Exposition on Electrical and Power Engineering, 16-18 October 2014, Iasi, Romania.

MANAGEMENT OF ELECTRICITY TO A COUNTY LIBRARY

Mircea **HORGOS**, Zoltan **ERDEI**, Cristian **BARZ**

Tehnical University of Cluj Napoca, North University of Baia Mare Centre,.

mircea.horgos@cunbm.utcluj.ro, zoltan.erdei@yahoo.com, cristian.barz@cunbm.utcluj.ro.

Keywords: Energy measurement, energy consumption, energy management

Abstract: *The effects that manifest themselves at the scale of the Organization, in which energy is consumed, are related to the influence of its cost in financial balance. The importance of energy cost depends on the area of activity of the company. There is, however, a high potential for energy saving in most sectors of economic activity and in most institutions. Energy conservation is often a "painless" reduction in operating expenses. This does not imply employment for employees, and the investments required are often reduced and have minimal risk.*

1. INTRODUCTION

In recent years it may find a constant increase in energy costs. Liberalization of energy prices will worsen and more than the increase in the near future. This price increase, particularly in motor fuels contributed to stimulating public interest in reducing consumption and efficient use of energy through the implementation of energy policies.

Energy savings management involves the development of a precise organizational structures within the society concerned, to conduct regularly a series of actions for the functioning of the well-defined with a higher energy efficiency of technological installations.

1.1. Power quality Problem

To ensure the quality of energy delivered at the point of consumption is not easy and there's no way that electricity that does not comply with the standards to be withdrawn from the food chain or refused by the consumer.

High-quality electricity-electricity available permanently (continuously) to the values of the parameters (frequency, RMS, sine shape, symmetry of three-phase system) within limits allowed by the rules. [5] Note that technical parameters are actually blood parameters, do not have the energy or power direct current.

Achieve the level of quality offered by the electricity suppliers cannot be obtained only under conditions ensuring technical and maintenance requirements at the level of the distributor, producer and transporter of electricity. In this way, monitoring quality indicators at the point of interface between carrier and distributor as well as providing the level of quality standard in these points are decisive in ensuring the level of quality offered by the supplier. Knowledge of quality indicators at the point of interface between manufacturer and carrier are of particular interest in assessing the level of quality of electric energy at the point of connection with distributors.

At the same time, the quality of electricity has a significant effect on the economic indicators of the transport network and is a defining parameter for evaluation of its performance.

To a large extent, disturbances that lead to diminishing the level of quality of electric power are determined by consumer activity (unbalance, flicker, harmonics, etc.). But production systems, transportation and distribution, thanks to specific requests occurring (lightning, wind, ice, damage deposits, etc.) may be the source of disturbance in the form of switches, Voltage dips, surges, and voltage variations and frequency. Also at overcoming the tape tension, permitted transmission network can be the source of voltage harmonics, so by downloading the corona as well as the operation of nonlinear characteristic on magnetic circuits.[1]

Power grid development must take into account to ensure the level of quality standard of electricity at the point of interface with the distribution network.

Knowledge of quality indicators, practical determination method, interpretation of the results of their monitoring, knowing the limits of disturbance, presents a particularly interest in securing energy as well as for decisions relating to measures to be taken in order to achieve the required quality level.

2. ENERGY POLICY OF THE INSTITUTION

Regardless of the size or type of organization, the common element of success is the commitment of the entire energy management organisations. [11]

A commitment of the organisation shall be effected by the allocation of staff and financial resources necessary to achieve continuous improvement in energy efficiency. To develop and implement their programme of energy management, the management of the institution must be:

- to establish a dedicated team energy management;
- to set up an energy policy.

Energy policy is the basic document for energy management success. This formalizes the support of senior management and articulates the Organization's commitment to energy efficiency for all employees, shareholders, the community and other stakeholders. [11]

One of the first tasks of the team designated for energy management within the institution will be drafting an energy policy to guide the process of energy management in the following stages.

3. PROCESSING AND ANALYSIS OF DATA

For this analysis the data obtained were processed on the invoices of electricity and natural gas for a period of 12 months, between October 2012 and September 2013. They also obtained data on the consumption of electricity and the Electrical Supply, S.C. Electrica Furnizare S.A. for the period 1 January 2013 to 31 October 2013.

Electricity consumption at the "Petre Dulfu" county library Baia Mare is measured by a single digital counter, which allowed production costs per one-hour intervals, on calendar days. In the period under review, the total consumption of electricity both active power and reactive power was 152.962 MWh, which represents a total cost of 82298.74 RON, at an average price of 0.55 euro/kWh active energy respectively 0.08 lei/ kVARh - reactive energy. Below are presented in graphical form, electricity consumption on different intervals.

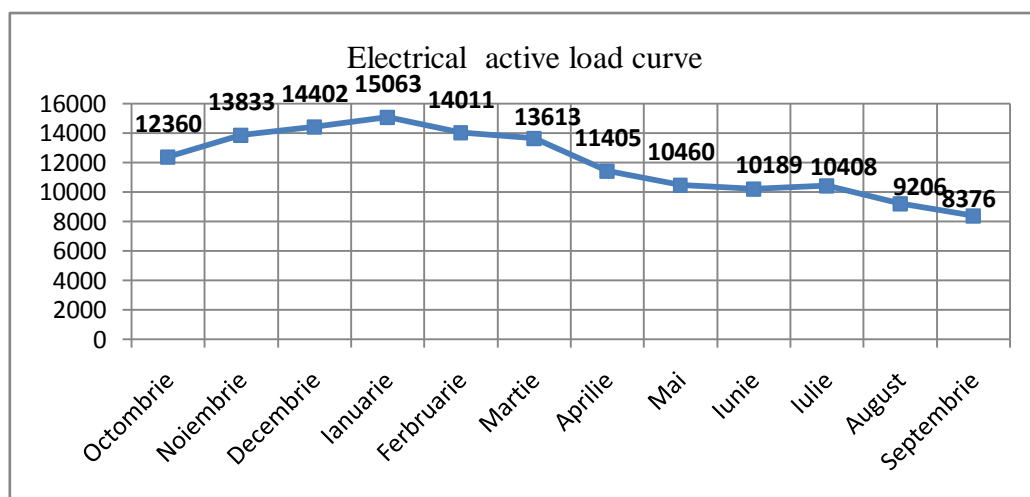


Fig. 1 Load curve-active energy [kWh]

Analyzing the graph with monthly consumption active energy [kWh] (fig. 1) can be noticed an increase in winter and a decrease in the hot season, from April to September

inclusive. This fluctuation of electricity consumption, according to the two periods, and can be explained by the fact that one of the main consumers of this institution, through specific activities, represent the lighting, a longer period of operation rises about 4 hours in cold season, also during summer Saturdays is non-working day and more than 70 % of its staff, schedule a part of summer vacation.

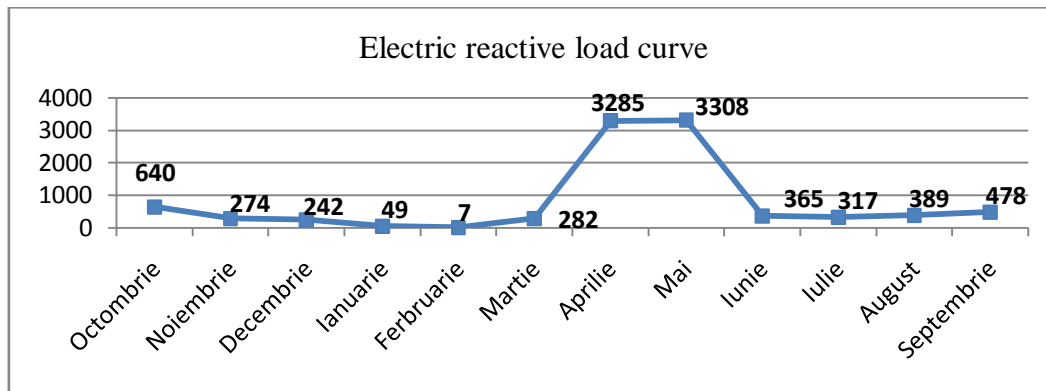


Fig. 2 Load curve-reactive energy [kVARh]

3.1. Energy intensity

The common parameter used to characterize the energy efficiency is energy intensity, defined as the ratio of resource consumption (energy) and the value of products (services) is achieved. In the case of public institutions, which are not productive units, energy consumption may be reported on the surface or the number of clerical staff.

In this case the relationship of energy intensity can be written in the form:

$$I = \frac{W}{S} \quad (1)$$

W – energy consumption [kWh];

S – the working surface [m^2]

In the case of energy intensity will be library:

$$I = 100.54 \text{ kWh/m}^2$$

or

$$I = 31.87 \text{ kBTU/sq.ft (to compare with the similar institution in the U.S.A.)}$$

To ascertaining the whereabouts of placed the library of energy efficiency it is necessary to compare the value of energy intensity with a similar institution. Energy audits in Romania is in its infancy, there is no data in this sector of activity, as a result will be used as a reference a public library in the United States of America.

The equivalent energy intensity in the United States is Energy Use Intensity (EUI) and is measured in kBTU/sq. ft. It should be noted that in the United States use two distinct values of the EUI Website: Energy Intensity, and the Source Energy Intensity.

Site Energy Intensity is the amount of energy (electricity and natural gas) consumption on one foot square (square foot) carpet surface, which is measured by counters located at the institution.

An analysis of load curve of reactive power consumption [kVARh] (Fig. 2) shows an average of about 400 kVARh, with a jump of over 8 times in April and may. In discussions with the administrator of the institution and with the electricity supplier has appeared that over that period there was a crash at the battery of capacitors, mounted in the library building, which has led to the emergence of anomalies in the network and the load graph tip.

An efficient management of energy consumption would have resulted in the failure to promptly remedy arising from the battery of capacitors.

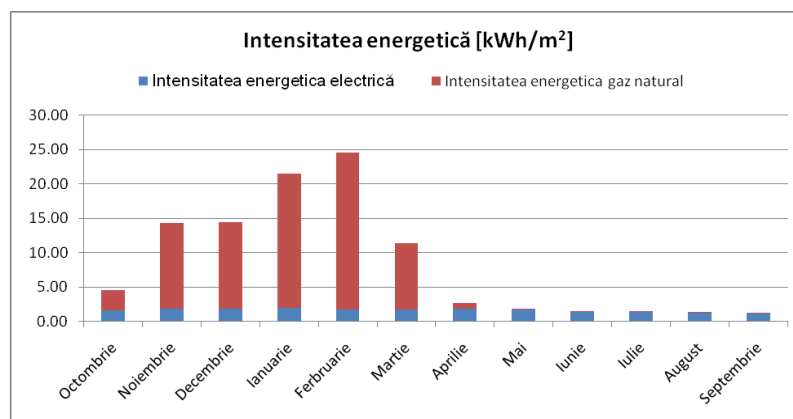


Fig. 3 Monthly energy intensity energy types

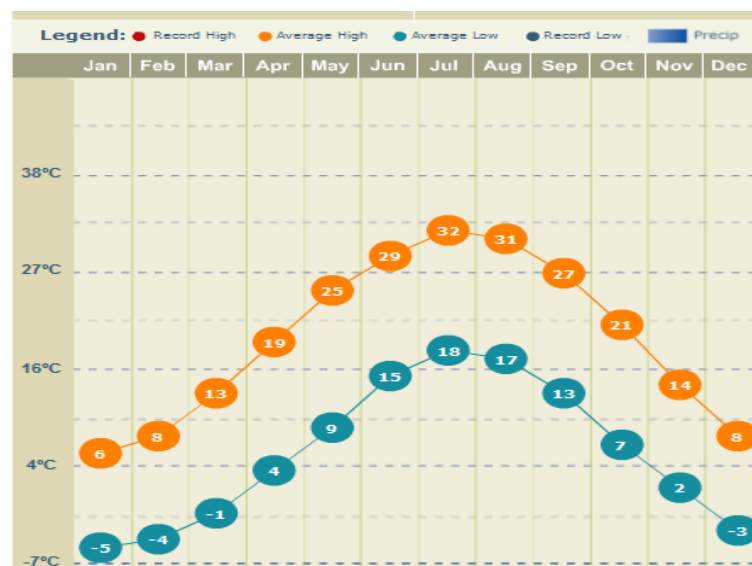


Fig. 4 Graph of average temperatures for Cherry Hill

Source energy intensity and take into account the energy consumption with production, transmission and distribution of electric energy, namely the energy lost to the storage and distribution of natural gas. The national average in the u.s. is: for every BTU of electricity

output used by the end user, it consumes an energy totaling 3.34 BTU for obtaining and transporting it. In the case of natural gas ratio is lower, 1.047, cost only reflected in its price, which is lower. In conclusion, the two may have the same value for energy intensity, but a different value to the source energy intensity. If you use different sources for the supply of electricity or natural gas.

For comparison was chosen at Cherry Hill public library in New Jersey, the main reasons being: public availability of energy intensity data (Library web site) [3], but the monthly average temperatures close to (less than higher) than those of Baia Mare.

3.2. Fluke 435 analyzer measurements

For this analysis were processed data obtained from measurements made with a spectrum analyzer, power quality Fluke 435 model, connected to the main board of the consumer for a period of about 24 hours, thus being covered a whole period of activity of the institution.

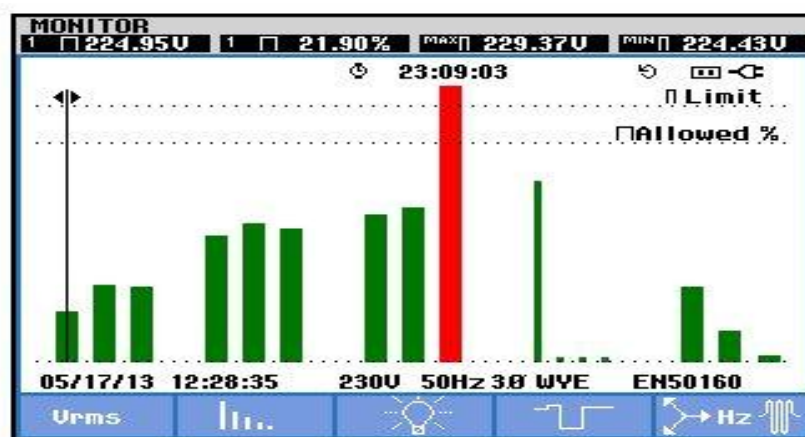


Fig.5 Monitoring power quality energy

During the monitoring of the quality of electric power has been an overrun of the index of severity of flicker, $P_{lt} = 1.3$

MONITOR EVENTS URMS				
START 05/16/13 13:19:32			EVENT 3 / 3	
			23:09:03	  
DATE	TIME	TYPE	LEVEL	DURATION
05/16/13	15:05:16:153	L2 DIP	203.5 U	0:00:00:280
05/17/13	03:10:47:125	L3 DIP	186.4 U	0:00:00:070
◀ 05/17/13	01:19:32:428	L3 Pit	1.3	0:00:00:000

Fig. 6 Monitor events

4. SETTING GOALS

Establish clear and measurable objectives is essential to understanding the desired results, the development of effective strategies and obtain financial gains. [5]

Establish clear objectives help in decision making and are daily base for monitoring and assessment of progress.

Communication and recording goals can motivate staff to support energy management efforts across the institution.

The purpose of the performance goals may require several levels of organization, and various time frames for the completion of specific objectives.

The library will be established both in the institutions and departments. In respect of installations and equipment which are the subject of the process efficiency, these are as follows:

- interior lighting (particularly in the area of reading rooms and stacks of books);
- exterior lighting;
- computing equipment;
- server room.

From the point of view of eşalonării in time of the objectives set for “Petre Dulfu” county library Baia Mare there are two basic categories:

- annual objectives which allow tracking and reporting progress regularly and throughout the conduct of the trial;
- long-term objectives, between 3-10 years.

After analyzing data, the management team of electricity established to achieve the following objectives:

- reduce energy consumption by 10 % over the next two years (2014-2016). In the current annual energy consumption is 784252 kWh, which would supposedly reduce 78.5 MWh by 2016;
- implementation in 2014 has a system for monitoring of electricity consumption, allowing for real-time observation of the occurrence of any failure and fix them in a timely manner; identification of possible sources of financing for the installation on the roof of the buildings of a photovoltaic solar system with a capacity of 10 KW.

5. MEASURES TO REDUCE THE ENERGY CONSUMPTION

Measures to reduce energy consumption (MRCE) are recommendations for public library, based on improvements in conditions at present. As a result of the analysis of data, the following measures have been identified to streamline the energy consumption:

Table 1

No. crt.	MRCE recommended. The investment recovery period 0-5 years
1	Replacement of 48 of filament lamps with compact fluorescent lamps (CFL)
2	Replacement of 16 monitors with CRT monitors LED equivalent
3	Replacement of halogen exterior floodlights 8 with metal iodide lamps
4	Optimisation of consumption in server room
5	Replace the 3 refrigerators (10 years old) with class A models
6	The change has the halogen spotlights with 202 spotlights LED
7	Replacement of 20 desktop computers with thin-client terminals
8	Installation in the reading rooms and stacks of 33 light presence sensor
9	Installation of taps thermostat for 30 radiators
	MRCE recommended. The use of energy from renewable sources
10	The installation of a photovoltaic system on the roof of the building 10 kW

Apart from the measures mentioned above, it is recommended to also:

- the installation of more efficient engines from the energetic point of view at the time that it is necessary to replace them, especially those of higher powers of 1 KW (elevators, circulating pumps of the heating, etc.);
- the repair or replacement of the gaskets with problems from windows;
- the use of a system for real-time monitoring of electricity consumption;
- achieve publicity of the measures implemented and results obtained, both among employees and in the local press.
- employee awareness regarding the efficient management of energy consumption through various campaigns.

5 CONCLUSIONS

Without a doubt, it is found, a must all the more acute for reducing energy consumption, especially in the conditions in which it is increasingly expensive and each kWh saved is a kWh won.

From the analysis made at the county library is found that is justified, in economic terms, the implementation of measures to rationalise energy consumption. Thus it appears that the majority of the proposed measures to save energy have recovery time under 2 years less *MRCE no. 2: replacement of 16 monitors with CRT monitors LED equivalent*, which pays off in about 3.6 years.

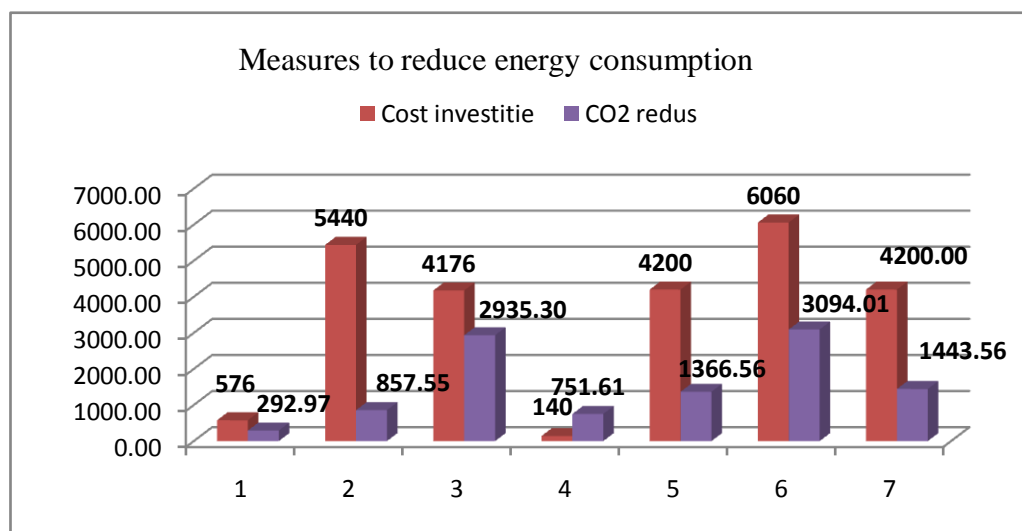


Fig. 7 The analysis of measures to reduce energy consumption

There is a preconception that pollution is caused especially heavy industry and traffic, but currently, an increasingly important role in polluting the atmosphere is getting electricity from conventional sources, especially that produced by burning fossil fuels. In conclusion, a reduction in energy consumption assumes the default mitigation a carbon emissions into the atmosphere.

If the county library, with investments of approximately \$ 25,000 would save over 34 MWh annually, avoiding the emission into the atmosphere over 10741 kg/year CO₂ emissions, equivalent to the amount generated by the 18 cars (Euro Euro 3), within a year.

At the same time carrying out a monitoring system to provide real-time information about electricity consumption, is one of the first steps that should be made for the efficient management of electricity consumption.

Whichever solution is chosen, the institution or solutions, but last but not least the local community will have won, by saving the public money and use the amounts obtained in this way, the purchase of books for the library users.

REFERENCES

1. Albert, H.; Golanov, C. *Probleme actuale privind monitorizarea calității energiei electrice în România*, Montenegro, Octombrie, 2004;
2. Capehart, Barney; Turner, L.; Kennedy, Wayne C.; William J., *Guide to energy management. Fifth Edition*, The Fairmont Press, 2006;
3. Cherry Hill Public Library, New Jersey - <http://www.chplnj.org> (accessed at 10.2013);
4. De Keulenaer, H. *Ghid de autoevaluare a calității energiei electrice*, European Copper Institute, 2002;
5. Dugan, R. C.; Santoso, S., *Electrical power systems quality*, McGraw-Hill, 2003;

6. **European Commission, Directorate-General for Energy** - <http://www.eu-energystar.org> (accessed at 10.2013);
7. **Fluke**. Monitorizare calitatea energiei - <http://www.fluke.com/fluke/ro/centru-solutii/calitatea-energiei> (accessed at 04.2014);
8. **Markiewicz, H.; Klajn, A.**, *Perturbații de tensiune. Standard EN 50160 - Caracteristicile tensiunii în rețelele de distribuție publice*, Wrocław University of Technology, 2004;
9. **Materiale electrice si corpuri de iluminat** - <http://www.materialeelectrice.ro> (accessed at 01.2014);
10. **TechSoup for Libraries** - <http://www.techsoupforlibraries.org> (accessed at 10.2013);
11. **Vuc, Gh.**, *Gestiunea energiei și managementul proiectelor energetice: note de curs pentru managerii energetici*, Orizonturi Universitare, Timișoara, 2004;

CONSIDERATIONS ABOUT SHIELDING MATERIALS IN LOW FREQUENCY MAGNETIC FIELDS

Liviu NEAMȚ, Olivian CHIVER, Eleonora POP

Technical University of Cluj-Napoca, North University Centre, Electrical, Electronic and Computer Engineering Department

liviu.neamt@cunbm.utcluj.ro, olivian.chiver@cunbm.utcluj.ro

Keywords: Magnetic fields, magnetic shielding, Finite Element Analysis;

Abstract: *This work analyses the magnetic shielding for a large variation interval of perturbative field in terms of both amplitude and frequency. Founded on Finite Element Analysis, shields constructed from different materials are studied. Conclusions about materials behavior for a given frequency but different amplitudes are focused on magnetic nonlinearity influence about shielding efficiency. In the final part of the research, there are presented some tips about an acceptable shielding attenuation realized with one single layer of material capable to deal with a large spectrum of frequencies and amplitude of magnetic interferences.*

1. INTRODUCTION

A magnetic shielding, suitable for the entire spectrum of electromagnetic field and also for any strength of external interference, is a very complicated task to be achieved in practice. For example, the biomagnetic signals ($\sim 10^{-13}$ T), must be processed in absence of other electromagnetic signals in medicine, while the Earth magnetic field range is between approximately 25,000 and 65,000 nT – static field, but also for harmonic, up to mT order values - fields generated by power distribution and bigger frequencies fields used in communications.

For higher magnetic flux densities and frequencies the shielding effect is altered, in magnetic materials cases, by saturation, [5] and induced magnetic fields.

Analytical solutions for attenuation factor, S ,

$$S = \frac{B_0}{B_i} \quad (1)$$

are available only for linear, isotropic and homogenous materials, and also for simple geometrical configurations. The proper tool to design, evaluate and optimize the magnetic shielding is the Finite Element Method, [1], [2], [7], [8].

Mostly shielded rooms are quasi-cubic enclosure, analyzed in first time as a spherical volume and only when this configuration was optimized in terms of inputted data, the real geometry is tacked into account, for last retouching, [6]. This paper analyzed the 2 m diameter spherical room, 2 mm thickness, t , of material in one layer shield, for different materials and different applied fields, fig. 1.

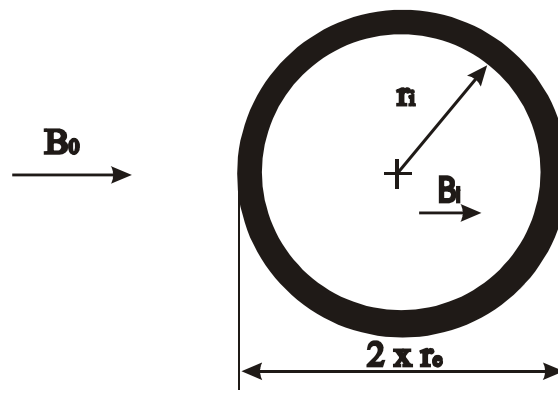


Fig. 1. Spherical one layer shield model

2. ANALYTICAL COMPUTATIONS

The chosen geometrical configuration is a very simple one, so if the material of the shield is considered linear, homogenous and isotropic there are available analytical relations.

For static fields, the attenuation factor, based on variable separations, [3], is:

$$S = 1 + \frac{2}{9} \left[1 - \left(\frac{r_i}{r_e} \right)^3 \right] \left(\frac{1}{\mu_r} + \mu_r - 2 \right) \quad (2)$$

where μ_r is the relative magnetic permeability of the shield magnetic material.

The maximum value of magnetic flux density in magnetic material is:

$$B_{Fe \max} = \frac{6 \cdot B_0 \cdot \mu_r \cdot \left(1 + \frac{M-1}{M+2} \right)}{1 + 2 \cdot \mu_r - 2 \cdot (\mu_r - 1) \cdot \left(\frac{r_i}{r_e} \right)^3} \quad (3)$$

with M being:

$$M = 2 \cdot \mu_r \cdot \frac{1 - \frac{2 \cdot (\mu_r - 1) \cdot \left(\frac{r_i}{r_e}\right)^3}{1 + 2 \cdot \mu_r}}{2 + \frac{2 \cdot (\mu_r - 1) \cdot \left(\frac{r_i}{r_e}\right)^3}{1 + 2 \cdot \mu_r}} \quad (4)$$

For variable magnetic fields, the attenuation factor can be computed as [3]:

$$S = \sqrt{\text{Re}^2(\underline{S}) + \text{Im}^2(\underline{S})} \quad (5)$$

where,

$$\underline{S} = \left(\frac{2}{3} + \frac{1}{3} \cdot \frac{r_i}{r_e} \right) \cdot \cosh(k \cdot t) + \frac{1}{3} \cdot \left(\frac{k \cdot r_i}{\mu_r} + \frac{2 \cdot \mu_r}{k \cdot r_e} \right) \cdot \sinh(k \cdot t) \quad (6)$$

and,

$$k^2 = j \cdot 2 \cdot \pi \cdot f \cdot \mu \cdot \sigma \quad (7)$$

where f is the frequency of the field, μ is the magnetic permeability and σ the conductivity, these two last variable referring to the shield material.

The limitations of analytical computation are not just the insufficient material properties countable, but also a lot of hypothesis that have to be considered to reduce the form of equations to a solvable ones. These hypothesis concern the aspect of induced current, the ways that magnetic field varies, etc.

Using Finite Element Method (FEM), the real behavior of a magnetic shield is more exactly described.

3. FNITIE ELEMENT ANALYSIS

Maxwell equations applied for magnetostatic, and for harmonic problem leads to equations (8), respectively (9). These equations are to be solved by FEM. All configurations are computed in David Meeker's Finite Element Method Magnetics, FEMM®, in 2D configurations, [4].

$$\nabla \times \left(\frac{1}{\mu(B)} \nabla \times \bar{A} \right) = 0 \quad (8)$$

$$\nabla \times \left(\frac{1}{\mu(B)} \nabla \times \bar{A} \right) = -\sigma \cdot \frac{\partial \bar{A}}{\partial t} + \bar{J}_{SRC} - \sigma \cdot \text{grad}V \quad (9)$$

where \bar{A} represents the magnetic vector potential and \bar{J}_{SRC} represents the applied currents sources.

The chosen geometrical configuration is a very simple one, so if the material of the shield is considered linear, homogenous and isotropic there are available analytical relations.

If the magnetic field oscillates at one fixed frequency, a phasor transformation for magnetic vector potential is available:

$$A = \text{Re}[a(\cos \omega t + j \cdot \sin \omega t)] = \text{Re}\left(a \cdot e^{j \cdot \omega t}\right) \quad (10)$$

FEMM® solves, for harmonic magnetic problems, the resulted equation, [4]:

$$\nabla \times \left(\frac{1}{\mu(B)} \nabla \times a \right) = -j \cdot \omega \cdot \sigma \cdot a + \underline{J}_{SRC} - \sigma \cdot \text{grad}V \quad (11)$$

with \underline{J}_{SRC} representing the phasor transform of the applied current sources and a being the complex amplitude of the phasor transformation, of A .

4. RESULTS

In [1], the influence of nonlinearity of the magnetic materials in shielding efficiency is treated for magnetostatic regime. In this work were considered the same materials, meaning: low carbon steel, “1010 Steel” with a constant relative magnetic permeability (linear consideration of material) $\mu_r = 902.6$ and a conductivity $\sigma = 5.8$ MS/m; cobalt iron “Hiperco 50” with $\mu_r = 3520$, $\sigma = 2.5$ MS/m and nickel alloys “Mu metal” with $\mu_r = 82910$, but supplemented with Cooper, $\mu_r = 1$, $\sigma = 58$ MS/m.

The magnetic characteristics of the ferromagnetic materials are illustrated in fig. 2.

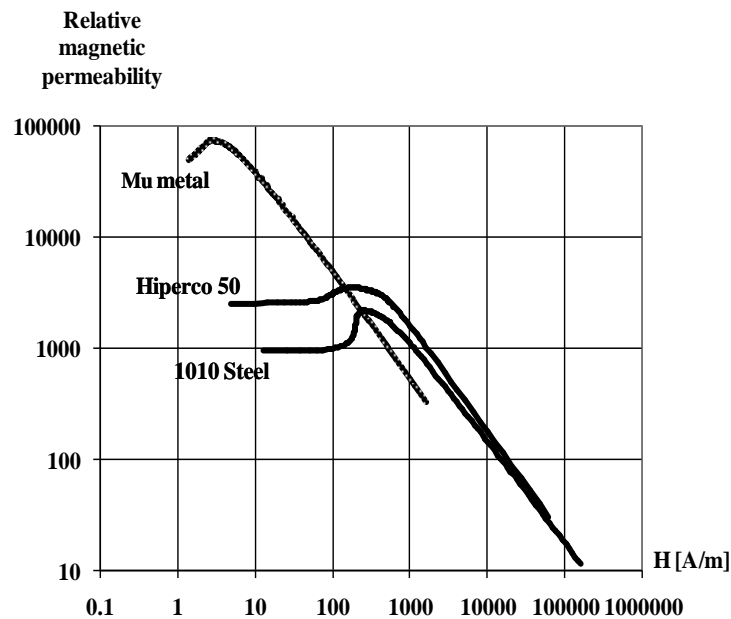


Fig. 2. Relative magnetic permeability of analyzed magnetic materials

Graphically presentation of equation (2) shows the attenuations of the studied shields, fig 1, in terms of exterior magnetic field density and having the relative magnetic permeability as a parameter, fig. 3, as straight lines, due to the linearity of materials. Of course the Cu shield has no effect on magnetostatic fields.

Considering the nonlinearity, the shield efficiency drops as the magnetic flux density increases, fig. 3.

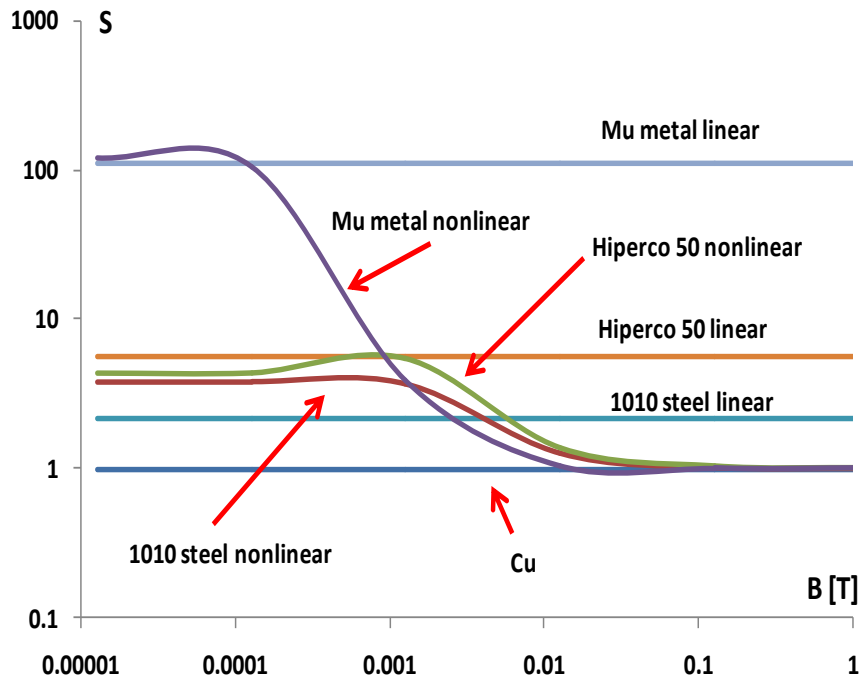


Fig. 3. The attenuation for magnetostatic interferences

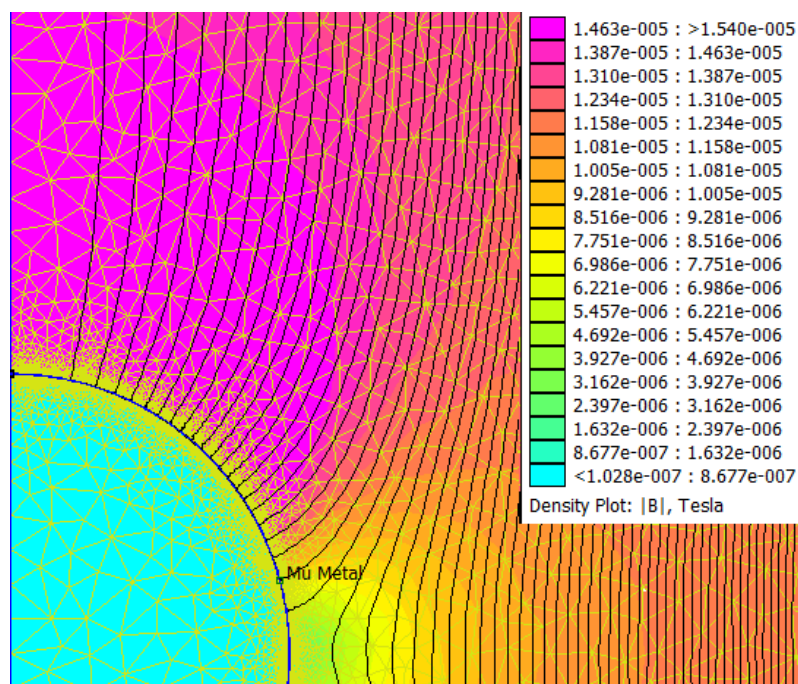


Fig. 4. Discretization and magnetic field spectrum for Mu metal, $B_0 = 1.26 \cdot 10^{-5} \text{ T}$, $f = 0 \text{ Hz}$

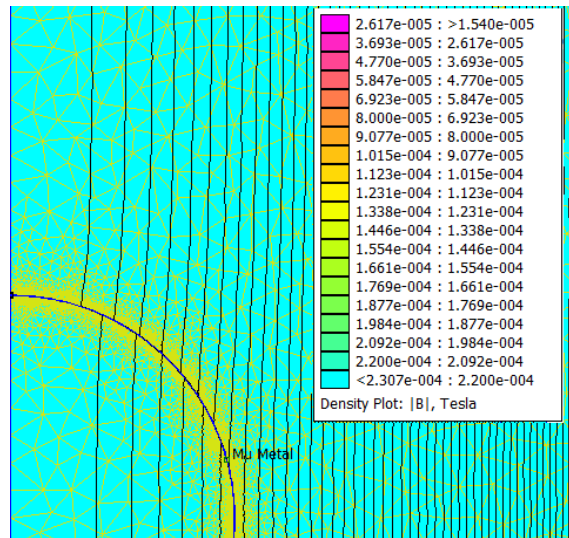


Fig. 5. Discretization and magnetic field spectrum for Mu metal, $B_0 = 0.0126 \text{ T}$, $f = 0 \text{ Hz}$

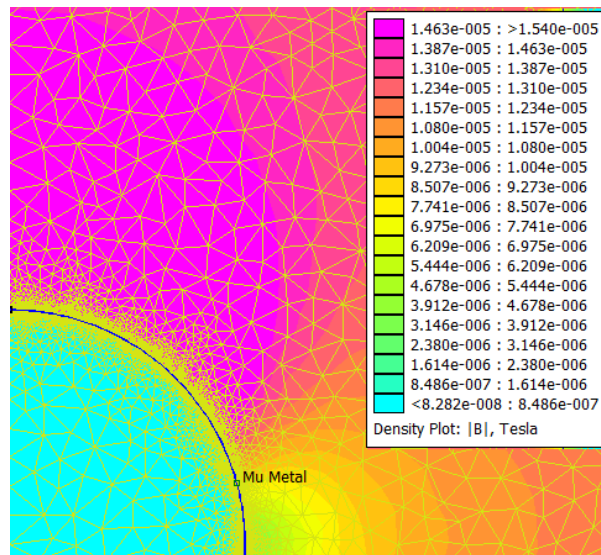


Fig. 6. Discretization and magnetic field values for Mu metal, $B_0 = 1.26 \cdot 10^{-5} \text{ T}$, $f = 50 \text{ Hz}$

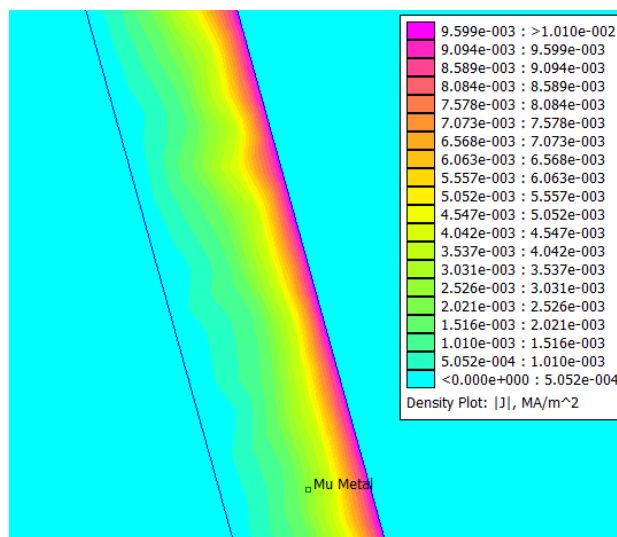


Fig. 7. Induced current in shield for Mu metal, $B_0 = 1.26 \cdot 10^{-5} \text{ T}$, $f = 50 \text{ Hz}$

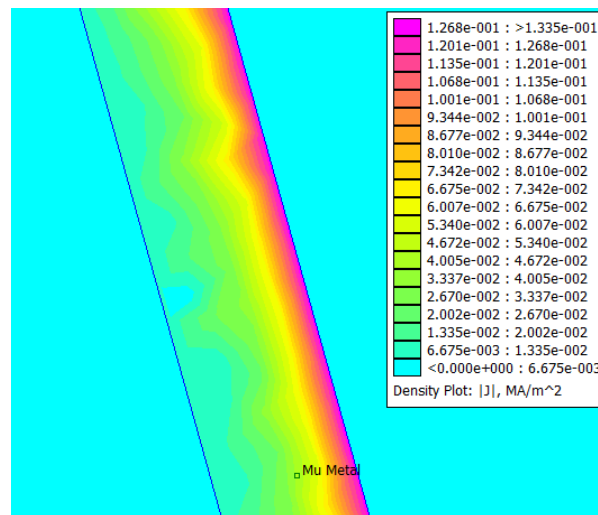


Fig. 8. Induced current in shield for Mu metal, $B_0 = 0.0126$ T, $f = 1$ kHz

The magnetic saturation is obviously in fig 5 compared to 4.

Also for variable magnetic field, the induced currents in shields are bigger, which leads to a bigger attenuation factor.

Again if we considered the materials as linear, the equation (5) conducts to results far from reality in case of magnetic materials at high values magnetic fields applied. The differences can be observed in fig. 9 and fig. 10-11.

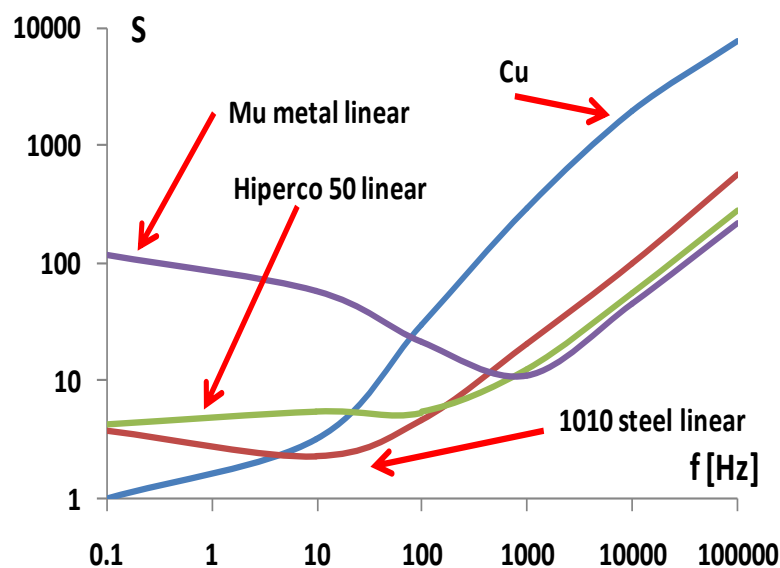


Fig. 9. The attenuation for variable magnetic interference - linear material shields

Magnetic materials, due to smaller conductivity than cooper, are inferior shielding materials for bigger frequencies. Cooper instead has no shielding effect for magnetostatic field.

Carefully observation of above mentioned figures shows that the importance of knowing the magnetic flux density value of the field that must be blocked to create

interferences inside the shielded room is very important.

As a general behavior, the better conductivity of the shield material goes to an improved shielding effect for high frequencies and the same proportionality is available between magnetostatic shielding and relative magnetic permeability, but carefully considers the saturation effect.

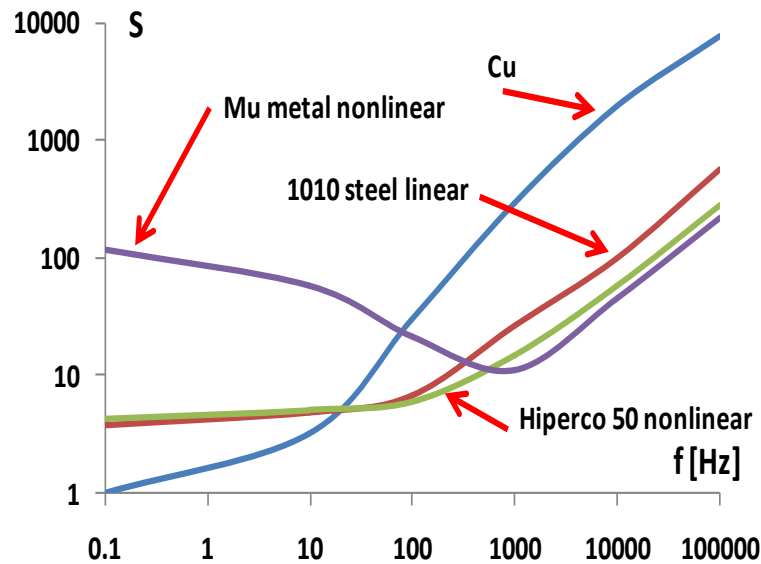


Fig. 10. The attenuation for variable magnetic interference-nonlinear material shields, $B_0 = 1.26 \cdot 10^{-5} T$

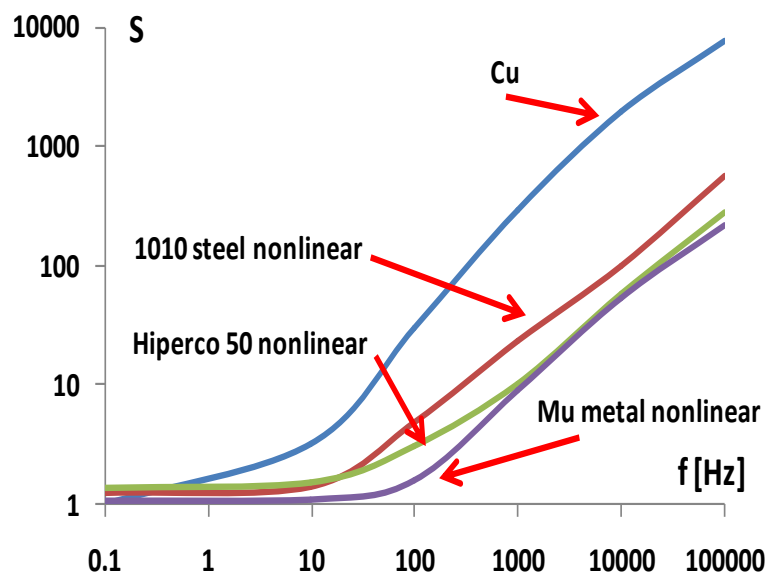


Fig. 11. The attenuation for variable magnetic interference - nonlinear material shields, $B_0 = 0.0126 T$

5. CONCLUSIONS

The most significant conclusion of this research is the importance of magnetic

properties of materials in shielding techniques. Because it is very unlikely to be able to predict the real incident magnetic field, generally, the designers must consider a very extend ranges of both magnetic flux density and frequency. If we are dealing with medical applications, for example, the geomagnetic field is a very important perturbation, so only a magnetic material shield must be taken into account.

For higher frequencies, only matters the electric conductivity and for lower frequencies, only matters the relative magnetic permeability. If it is possible to reduce the range of variation for applied magnetic field parameters, it is possible to choose an optimum material for shield from fig. 3, 10 and/or 11.

REFERENCES

1. **Becherini, G., Di Fraia, S., Schneider, M.; Ciolini, R.; Tellini, B.,** *Shielding of High Magnetic Fields*. 14th Symposium on Electromagnetic Launch Technology, pp.1-6, 2008.
2. **Cazacu, D., Castravete, S.,** *Efficiency evaluation via finite element method of 3D magnetostatic shields using different types of magnetic potentials*. 2012 IEEE 18th International Symposium for Design and Technology in Electronic Packaging (SIITME), pp.25-30, 2012.
3. **Hortopan, Gheorghe,** *Compatibilitate Electromagnetică*, Editura Tehnică, București, 2005, pp. 81-112, 2005.
4. **Meeker, David,** (2006). *Finite Element Method Magnetic*, Users Manual, <http://femm.info>, 2006.
5. **Neamț, Liviu, Neamț, Alina, Horgoș Mircea,** *The influence on the magnetic non-linearity on the magnetostatic shields design*. Rev. Roum. Sci. Techn. – Électrotechn. et Énerg., vol. 53, no. 2 bis, ISSN 0035-4066, pp. 129–135, 2008.
6. **Neamț Liviu, Neamț Alina, Chiver Olivian, Horgos Mircea,** *A flexible design method for double-shell magnetostatic shields*. Journal of Electrical and Electronics Engineering, volume 4 - nr. 1, ISSN 1844-6035.
7. **Yoshizawa, K., Noguchi, S., Igarashi, H.,** *Influence of Magnetic Property of Ferromagnetic Shield on High Field Magnet Analysis*. IEEE Transactions on Applied Superconductivity, vol. 21, no. 3, pp.2088-2091 2011.
8. **Takahashi, Y., Wakao, S., Kameari, A.,** *Large-scale and highly accurate magnetic field analysis of magnetic shield*. Journal of Applied Physics, vol. 99, no. 8, pp.08H904-08H904-3, 2006.
9. **Liviu NEAMT, Olivian CHIVER,** *The influences of different materials on low frequencies magnetic shielding*, Proceedings of the international conference of the carpathian euro-region's specialists in industrial systems - 10th edition – BAIA MARE, Sept., 11st – 13rd, 2014

REACTIVE POWER ON A POWER LINE CONNECTED FROM ONE END

Ioan BERINDE, Horia BĂLAN, Teodora OROS(POP)

Technical University of Cluj-Napoca

ioan_berinde@yahoo.com, horia.balan@eps.utcluj.ro, teodoraoros_87@yahoo.com

Keywords: line testing; reactive power;

Abstract: *Reactive power generated by power lines is one of the factors determining the level of voltage substations bars. Lines are often used for raising or lowering the voltage level. It is very important to monitor the level of voltage and reactive power supply lines. When the power consumption decreases, increases the voltage on transformer stations bars. As a preventive measure off lines that do not impair the operation of the national energy system(SEN). Disconnecting lines produce a decrease in the level of voltage.*

1. INTRODUCTION.

The development of electric power facilities during time had several stages, from energy supplying of each electric power consumer till organizing the grid elements in an electric power system, following the technical development of the equipments and with a high level of reliability and economic efficiency [1].

The electric power system comprises the producing and distribution facilities for the electrical energy on a certain territory [1].

The electric lines from the power grid are air-isolated. The major benefit of this is that they are cheaper comparing with the electrical cables but they will certainly have a reduced exploit being subject to direct weathering [1].

During the analyses of the operation mode of an electric grid we shall build the equivalent circuit of that grid, which results from interconnecting the equivalent wiring

diagrams of each system element. Thus we shall calculate the electrical parameters for the grid elements in two cases: for steady state and for electric fault [2].

The computing of the electrical parameters of the power grid it means knowing some factory data or experimental data obtained for each grid element [2].

The electric grid is modeled using equivalent circuits which are connected accordingly with the real situation from the ground. The equivalent circuits of the transmission and distribution grid usually consists of nonlinear passive elements, series or shunt connected. The electrical parameters are (fig.1) R – resistance, X – reactance, B – susceptance, G – conductance[1]

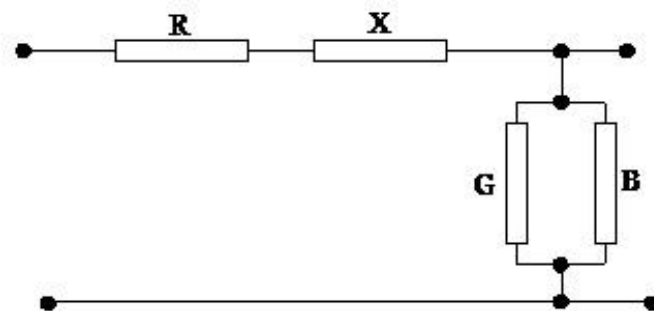


Fig. 1 – Equivalent schematic of the installations for transport and distribution

1.1 The electrical parameters of the overhead power lines

The overhead power lines are three-phase elements of the transmission and distribution grid which sometimes are protected against thunder stroke with a special conductor[1].

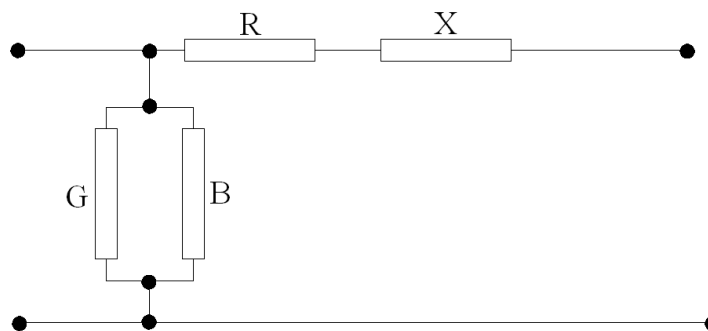


Fig. 2 – Equivalent of a Schematic overhead power lines

The equivalent circuit for an overhead power line consists of the series parameters resistance R and $X = \omega L$ wich together makes the series impedance $Z = R + jX$, the shunt parameters conductance G and susceptance $B = \omega C$, wich together makes the shunt admittance $Y = G + jB$, [1].

If the three-phase currents wich flows in the power line are symmetrical and balanced than the addition of these current makes zero so they have no impact on the power line electrical parameters[3].

For the zero phase-sequence currents which are flowing through the ground, the single-phase loops connecting the line and the ground provides the path for the return of their. In the zero phase-sequence state the grounding system turn path influences the power line electrical parameters[3].

1.1.1 The Power Line Resistance

The resistance of the power line is the active series electrical parameter which represents the series active power losses into the real power line.[1]

For the direct current:

$$R = \rho * \frac{l}{S} [\Omega] \quad (1)$$

In which: ρ – is the resistivity of the electrical conductor, in $\Omega mm^2 / m$

l – is the electrical conductor's length, in m

S – is the conductor's cross-section in mm^2

For the alternating current:

$$R = \frac{\Delta P}{I^2} [\Omega] \quad (2)$$

In which: ΔP are the series active power losses

1.1.2 The Power Line Reactance

The inductive reactance for a single phase circuit is:[1]

$$X = \omega L = 2\pi f L [\Omega] \quad (3)$$

In which: L is the phase inductance in H , and f is the a.c. current frequency in Hz .

The inductance is given by the total magnetic flux through a surface surrounded by a loop divided by the electrical current flowing through that loop.

$$L = \frac{\Phi_t}{i} [H] \quad (4)$$

1.1.3 The Power Line susceptance capacitive

Conductors of power lines form a capacitor, with the metal conductors and earth reinforcement. Thus, if a three-phase line without protective conductor are six capacitors, three between line and earth conductors with capacity C_{10}, C_{20}, C_{30} , and three between pairs of capacitors, with partial capacity C_{12}, C_{23}, C_{31} (fig.3)[1]

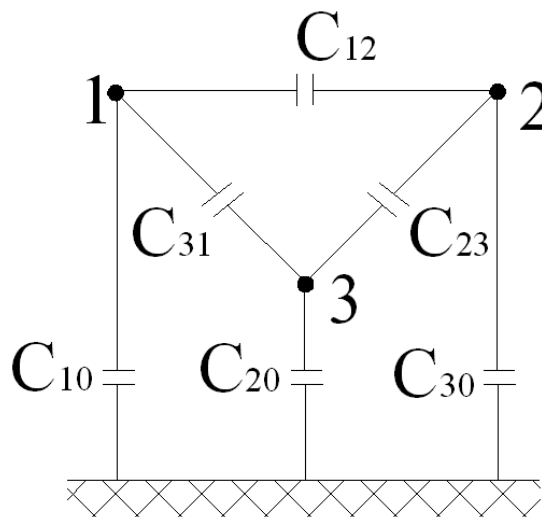


Fig.3 – The Power Line partial capacity

The capacity of a parallel earth conductor is defined by the relation (5):

$$C = \frac{q}{V} [\mu F] \quad (5)$$

1.1.4 The Power Line conductance

Transverse conductance parameter of the scheme is equivalent to a corresponding power lines cross the active power losses [1].

Overhead electrical lines these losses are due to imperfection of insulation and corona phenomenon. [1] The conductance of an airline per unit length of the line (1km) is determined by the relation (6):

$$G_0 = \frac{\Delta P_{iz} + \Delta P_c}{U_n^2} * 10^{-3} [S / km] \quad (6)$$

In witch: ΔP_{iz} și ΔP_c three phase power losses are due to imperfection of insulation that corona phenomenon, in kW/km, and U_n is the nominal voltage of the grid [1].

Due to the imperfection of cable insulation at points of attachment to a current leakage occurs posts by insulation to earth. They are more intense as the weather conditions are adverse (fog, rain, etc.) [4, 7]

1.2 Presentation power transmission line model SEL-1/EV

In order to study the reactive power flow we use power transmission line mod. SEL 1-/EV manufacturing Elettronica Veneta Italy (fig. 4).[5]

Two high-voltage power transmission lines with the possibility of varying their parameters are reproduced in this equipment. This simulator enables to learn and test the characteristics and the management of high-voltage mains systems on components of reduced

scale. The various electric devices installed, partially connected with each other and with safety terminals, start working with very simple and fast operations offering the possibility of modifying parameters and circuits at operators' will.[5,6,8]

The frontal panel is made of aluminum alloy, the power transmission lines are represented with international electric symbols; using unified educational terminals and safety jumpers with a high degree of protection against accidental contacts, will enable to carry out series / parallel connections. Acting some lever switches will change the electrical parameters (resistance, inductance and capacitance) according to different sections and lengths of the line. Voltage is signaled by warning lights, whereas the protection against overloads and/or short circuits is carried out by fast-blow fuses. [5,6,8]

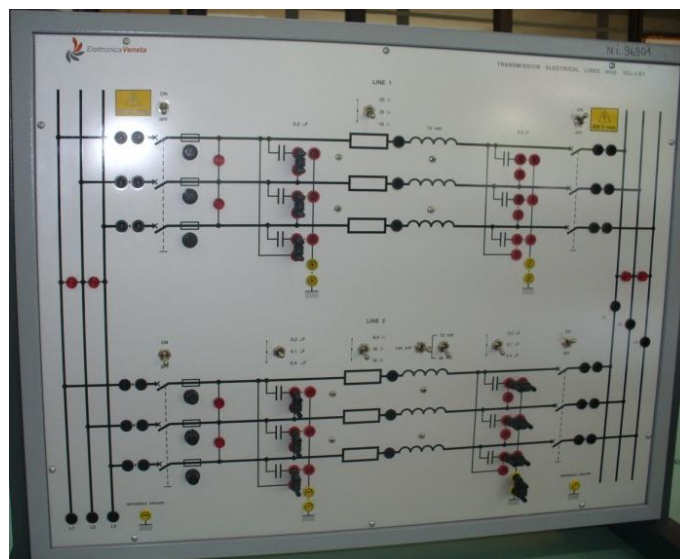


Fig.4 Power Transmission line mod SEL-1/EV- Front view

1.2.1 Technical characteristics

Line 1[5]

- | | |
|--|-----------------------|
| ➤ Modifiable parameter: | Section |
| ➤ Model of line used: | P I |
| ➤ Simulated voltage:120 kV(working U 3x400Vmax.) | |
| ➤ Simulated power: | P 10 - 15 - 20 MVA |
| ➤ Working current: | 1 A |
| ➤ Equivalent resistance: | 18 - 25 - 35 Ω |
| ➤ Equivalent inductance: | 72 mH |
| ➤ Equivalent distributed capacitance: | 2 x 0.2 μ F |
| ➤ Breakers at the beginning and at the end of the line | |
| ➤ Protection fuses | 1A |

Line 2 [5]

- | | |
|--|------------------------|
| ➤ Modifiable parameter: | Section |
| ➤ Model of line used: | P I |
| ➤ Simulated voltage:120 kV(working U 3x400Vmax.) | |
| ➤ Simulated power: | P 20 MVA |
| ➤ Working current: | 1 A |
| ➤ Equivalent resistance: | 8.9 - 25 - 35 Ω |
| ➤ Equivalent inductance: | 144-72-36 mH |
| ➤ Equivalent distributed capacitance:2 x 0.1-0.2-0.4 μ F | |
| ➤ Breakers at the beginning and at the end of the line | |
| ➤ Protection fuses | 1A |

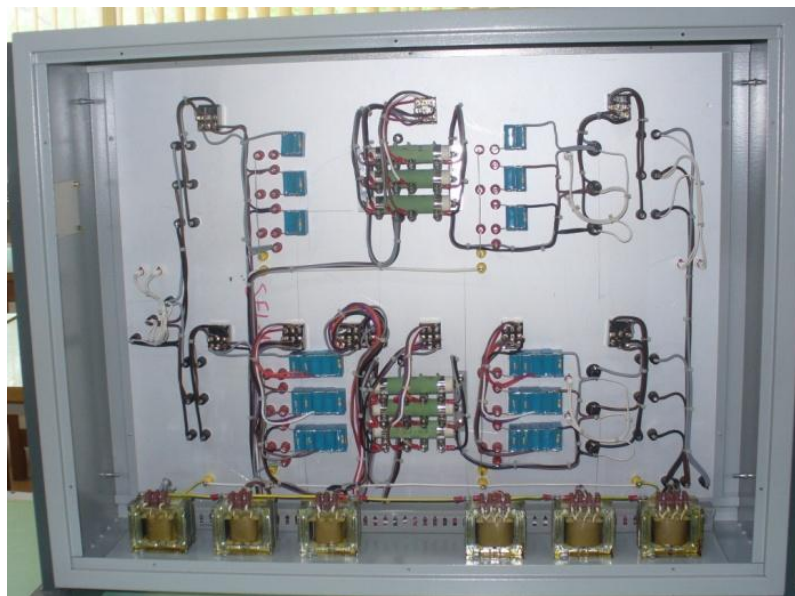


Fig.5 Power Transmission line mod SEL-1/EV- Connect components

1.2.2 Using the simulator

— Generally the power transmission lines reproduced in the simulator are powered on the left side of the schematic diagram so that the protection fuses are located at the origin of the line [5].

— The busway (vertical lines of the left side) is powered through the terminals indicated by L1 - L2- L3; the warning lights indicate the availability of mains voltage[5].

— The LINE 1 and/or the LINE 2 will be shunted from the left busway, through jumpers or leads with plugs. The lever switches available at the origin of each line enable to cut them out of the starting busway . Each line is also protected from overcurrents (overload and short circuit) with fast-blow fuses, and provided with warning lights for indicating the availability of mains voltage, at its origin[5].

— The right busway is connected at the end of the lines (right side) still through jumpers or leads with plugs; the transferred energy can be drawn from this busway. The lever switches available at the end of each line enable to cut them out of the destination busway[5].

1.2.3 Configuration and typical use of a line

- Remove all the jumpers of the LINE 2 not considered.
- Connect the jumpers at the origin and at the end of the LINE 1.
- Turn the breakers at the origin and at the end of the LINE 1, to OFF.
- Connect the jumpers with the left capacitors, only in the LINE 1, to reproduce the capacitance between active conductors.
- Connect the jumpers with the right capacitors, only in the LINE 1, to reproduce the capacitance between the active conductors and the ground.
- Adjust the position of the selector Resistance LINE 1 at the desired value.
- Connect with the three-phase power supply, and power (the allowed voltage value ranges from 0 to 400 V, and only if this value is around at half range, the warning lights available on the left busway will be on).
 - Turn the breakers at the origin and at the end of the LINE 1, to ON, in sequence; now the destination busway is energized and the voltage will be indicated by respective warning lights.

2. MEASUREMENTS AND DISCUSSIONS

2.1. Studying the operation of a power transmission line in no-load conditions (no-load current of the transmission line).

To perform the measurements we will need:

- Simulator of electric lines mod. SEL-1/EV
- Variable three-phase power supply mod. AMT-3/EV, in option threephase line generated by the generator control board mod. GCB-1/EV, or a fixed three-phase line 3 x 380 V
- Three-phase transformer mod. P 14A/EV
- Set of leads/jumpers for electrical connections
- 2 electromagnetic voltmeters with range of 250 - 500 Vac
- 1 electromagnetic ammeter with range of 100 mAac
- 1 electromagnetic wattmeter with low power factor 1-2 A / 240-480 V
- The instruments of the generator control boards mod. GCB-1/EV or two digital instruments for measuring the parameters of electric energy in three- phase systems mod. AZ-VIP, can be used as alternative.

Preparing the exercise:

— Considering the transmission LINE 1 with the following constants: Resistance = 25 Ω ; Capacitance = 0.2 μF ; Inductance = 0.072 H; Length = 50 km; Section = 35 mm² – conductor of copper.

— Remove all the jumpers of the LINE 2 not considered.

— Turn the breakers at the origin and at the end of the LINE 1, to OFF.

— Connect the measuring instruments between the left busway and the terminals at the beginning of the LINE 1.

— Connect the measuring instruments between the end terminals of the LINE 1 and the right busway.

— Connect the jumpers with the set of left capacitors, only in the LINE 1, to reproduce the capacitance between active conductors (called CL). These capacitors can be connected either in star or delta configuration. The delta connection will ensure stronger capacitive currents.

— Connect the jumpers with the set of right capacitors, only in the LINE 1, to reproduce the capacitance between the active conductors and the ground (called CE); connect also the jumper that grounds the star centre of the capacitors. In this case the only star connection can be carried out because each line conductor generates a capacitance to the ground.

— Adjust the position of the selector Resistance LINE 1 at the value of 25 Ω .

— Connect with the variable three-phase power supply by inserting the three-phase insulation transformer.

The reference electric diagram, the connections and configuration of the line are respectively shown in the figure 6.

— Enable and adjust the voltage of the power supply at 380 V. The warning lights of the left busway will be on. Turn the breaker at the origin of the LINE 1, to ON.

— All the parameters of the starting energy can be measured with the digital instrument available at the origin of the line.

— Turn the breaker at the end of the LINE 1, to ON.

— Read the electric quantities on the measuring instruments and write them down in the following table. Compare the reactive power measured on the line to that calculated with the following formulae:

$$Q_L = \Omega * C_L * U_1^2 = 2 * \pi * 50 * 0,2 * 10^{-6} * 380^2 = 9\text{VAR} \quad (7)$$

$$Q_E = \Omega * C_E * U_0^2 = 2 * \pi * 50 * 0,2 * 10^{-6} * 220^2 = 3\text{VAR} \quad (8)$$

Q_L - reactive power due to the capacitance between two active conductors;

Q_E - reactive power due to the capacitance between an active conductor and the ground.

Q_L and Q_E resulting from the formulae indicated above are calculated for only one phase. The total reactive power of the three-phase system will result from the sum of the powers of both the three line capacitors and the three capacitors to the ground.

Total reactive power of the transmission line:

$$Q_{TOT} = 3 * Q_L + 3 * Q_E = 36VAR \quad (9)$$

The sign – (minus) indicates that the reactive power is of capacitive type

2.1.1 Reactive power calculation as a function of variations in voltage.

$$Q_L = \Omega * C_L * U_1^2 = 2 * \pi * 50 * 0,2 * 10^{-6} * 400^2 = 10VAR \quad (10)$$

$$Q_E = \Omega * C_E * U_0^2 = 2 * \pi * 50 * 0,2 * 10^{-6} * 220^2 = 3VAR \quad (11)$$

$$Q_{TOT} = 3 * Q_L + 3 * Q_E = 39VAR \quad (12)$$

$$Q_L = \Omega * C_L * U_1^2 = 2 * \pi * 50 * 0,2 * 10^{-6} * 390^2 = 9,55VAR \quad (13)$$

$$Q_E = \Omega * C_E * U_0^2 = 2 * \pi * 50 * 0,2 * 10^{-6} * 220^2 = 3VAR \quad (14)$$

$$Q_{TOT} = 3 * Q_L + 3 * Q_E = 37,66VAR \quad (15)$$

$$Q_L = \Omega * C_L * U_1^2 = 2 * \pi * 50 * 0,2 * 10^{-6} * 380^2 = 9VAR \quad (16)$$

$$Q_E = \Omega * C_E * U_0^2 = 2 * \pi * 50 * 0,2 * 10^{-6} * 220^2 = 3VAR \quad (17)$$

$$Q_{TOT} = 3 * Q_L + 3 * Q_E = 36VAR \quad (18)$$

$$Q_L = \Omega * C_L * U_1^2 = 2 * \pi * 50 * 0,2 * 10^{-6} * 370^2 = 8,56VAR \quad (19)$$

$$Q_E = \Omega * C_E * U_0^2 = 2 * \pi * 50 * 0,2 * 10^{-6} * 220^2 = 3VAR \quad (20)$$

$$Q_{TOT} = 3 * Q_L + 3 * Q_E = 34,7VAR \quad (21)$$

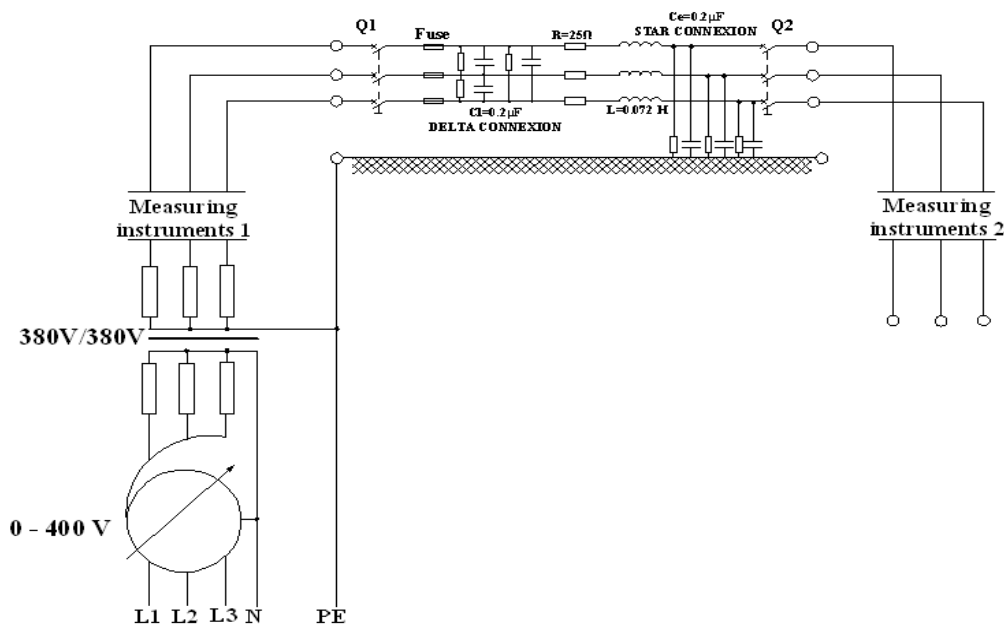


Fig.6 Power transmission line in no-load condition. Reference electric diagram

$$Q_L = \Omega * C_L * U_1^2 = 2 * \pi * 50 * 0,2 * 10^{-6} * 360^2 = 8,14VAR \quad (22)$$

$$Q_E = \Omega * C_E * U_0^2 = 2 * \pi * 50 * 0,2 * 10^{-6} * 220^2 = 3VAR \quad (23)$$

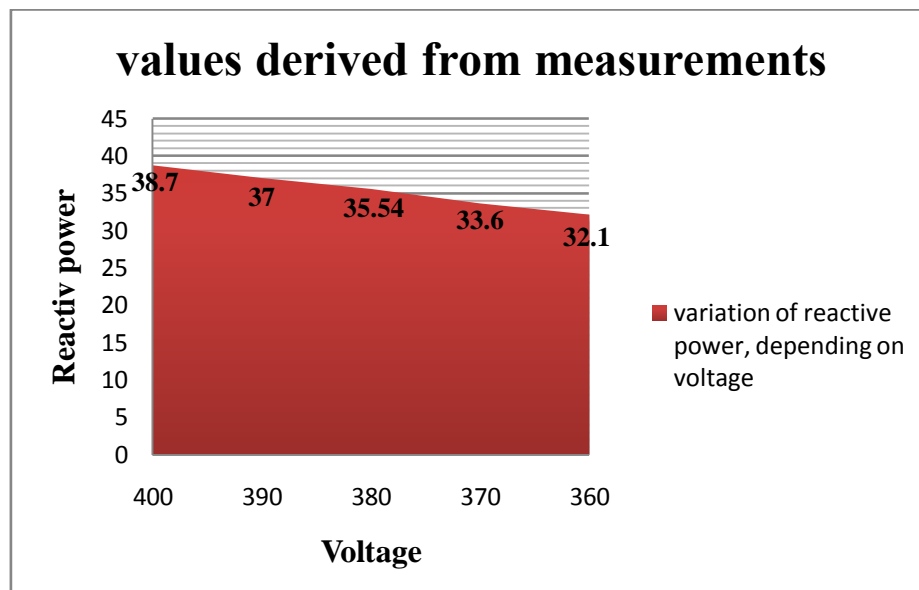
$$Q_{TOT} = 3 * Q_L + 3 * Q_E = 33,42VAR \quad (24)$$

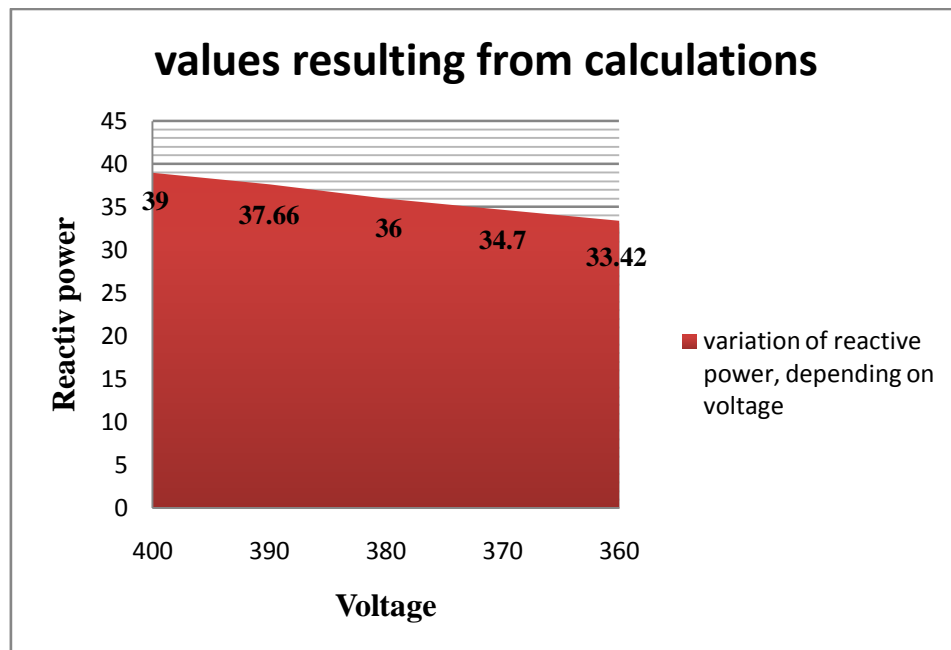
Table 1. The value measurements carried out on the basis of voltage variation

Interlinked voltage measured at the rigin of the line U1 (V)	Line current measured at the origin of the line I1 (A)	Active power measured at the origin of the line P1 (W)	Interlinked voltage measured at the end of the line U2 (V)	Reactive power measured at the origin of the line Q1 (Var)
400V	0,056A	0W	400V	-38,7Var
390V	0,055A	0W	390V	-37Var
380V	0,054A	0W	380V	-35,54Var
370V	0,052A	0W	370V	-33,6Var
360V	0,051	0W	360V	-32,1Var

Table 2. reactive power and current results of calculations

Voltage U1[V]	Current I [A]	Reactive power Q1 (Var)
400V	0,057A	39Var
390V	0,056A	37,66Var
380V	0,055A	36Var
370V	0,054A	34,7Var
360V	0,053A	33,42Var





2.2. Studying the operation of a transmission line in no-load conditions with increased capacitance (no-load current of the transmission line)

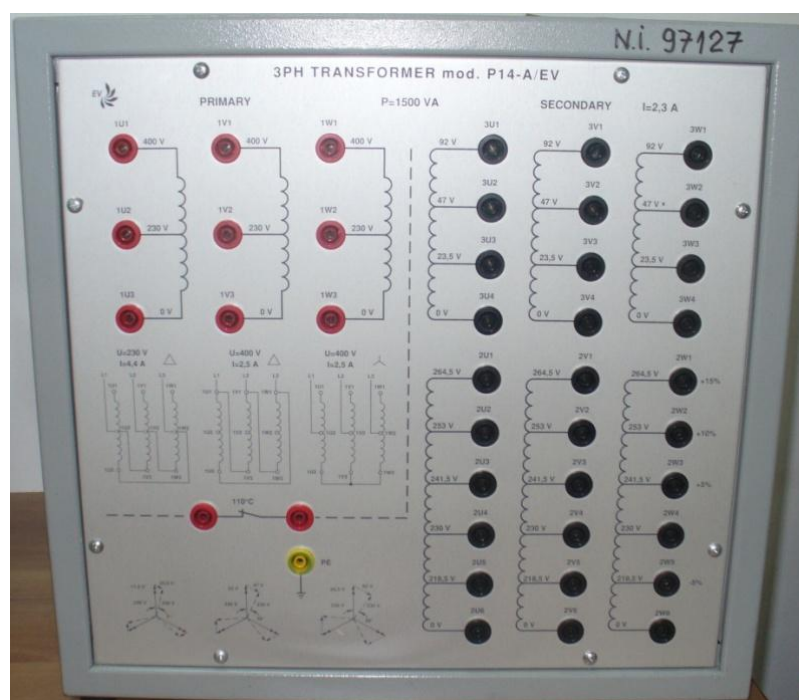


Fig 7. Three-phase transformer mod. P 14A/EV

Preparing the exercise:

It uses the same type of equipment as the previous year following completion:

- Battery of capacitors, for instance that of $3 \times 2 \mu\text{F}$ of the module AZ 191b, with the respective discharge resistances.

Prearrange the simulator as in the previous exercise(fig 6) and connect the capacitors of the module AZ 191a in parallel with CL(becoming CLaux).-fig 8

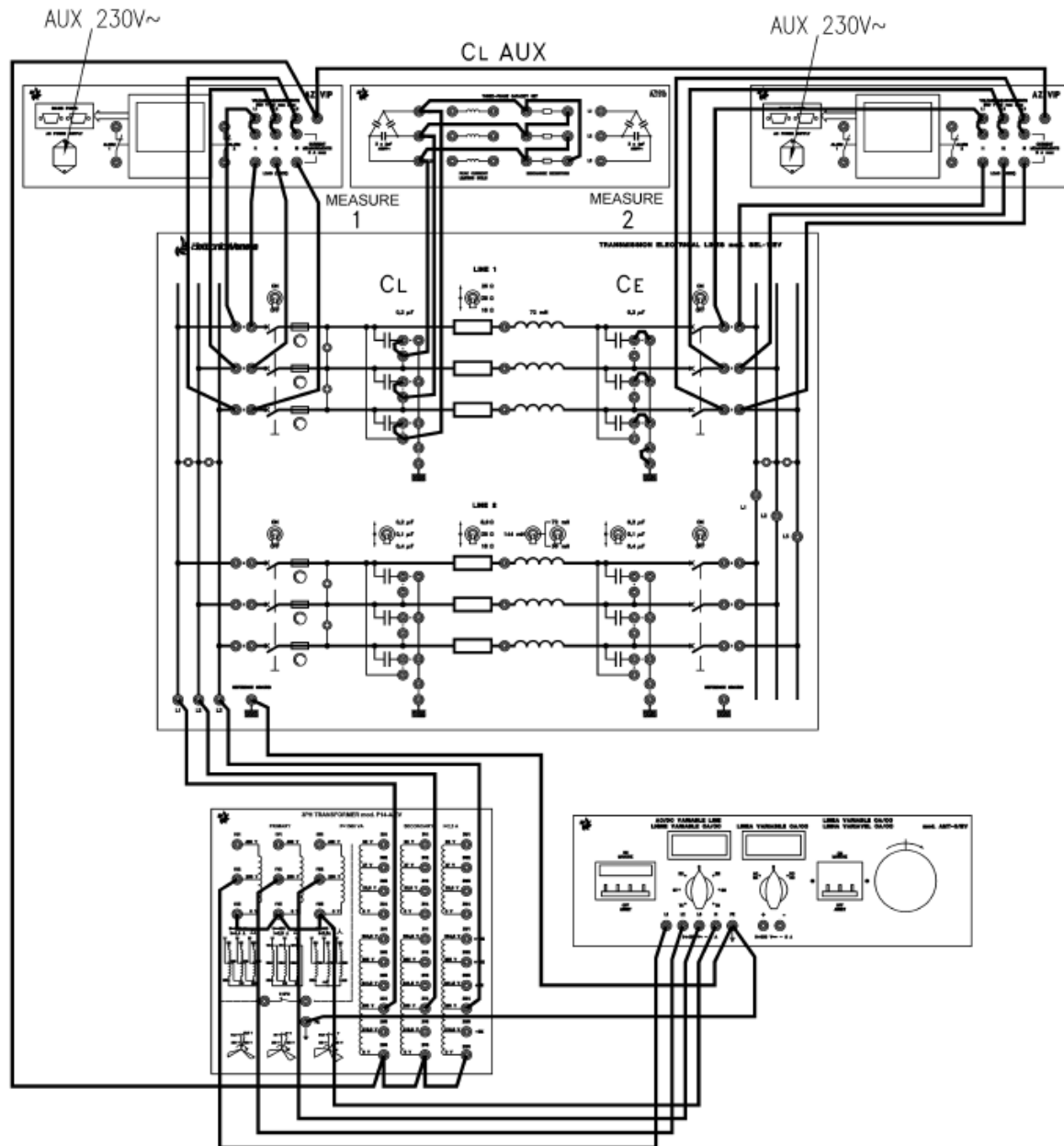


Fig 8. No-load performance of a power transmission line with increased capacitance

Actual measurements carried out on the LINE 1 with: Resistance = 25Ω ; Capacitance = variable $0.2 - 2.2 - 4.2 \mu\text{F}$; Inductance = 0.072 H

Table 3 - transmission lines with auxiliary capacitors CL_{aux} from the origin of the line

Capacitance (μF)	Interlinked voltage at the origin of line $U1 (V)$	Current at the origin of the line $I1 (A)$	Active power at the origin of line $P1 (W)$	Interlinked voltage at the end of the line $U2 (V)$	Reactive power at the origin of line $Q1 (Var)$
0.2 μF	380 V	0.052 A	0	380 V	- 34.5 VAr
2.2 μF	380 V	0.520 A	0	380 V	- 340 VAr
4.2 μF	380 V	0.860 A	0	380 V	- 568 VAr

Studying the transmission lines represented with concentrated parameters will lead to consider that shifting the set of auxiliary capacitors CL_{aux} from the origin of the line to the half length of the line and to the end of the line determines what is explained herebelow:

- when the auxiliary capacitors CL_{aux} are connected at the origin of the transmission line, the capacitive current crossing it will concern only the generator and it does not provoke any effect on the line resistance inductance;
- when the auxiliary capacitors CL_{aux} are connected at half length of the transmission line, the capacitive current crossing it will also affect the resistance where it provokes a power loss by Joule effect $R \times I^2$;
- when the auxiliary capacitors CL_{aux} are connected at the end of the transmission line, the capacitive current will cross not only the resistor (as in the previous point), but also the coil where it provokes a further power loss $R \times I^2$ due to the resistive component of the coil (the coils of the simulator are wound on a ferromagnetic core and consequently they also have a resistive component).

Actual measurements carried out on the LINE 1 with: Resistance = 25 Ω ; Capacitance = variable 0.2 – 2.2 – 4.2 μF ; Inductance = 0.072 H

Table 4 - transmission lines with auxiliary capacitors CL_{aux} from the origin of the line to the half length of the line and to the end of the line

Capacitance (μF)	Interlinked voltage at the origin of line $U1 (V)$	Current at the origin of the line $I1 (A)$	Active power at the origin of line $P1 (W)$	Interlinked voltage at the end of the line $U2 (V)$	Reactive power at the origin of line $Q1 (Var)$
0.2 μF origin of line	380 V	0.052 A	0	380 V	-34.5 VAr
0.2 μF half line	380 V	0.044 A	4 W	380 V	-29VAr
0.2 μF end of line	380 V	0.055 A	6 W	380 V	-36 VAr
2.2 μF origin of line	380 V	0.52 A	0	380 V	-340 VAr
2.2 μF half line	380 V	0.51 A	18 W	380 V	-335VAr
2.2 μF end of line	380 V	0.53 A	23 W	380 V	-350 VAr

4.2 μF origin of line	380 V	0.86 A	0	380 V	-568 Var
4.2 μF half line	380 V	0.82 A	26 W	380 V	-540Var
4.2 μF end of line	380 V	0.90 A	32 W	380 V	-590 Var

The sign – (minus) indicates that the reactive power is of capacitive type. The measured power can have a deviation of +/- 10 % for the tolerance of capacitors

3. CONCLUSIONS

Following measurements it was found that the values resulting from calculations are very close to the results of measurements. The difference is due to errors of measurement devices. It is found in the presented reactive power measured is directly proportional to the mains voltage.

The parameter of capacitance is directly proportional to the length of the transmission line .It is concentrated into an equivalent total capacitance only for an easier study. Actually the “parameters” of a transmission line (capacitance and resistance in this particular case) are distributed; crossing the line resistors the capacitive currents will provoke power

The values obtained from the calculations can help both the operating personnel, working with the line having voltage levels 6,10,20,35,110,220,400,750 kV, the understanding of how power flows reactive Upon awakening in the line is in operation only one end the other is the backup, and the measures to be taken to control reactive power influencing the nodes tensions.

ACNOWLEDGMENT

This paper is supported by the Sectoral Operational Programme Human Resources Development POSDRU/159/1.5/S/137516 financed from the European Social Fund and by the Romanian Government

REFERENCES

1. Dan Călin Peter;Radu, Adrian Tîrnovan,2014. *Transportul și Distribuția Energiei Electrice*, p1-7,76-109 ISBN 978-973-662-960-0
2. Darie, S., Vădan, I., *Producerea, Transportul și Distribuția Energiei Electrice. Instalații pentru producerea energiei electrice*, U.T. PRES, Cluj-Napoca, 2003.

3. **Hortopan, G.**, “*Aparate Electrice, Teorie, Proiectare, Incercari*”, Editura Didactica si Pedagogica, Bucuresti, 1978
4. **Ionescu, I., Racovitan, I.**, “*Using Modern Methods of Diagnosis Off-line Medium and High Voltage Circuit Breakers in the Context of Transition to Maintenance Based on Reliability*”, FOREN-2008, Neptun, 15-19 june 2008
5. *** **Electronica Veneta** – Power Transmission Line – *mod.SEL-1/EV. Practical Testing Section-teacher/Student handbook.*
6. **Berinde I, Bălan H, Oros(Pop) Teodora** – *Study about the reactive power overhead power lines high voltage - THE INTERNATIONAL CONFERENCE OF THE CARPATHIAN EURO-REGION SPECIALISTS IN INDUSTRIAL SYSTEMS CEurSIS 2014*, 10th Edition, 11-13 September, 2014, BAIA MARE, ROMANIA
7. **G. Schickhuber and O. McCarthy.** *Control using power lines. IEE Computing and Control Engineering Journal*, pp 180-184, August 1997.
8. <http://www.neduet.edu.pk/electrical>

PRACTICAL APPLICATION WITH PLC IN MANIPULATION OF A ROBOTIC ARM

Cristian **BARZ**, Tihomir **LATINOVIC**, Zoltan **ERDEI**, Gherasim **DOMIDE**, Alina **BALAN**

Technical University of Cluj-Napoca, North University Center of Baia Mare, University in Banja Luka, Faculty of Mechanical Engineering, Technical University of Cluj-Napoca, North University Center of Baia Mare,

*cristian.barz@cunbm.utcluj.ro, drtiho@gmail.com, zoltan.erdei@cunbm.utcluj.ro,
gherasim.domide@cunbm.utcluj.ro, alina_balan91@yahoo.com*

Keywords: PLC, control systems, process interface, robotic arm

Abstract: *This paper presents the use of a robotic arm PLC Siemens in order not using CNC commands. This is done by programming the PLC ladder diagram language that makes movement on the three axes of the arm by means of stepper motors. Required command console PLC is built with the help of a touch screen HMI Weintek. In the user interface are introduced distances and displacement speeds on the three axes.*

1. INTRODUCTION

Industrial robots have emerged in response to the human need for automation of production processes, especially those repetitive. Besides stationary industrial robots, built mainly from the need to increase productivity in recent years have also been used the mobile robots. The main activities that can be taken by industrial mobile robots are linked to transport and manipulating objects and sometimes achievement of processes (painting, inspection, assembly, etc.).

In order to optimize the execution of these activities, many current field studies based programming lead to the cognitive attributes (reason, perception, understanding and learning)

that the abstraction, generalization, specialization, representation, knowledge, concentration, socialization gives robots a level high intelligence.

Industrial robots are point of intersection of the latest discoveries in a number of areas: mechanics, automation, electronics, computers and drives. The complexity of this sector is reflected on the mechanical architecture and the system management.

The automation of the manufacturing processes was required by the general effort of the industrial manufacturers to obtain high productivity and to improve the quality and reliability of products. The decrease of manufacturing costs and the improvement of work conditions are aimed. PLC's are used in numerous applications, particularly in industry and has a number of advantages, most of which important are reducing production time and lower costs. In principle, any application that requires electrical control needs a PLC. [2, 3]

Sending commands from the PLC program to the robotic arm elements require the use of stepper motors, which makes the transmission travels on mechanical components. Robotic arm allows movement in three axes and is equipped with three stepper motors.

2. APPLICATION COMPONENTS

2.1. PLC Siemens CPU 313C

PLC (Programmable Logic Controller) Siemens CPU 313C is composed of a power supply, a CPU and modules input and output (I/O modules). It monitors and controls equipment (installation) using Step7 software which through the addresses accessed I/O modules and internal elements entering the programming applications.

2.2. HMI Weintek

All PLCs do not dispose a graphical interface control (Human Machine Interface - HMI), requiring the use of an HMI to enter input data and monitor progress made by the program (*fig. 1*).

HMI MT8070 iH is a touch screen produced by Weintek, which facilitates the creation of a graphic interface for a large number of PLCs found on the market. MT8000 series is the new generation of HMI from Weintek.

EasyBuilder Pro is software developed by Weintek for programming various types of graphical user interface to controlling and command the various types of PLCs. The software has a diverse library of images, buttons, graphics, and sound monitoring screen, but also allows the insertion of other elements that can be used to create interfaces, depending on the project conducted.



Fig. 1 - Touch screen Weintek

2.3. Stepper motors

The applications of the stepper motors are limited to cases where high power is not required (usual powers between field's microwatt and kilowatt).

Stepper motors are used in low power applications that are characterized by quick movements, precise, repeatable: xy plotters, floppy disk drive, moving print head printers, operating mechanisms and pressure oriented robots axial displacement systems elements optical, tables positioning 2D drilling machines, in aviation etc. [1]

The stepper motor is used in control schemes with software systems and pulse. The use of computers for the control of complex processes is necessary to process signals, impulses form is what can be done with stepper motors.



Fig. 2 - Stepper motor Nema 42

Nema 42 stepper motor was developed primarily for users who have restricted installation space available and want a motor with increased torque (*fig. 2*). Nema 42 motor uses advanced magnetics technology to give the couple a level significantly higher than that of a standard motor device.

3. APPLICATION DEPLOYMENT

The project was realized using two software: Simatic Step 7 Manager, software for programming PLCs manufactured by Siemens, and EasyBuilder Pro software used to create graphical interfaces used in the simulation.

The programming using Ladder Diagrams appeared in the case of programmable controllers due to the necessity to have an easy programming way which allows the realization of applications without having complex programming knowledge.

The Ladder Diagrams are taken from electrical field and they inherit certain names and representations from this field. The base elements of the ladder diagrams are the contacts and coils. [5]

3.1. Movement of robotic arm in the PLC

For starters we established the entries will start or stop operation scheme, starting scheme is through the PLC inputs I124.0, I124.1 so that starting or stopping operation scheme is performed by simply flipping the inputs who are rebound.

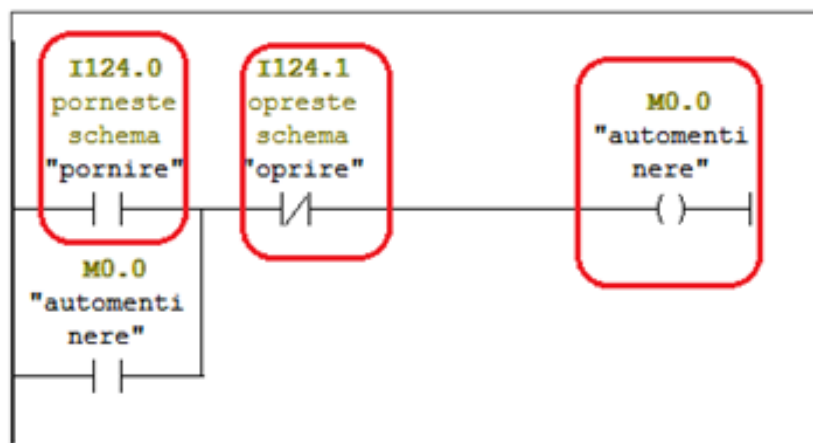


Fig. 3 - Start/Stop of process

In figure 4 it can be observed operation outputs Q124.0, Q124.1, Q124.2, these outputs are required to give impulses of the stepper motors through frequency converters, which are connected to the PLC terminals corresponding user exit.

As can be seen these outputs will be active when the program starts and the necessary buttons are enabled conditioning the axes functions as timers to be in working. These output besides the impulses getting from the operating time are on also for the markers corresponding directions.

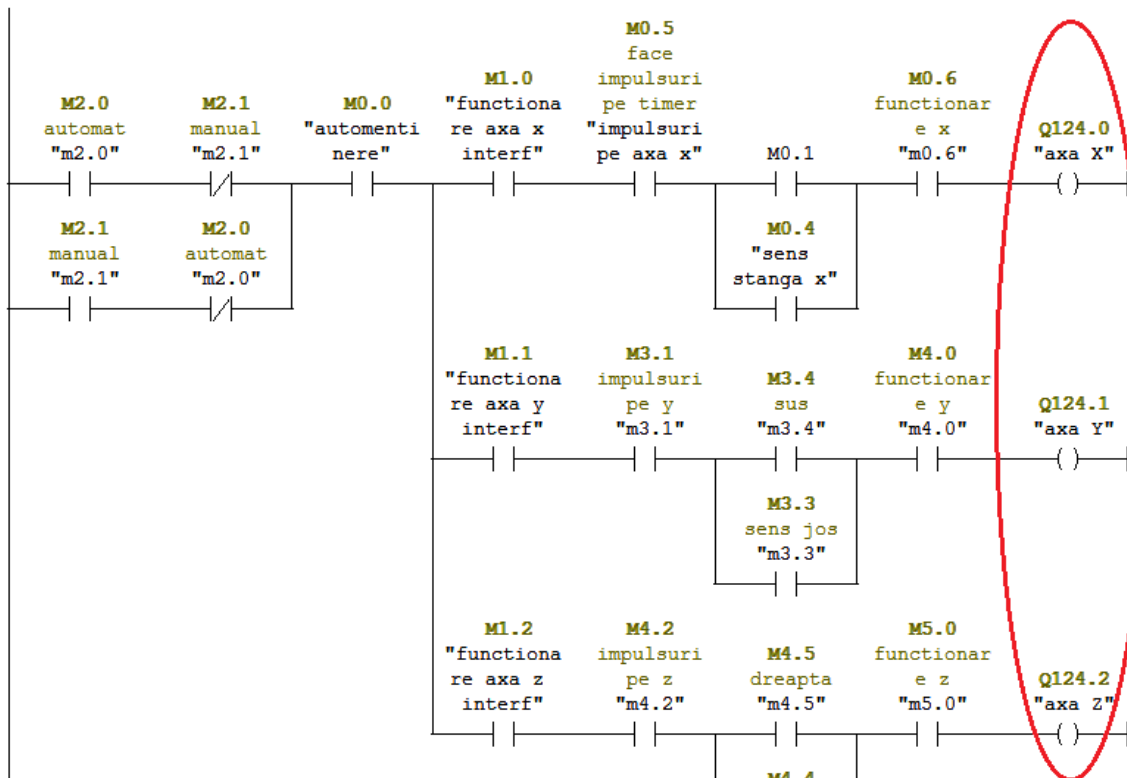


Fig. 4 - Commands on X, Y, Z axis

Time relay is one of the most important components of the programming in the works scheme we decided that it will be active only when one of the two inputs automatic/manual is active. In the network has introduced a marker M1.5 in order to establish its operation only when we want, marker M1.5 is designed for interface.

For making impulses every 30ms (value set by us) we inserted a marker M0.5 (fig. 5), it starts and stops the relay operation time doing a loop sending one pulse every 30ms.

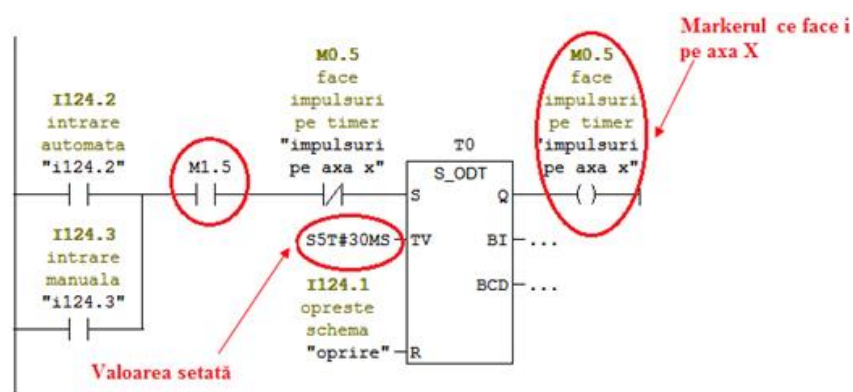


Fig. 5 - Making impulses 30ms

Time relay sends these pulses and impulses counter that counts up the number if entry CU (count up) incrementing by 1 the value of each pulse received from the relay time or the entry CD (count down) it decrements by 1 the value of the which is in the time counter.

4. HMI INTERFACE OF THE PROGRAM

4.1 Main menu panel

Main Menu panel (*figure 6*) present major information to any user, while having windows (screens) for additional axes robotic arm that works. This panel consists of buttons with which we communicate with the other interface windows, buttons and switches automatic and manual start and stop the operation of the program



Fig. 6 - Main menu panel

Start and stop buttons are buttons of starting and stopping set the programmed bit, we're still here and start and stop lights working distance when inputs I124.0 (start) and I124.1 (stop) operates the same from the PLC program (*fig. 3*).

4.2. X axis menu

Accessing window X axis is done by pressing the X axis in the Main Menu window. In this window you can find the main buttons for operating the robotic arm on the direction of X (*fig. 7*).

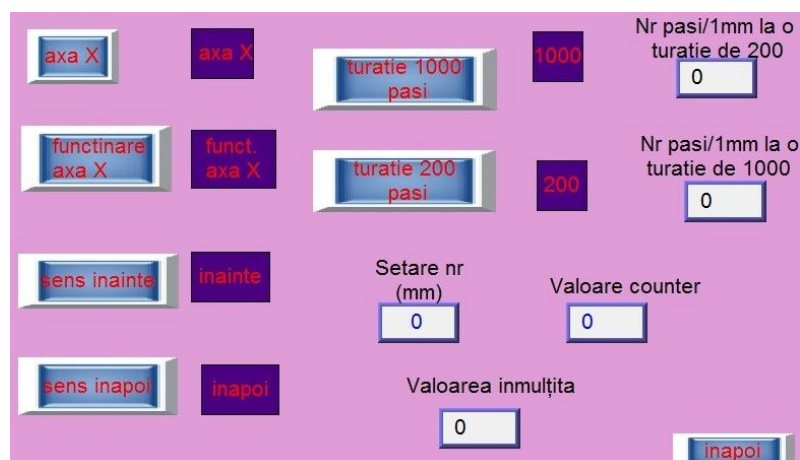


Fig.7 - Menu of X axis

The numerical indicators, *setare pași/mm la o turație de 200, valoarea înmulțită, valoare counter, setare pași/mm la o turație de 1000* and numerical button *setare număr* we finding also on the windows of Y and Z axis.

The numeric display can be set from Weintek panel and input to the PLC through the marker word (fig. 8):

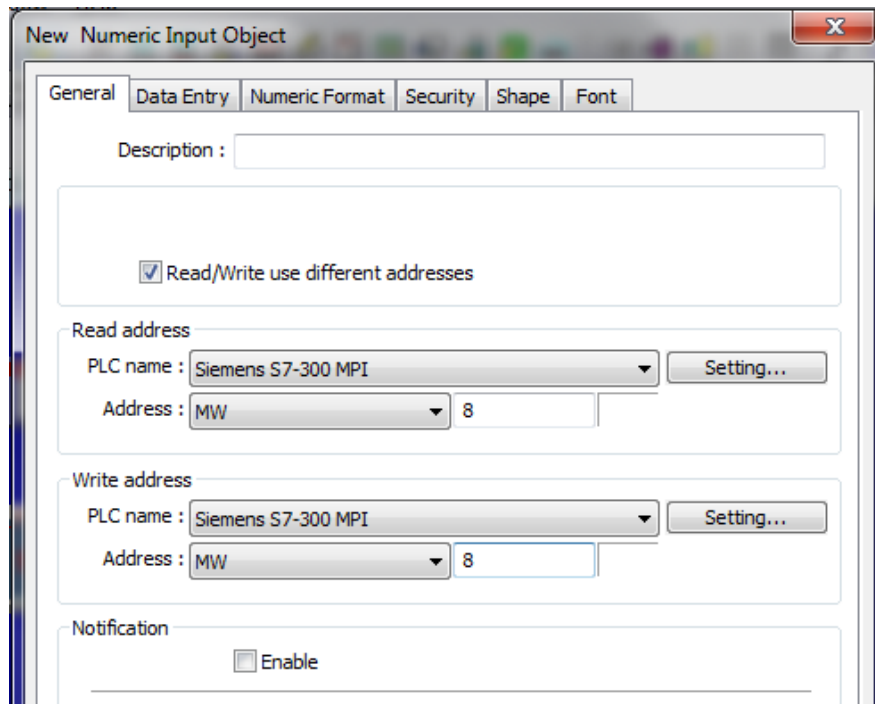


Fig. 8 - Setting of the numeric display

Numeric indicator *Setare pași/mm la o turatie de 200* (MW8) indicates how many steps must be at a speed of 200 steps in order to move a millimeter.

The button Axa X (M1.0) starts axis x along with relay output time (timer) and output counter.

LED Axa X (M1.0) indicates the function on X axis, the button works when the X axis button is pressed. The button Sens înainte (M0.3) controls robotic arm in the forward direction.

The interface consists of windows which make it possible to navigate between the X, Y and Z of the robotic arm. It performs the following commands:

- Establish starting and stopping application with Weintek panel,
- Set the distance you want to made the arm on the axes X, Y and Z,
- Setting impulses which they receive stepping motors, engines impulses have different configurations from 200 to 12800 pulses.
- Setting the direction of movement of the robotic arm in the X, Y and Z.

In this window is represented the functioning of the robot arm on the directions X and Y accessing is done from the Main Menu window. Window animation follows the movement

of the robotic arm on the X and Y directions in both automatic and manual modes (*fig. 9*). This shows how the robotic arm moves in X and Y was set as the the range of movement of the arm on axis.



Fig. 9 - Manual mode

5. CONCLUSIONS

The paper highlights the utility and importance of programmable automates in the control of the industrial processes, command the function over 3 axis of a robotic arm, in order not using CNC commands.

This is done by programming the PLC ladder diagram language that makes movement on the three axes of the arm by means of stepper motors. PLC command console is built with the help of a touch screen Weintek for introducing the distances and displacement speeds on the three axes. It allows to start and stop the application on the panel WEINTEK, as well as monitor the movement on the axes

PLC programming has the advantage of creating artificial intelligence by implementing control algorithms in the software and the ability to perform movements based on data provided by the sensors imposed by the developed.

REFERENCES

1. **Biro K.A., Viorel I.A., Szabo L., Henneberger G.** *Mașini electrice speciale*, Ed. Mediamira, Cluj-Napoca 2005
2. **Dunning G.** *Introduction to Programmable Logical Controllers*, Ed. TWI Press Inc. 2002

3. **Mărgineanu I.** *Automate Programabile*, Editura Albastră, București 2005
4. **Oprea Ctin, Barz C.** Elemente de inginerie electrica, reglare automata si automatizari, *Ed. Risoprint, Cluj Napoca 2011*
5. **Webb J. W., Reis R. I.** Programmable Logic Controllers, *Prentice Hall* 2000
6. *** *Simatic S7*, Siemens documentation
7. *** www.automation.siemens.com
8. *** www.weintek.com

THE STUDY, DESIGN AND SIMULATION OF A FREE PISTON STIRLING ENGINE LINEAR ALTERNATOR

Teodora Susana **OROS (POP)**, Ioan **BERINDE**

Technical University of Cluj Napoca

teodoraoros_87@yahoo.com

Keywords: free piston Stirling engine, permanent magnet machines, linear alternators, SIMULINK simulations

Abstract: *This paper presents a study, design and simulation of a Free Piston Stirling Engine Linear Alternator. There are presented the main steps of the magnetic and electric calculations for a permanent magnet linear alternator of fixed coil and moving magnets type. Finally, a detailed thermal, mechanical and electrical model for a Stirling engine linear alternator have been made in SIMULINK simulation program. The linear alternator simulation model uses a controllable DC voltage which simulates the linear alternator combined with a rectifier, a variable load and a DC-DC converter, which compensates for the variable nature of Stirling engine operation, and ensures a constant voltage output regardless of the load.*

1. INTRODUCTION

Environmental concerns and increasing electricity demand increased interest on the use of renewable energy, the energy recovery from organic waste, in special agricultural waste and wood waste. Stirling engines technology was developed based on their advantages over other heat engines:

- higher efficiency;
- possibility of using a large class of fuels or other sources of unconventional heat;
- the noiseless operation without vibration.

A potential market is that a small-power systems for electricity generation in cogeneration mode for residential applications.

So far, the research done in of Stirling engines field have not given importance to the interaction between the thermo-mechanical part and the electrical of a Stirling engines. This paper tries to compensate for this shortcoming by developing a model in SIMULINK simulation environment for electrical part of a cogeneration system of electricity and heat based on Stirling engine. Has been designed an electrical system which assure an adaptation between the variable voltage of a Stirling engine linear alternator based cogeneration system and a variable load connected to the power consumer, based on a DC-DC converter of the buck-converter type. The principle of operation, the design, the achievement of this system and the simulation results will be presented in the following paragraphs.

2. FREE PISTON STIRLING ENGINE DESIGN

For this paper, a typical cogeneration system based on Stirling engine is studied, designed, modeled and simulated, this system is shown in figure 1.

The heat produced by burning organic waste put the free-piston Stirling engine in operation. The operation the linear alternator produces a variable single-phase alternating voltage, that will be rectified with a diode rectifier. This voltage will be converted in a prescribed DC constant voltage by using a DC-DC converter of the type buck-converter by means of a feedback controller based on a PI controller.

Engines using the Stirling cycle have clear advantages compared with the small internal combustion engines in the field of power generation as: dish solar systems, biomass energy conversion, residential heat and power cogeneration and another applications. The main advantages are: bigger thermal efficiency; long life and multiple fuel capability.

In the last sixty years, hundreds of millions of dollars have been invested in development of kinematic Stirling engines, in which the pistons are conected in various mechanical linkages. Despite this significant effort, neither efficient mechanically reliability nor large scale commercial production of kinematic Stirling engines has been achieved.

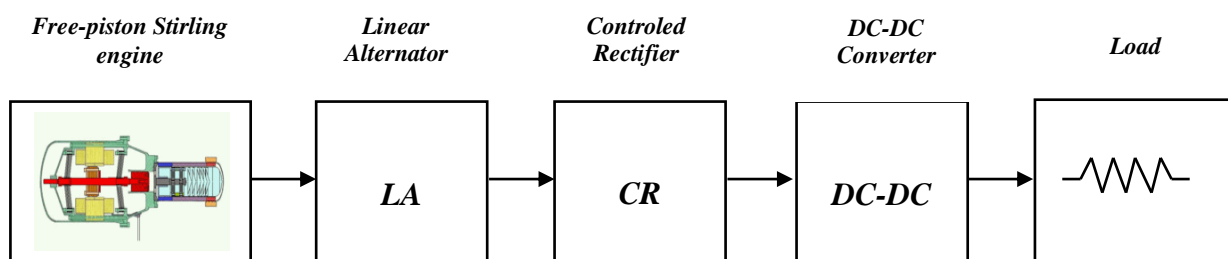


Fig. 1. The studied system configuration.

In order to avoid the kinematic Stirling engines design problems, a new class of Stirling engines have been developed: free piston Stirling engines.

The free piston Stirling engines have the following characteristics:

- mechanically simple construction – only two pistons in a common cylinder;
- the using of mechanically springing;
- high mechanical and electrical efficiency;
- the using of a direct driven permanent magnet linear alternator;
- extremely easy starting;
- no lubricant other than working gas.

In this configuration, the power piston is not mechanically connected to an output shaft. It bounces alternately between the space containing the working gas and a spring (usually a gas spring). In many designs, the displacer is also free to bounce on gas springs or mechanical springs (figure 2). This configuration is called the Beale “free-piston” Stirling engine after its inventor, William Beale [1]. Piston stroke, frequency, and the timing between the two pistons are established by the dynamics of the spring/mass system coupled with the variations in cycle pressure. To extract power, a magnet can be attached to the power piston and electric power generated as it moves past stationary coils [2]. These Stirling engine/alternator units are called “free-piston” Stirling converters.

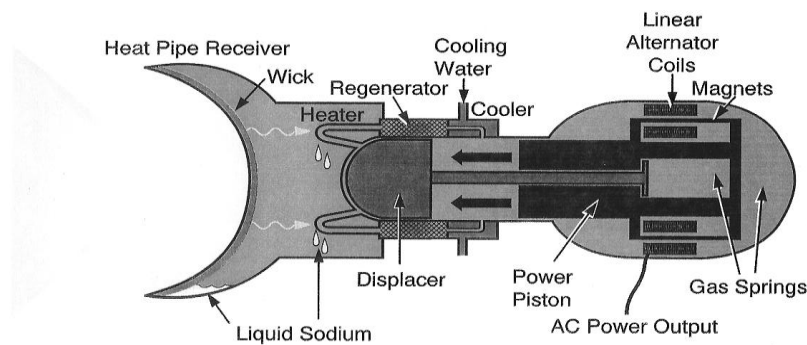


Fig. 2 Basic components of Beale “free-piston” Stirling engine [3].

The free piston Stirling engine can operate as a constant voltage generator. The linear alternator is the most expensive component of the system. The springs supports all and avoid any friction and wear during linear oscillation. The flexures can be designed for a long life of about 40,000 hours of operation. These flexures serve as friction free bearings to maintain the magnets in the flux gap. If the air gap is about 1 mm, there are no severe demands for radial position, and the springs can be made inexpensively.

The design starts with the Beale developed power formula [5]. Beale indicated that the power output of several Stirling engines observed could be calculated from the equation:

$$P = 0.015 \cdot p_m \cdot f \cdot V_p \quad (1)$$

where: 0.015 is the Beale number, P is the engine power output in Watts, p_m the mean cycle pressure in bar, f the cycle frequency in Hz, and V_p is the displacement of power piston in cm^3 . The Beale number was modified by West as follows:

$$P = F \cdot p_m \cdot f \cdot V_p \cdot \frac{T_H - T_C}{T_H + T_C} \quad (2)$$

where the factor $F=0.25-0.35$ can be used for practical use, T_H is the hot side temperature and T_C is the cold side temperature.

From this we can calculate:

$$V_p = \frac{P}{F \cdot p_m \cdot f} \cdot \frac{T_H + T_C}{T_H - T_C} = \frac{200}{0.25 \cdot 3 \cdot 10} \cdot \frac{766}{180} = 117 \text{ cm}^3, \quad (3)$$

where $P=200 \text{ W}$ is the power rate of the engine as design datum, $p_m=(0+6)/2=3 \text{ bar}$, $f=10 \text{ Hz}$, $T_H=473 \text{ K}$ and $T_C=293 \text{ K}$.

The oscillating amplitude must be as high as pole pitch, which has been chosen as high as permanent magnet height:

$$A = \tau = h_m = 0.0133 \text{ m} = 1.33 \text{ cm} \quad (4)$$

The oscillating amplitude A give us the swept volume of power piston.

$$V_p = A \cdot A_p \quad (5)$$

where A_p is the power piston area:

$$A_p = \frac{V_p}{A} = \frac{117 \text{ cm}^3}{1.33 \text{ cm}} = 88 \text{ cm}^2 \quad (6)$$

Now we can calculate the power piston diameter:

$$d_p = \sqrt{\frac{4 \cdot A_p}{\pi}} = \sqrt{\frac{4 \cdot 88}{\pi}} = 10.6 \text{ cm} = 106 \text{ mm} \quad (7)$$

This dimension was used in the drawing of the designed “free-piston” Stirling engine presented in figure 3.

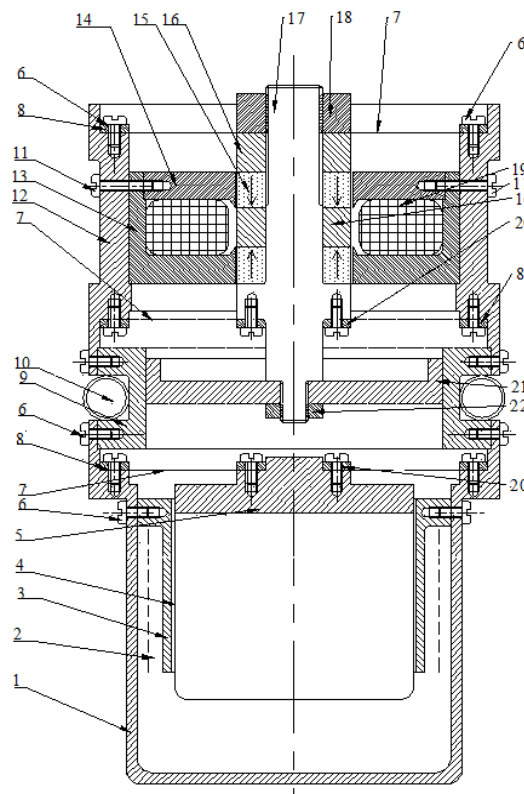


Fig. 3. The designed free-piston Stirling engine

3. PERMANENT MAGNET LINEAR ALTERNATOR DESIGN

3.1 The Magnetic Circuit Design

This alternator is of the synchronous type with excitation from the permanent magnets. From the figure 3 it can be seen that field line passes the air gap for two times, so the necessary magnetomotive force is:

$$F_{mm} = \frac{B_0}{\mu_0} \cdot 2 \cdot \delta = \frac{1}{4\pi \cdot 10^{-7}} \cdot 2 \cdot 1 \cdot 10^{-3} = 1592A \quad (8)$$

where $B_0 = 1T$ is the mean value of magnetic flux density in the air-gap, $\delta = 1mm$ is the air-gap length and μ_0 is the magnetic permeability of the air.

For the magnetization it was chosen two ring permanent magnets of the type EURONEOS 40x20x13.3, which have the properties presented in the table 1.

Table 1. The permanent magnets properties of the type EURONEO 3 40X20X13.3

Material	$B_r [T]$	$H_c [kA/m]$	$BH_{max} [kJ/m^3]$	$D [mm]$	$d [mm]$	$h [mm]$
N35	1.2	868	280	40	20	13.3

The magnetomotive force of the one magnet is:

$$F_{mm} = H_m \cdot h = 500 \cdot 0.0133 = 6,65kA \quad (9)$$

Can be seen that $6.65kA = 6650A > 1592A$, therefore, the magnets were chosen correctly.

3.2 The Coil Design

The induc coil design will be made according to the voltage that is aimed to be induced in the coil. We considered an induced voltage at 10 Hz frequency of $U = 18 V_{ef}$ voltage. The magnetic flux by this coil varies between $+\Phi_{max}$ and $-\Phi_{max}$ so that the magnetic flux variations:

$$\Delta\Phi = \Phi_{max} - (-\Phi_{max}) = 2\Phi_{max} = 2B_m A_m \quad (10)$$

The permanent magnet area is:

$$A_m = \frac{\pi(D^2 - d^2)}{4} = \frac{\pi(40^2 - 20^2)}{4} \cdot 10^{-6} m^2 = 942 \cdot 10^{-6} m^2. \quad (11)$$

Now, the magnetic flux variation is:

$$\Delta\Phi = 2B_m \cdot A_m = 2 \cdot \frac{B_r}{2} \cdot A_m = B_r \cdot A_m = 1.2T \cdot 942 \cdot 10^{-6} m^2 = 1130 \cdot 10^{-6} Wb. \quad (12)$$

The turn voltage is:

$$e = \frac{\Delta\Phi}{T} = f \cdot \Delta\Phi = 10Hz \cdot 1.13 \cdot 10^{-3} Wb = 11.3 \cdot 10^{-3} V / turn \quad (13)$$

considering $f = 10Hz$ from mechanical design stage.

For a voltage of $U = 18V_{ef}$ we will need:

$$N = \frac{\sqrt{2} \cdot U}{e} = \frac{\sqrt{2} \cdot 18}{11.3 \cdot 10^{-3}} = 2252 \text{ turns.} \quad (14)$$

The magnetic circuit window where the coil is placed has the area:

$$A_f = a \cdot b = 20 \cdot 30 = 600 \text{ mm}^2 \quad (15)$$

The coil conductor cross-section area is:

$$s_c = \frac{A_f \cdot k_1}{N} = \frac{600 \cdot 0.6}{2252} = 0.16 \text{ mm}^2 \quad (16)$$

where $k_1=0.6$ is the winding filling factor.

Now we can calculate the fixed coil conductor diameter:

$$d_c = \sqrt{\frac{4 \cdot s_c}{\pi}} = \sqrt{\frac{4 \cdot 0.16}{\pi}} = 0.45 \text{ mm.} \quad (17)$$

4. SIMULATION MODEL OF FREE PISTON STIRLING ENGINE LINEAR ALTERNATOR

In figure 4 is presented the SIMULINK model of the linear alternator (DC controlled source), DC-DC converter of buck type and the load composed from a fixed part and a cyclic load with 200 Hz frequency.

The linear alternator combined with a rectifier is designed to produce a variable voltage around the value of 18Vdc. The DC-DC buck converter is combined with a voltage control loop which assures to the load, just in case of variable load, a constant DC voltage of prescribed value, in the case above of 12 Vdc.

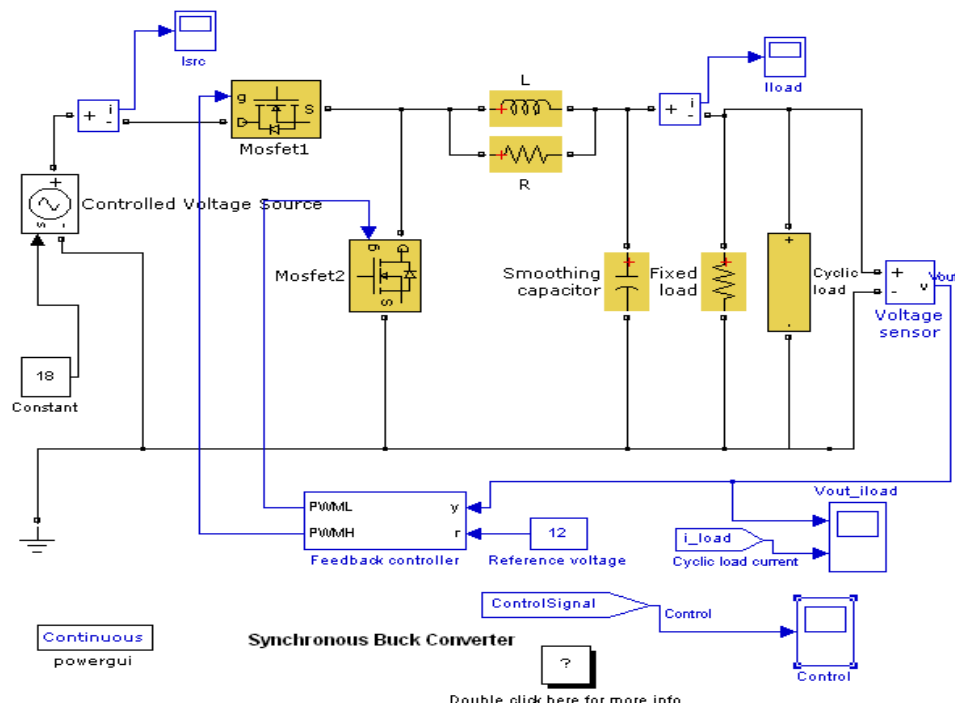


Fig. 4 The SIMULINK model of the Free piston Stirling engine linear alternator

5. SIMULATION RESULTS

In the next figures are presented some simulation results. In figure 5 is presented the out voltage V_{out} and the cyclic load current.

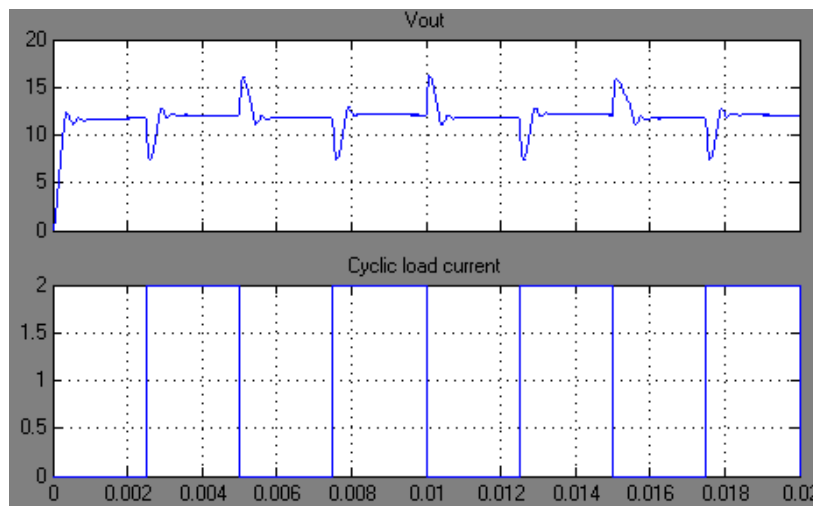


Fig. 5 The stabilized V_{out} and the cyclic load current.

In the figure 6 is presented the total load current.

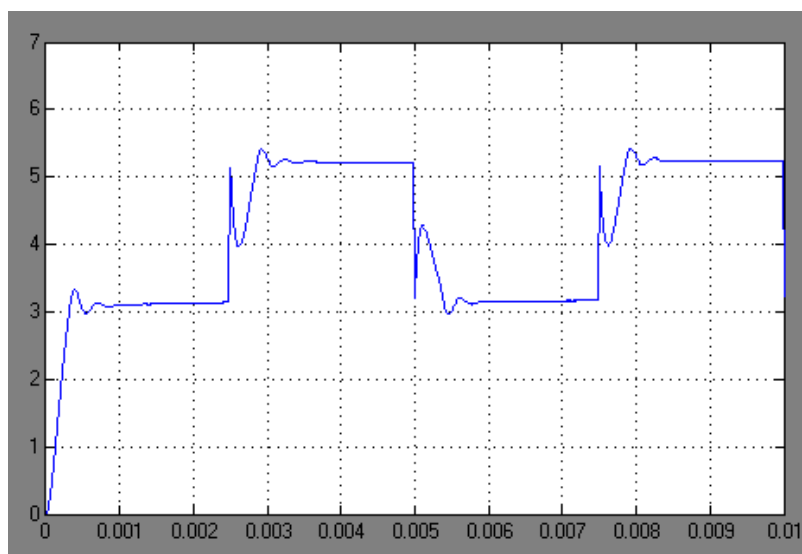


Fig. 6 The total load current.

Here can be seen the constant load of about 3 A and the cyclic load of 2 A.

In the figure 7 can be seen the PI control signal of PWM generator.

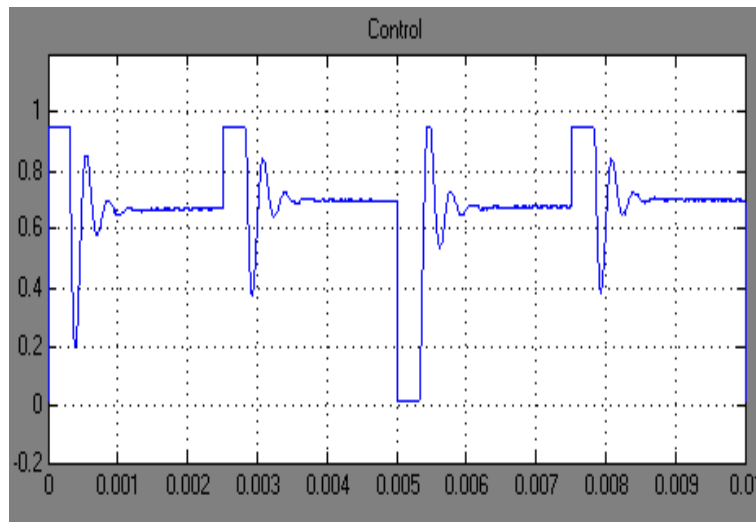


Fig. 7 The PI control signal of PWM generator.

6. CONCLUSIONS

In this paper a tubular type linear generator for a free piston stirling engine is studied and designed. The ring-shaped iron rotor with the rare earth axially magnetized permanent magnets is used as magnetic pole of the mover, because in the case of symmetric structure the leakage magnetic flux is smaller than that of the flat type one. Also, the mass of the copper coil is less than that in the case of flat-type generator because there is no end coil.

This paper also presents a SIMULINK simulation of the electrical part of a free piston Stirling engine cogeneration system. Because the linear alternator together with the diode rectifier produces a variable DC voltage, a voltage stabilizer loop is provided in order to assure a constant output voltage of prescribed value. This SIMULINK model is similar with a real electrical system used in the case of a free piston Stirling engine cogeneration system of small power for residential applications.

ACNOWLEDGMENT

This paper is supported by the Sectorial Operational Programme Human Resources Development (SOP HRD), ID/134378 financed from the European Social Fund and by the Romanian Government.

REFERENCES

1. **Thombare D.G., Verma S.K.**, 2008, “*Tehnological development in the Stirling cycle engine*”, Science Direct Renewable and Sustainable Energy Reviews 12 (2008) 1-38, Elsevier, 2008.

2. **Beale, W.**, 1981, "*Stirling Engines for Developing Countries*", U.S. National Academy of Sciences, Energy for Rural Development, 1981.
3. **Jahromi Z.M** et al, 2001, "*Simulation of a Stirling Engine Solar Power Generation System Using Simulink*", (ACEMP) and Electromotion Joint Conference, Istanbul, Turkey, 8-10 September 2011, ISSN: 978-1-4673-5003-7, pp. 676-681, 2011.

CONTRIBUTIONS TO THE MANAGEMENT OF WIND POWER IN ROMANIA. THE ABSORPTION SEN WIND ENERGY 2013. ELECTROMAGNETIC INTERFACE

Radu JOIAN, Mircea HORGOS, Alin GRAMA, Niculaie PALAGHIȚĂ

Technical University of Cluj-Napoca

yo5pcw@yahoo.com

Keywords: wind power capacity penetration level, installed capacity in wind power plants, management an dispatch control of power plants based on RES.

Abstract – Nowadays, Romania confronts with a storm of the already implemented projects or in development as regards the wind and photovoltaic power plants, located to a great extent in Dobrogea, an area where the power consumption is low. Also, the capacities of discharge power lines on this area are limited. Compare with the wind power plants, the photovoltaic power plants have a more uniform spreading in the country. A great importance have the aspects that concerns the level where the wind power plants penetrates the National Power System. Considering the practice used in EU countries, which have a high penetration potential of the renewable energy in the National Power System, Romania needs to reorganize the current structure taking into account the adopting of one organizational structure dedicated in that meaning. As follows, there are presented a number of solutions to be adopted for this purpose.

1. INTRODUCTION

In the European Parliament and European Council there is a mechanism which regulates the promotion and the use of renewable energy (Directive 2001/77/EC, replaced later with Directive 2009/28/EC).

The mentioned directives are designed to determine the share of renewable energy in the EU's GDP in 2010 and for the period 2010-2020 (20% in 2020). Therefore by the Law 220/2008 Romania established:

- The objectives regarding gross final consumption of electricity produced from renewable sources are: 35% for 2015 and 38% for 2020;
- The obligatory quotas for the electricity produced from renewable sources, with a promotion system are: 16% for 2015 and 20% in 2020.
- This system of green certificates promotion of E-RES (electricity produced by renewable energy sources) with the help of each 1 MWh produced or delivered by the E-RES producers receives two green certificates for wind power plants (until 2017).

The reasons to promote E-RES are likely:

- **economic:** aims particularly the security of the energy supply and the industries which use E- RES;
- **social:** aims the employment;
- **environmental:** as clean sources or as contribution to reduction of climate changes etc.

In Romania, there are today many projects implemented, located in a continuous development of wind power. Dobrogea region is dominated by the wind. In that part of the country's consumption is quite low, there is also a nuclear power plant. The region is lacking by the power plants able to take swings electricity production and for energy removal products to other areas there are severe limitations.

2. THE SITUATION IN ROMANIA INSTALLATION IN SEN A CEE

At the end of July 2013, in Romania, there were installed 2198.9 MW in 66 wind power plants. Regarding the maximum power that the wind power plants produced in Romania, we can say that it has tended the maximum of 1,840 MW on 04/14/2013 at 10:49 p.m. hours. In that time, this power was approximately 87.6% of the total capacity installed in the wind power plants which operated in Romania at that time (around 2,100 MW). Taking into account the data provided by NC Transelectrica, we find that the total capacity installed and affordable at the first octombre 2013 in the wind power plants, was 2,325 MW.

We present an overview about the situation existing projects in September 2013 of wind power plants, taking as reference points the connection requests and the situation commissioning.

Table 1 - The situation existing projects in September 2013 of wind power plants, taking as reference points the connection requests and the situation commissioning.

	CEE connected at RET [MW]	CEE connected at RED [MW]	Total [MW]

CEE with tehcnical connections	3.105	1.354	4.459
CEE with connection contracts	9.431	5.181	14.612
Total	12.536	6.535	19.071
CEE with completed commissioning	1.005,6	1.304,8	2.310,4

It is estimated that by the end of 2015 in Romania will exist a total installed capacity of wind power plants of about 4,200 MW. Also, it is possible that for periods of strong winds these plants will produce a maximum power around 3,680 MW and the average power will be 1,050 MW.

Following the studies made by experts, we can say that there are a lot of situations where the energy production related to the wind power plants sincreases or decreases rapidly, sometimes in short intervals. We conclude that the energy from renewable sources, particularly the wind and the solar, have certain special characteristics because they are intermittent and uncontrollable. Thus, it requires:

- providing electrical power sources;
- forecasting accurate, regularly updated and the control of energy from both renewable and distributed generation sources.

3. SOLUTION FOR A DEDICATED MANAGEMENT STRUCTURES INTEGRATED RENEWABLE ENERGIES

3.1 Preliminary Notions

If we want to integrate the production of electricity from renewable sources (wind, solar etc..), we will face some operational difficulties regarding the power systems. It requires finding solutions: dispatching balancing or control. These problems not depend only on the technical side, but are closely related with the organizational, economic or regulatory side, all of them can be solved with a balanced approach of all the parts together.

IWES Fraunhofer Institute in Germany has introduced and developed the concept of "Virtual Wind Power Plant" applied to a plant or a cluster (a group of wind power plants), which has led to the concept of wind power generation control. Currently, rising is the concept of Virtual Power Plants based on renewable energies that we apply to countries like USA, Germany, Portugal, Spain etc. Thus, more renewable sources are involved for the complementary generation (with priority access to the grid and dispatching).

Considering the previous context, we propose a dedicated structure in terms of leadership and management by dispatching.

3.2. The Grouping into Clusters of Wind Power Plants Based on RES

After the model of west countries, in such a group we have engaged plants based on RES with different locations, but connected directly or indirectly to the same node belonging to the electricity transmission network in order to form / function like a "Virtual Power Plant based on RES."

In Figure 1 we represent a cluster.

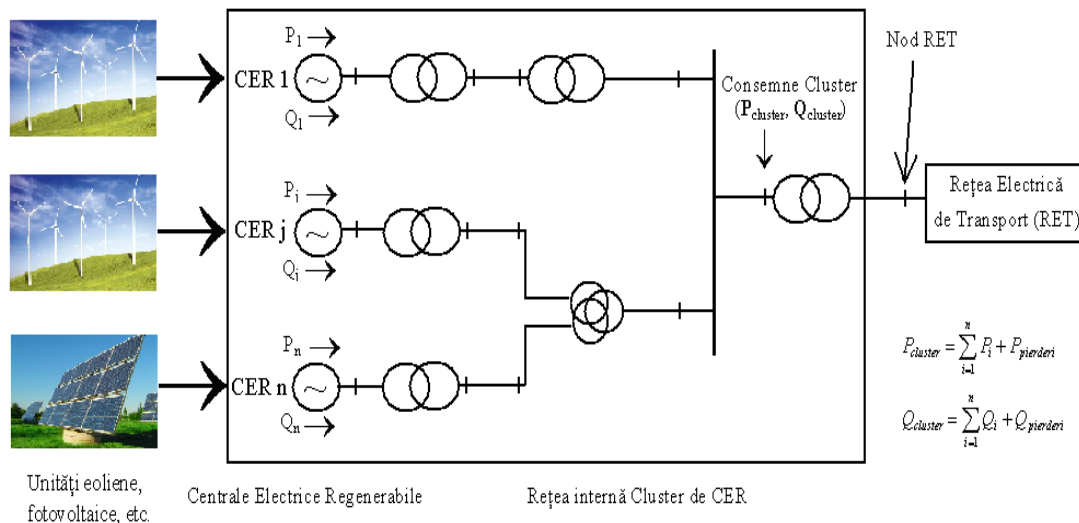


Figura 1 –The definition of a cluster of CER

If in a cluster there will be some unregulated plants, they will be filled by those where the control is possible. The fact that the engagement of these plants is made on the principle of direct or indirect connection to a common node grid (electricity transmission network , in order to achieve the Virtual Power Plant), is due to the transmission system operator (TSO) which is interested in power consumption, the injections and the grid node voltages in order to generate scheduling and real-time analysis with the objective : the power flows on the grid lines, the analyse of the wrong and random inputs in the grid, the transformers in grid nodes, the node voltage grid, the reactive power etc and, on the base of centralizing the data from grid nodes, we'll be able to execute a series of actions (in real time) aimed at: balancing, adjusting voltages of nodes, the power-frequency control, optimization, safety in operation RET and SEN.

In countries like Germany, USA etc. the concept "Virtual Power Plants based on Renewable Energy" (VRPP - Virtual Renewable Power Plants) is already widespread, thus generating electricity in photovoltaic power plants associated with the wind power plants (which produce energy at night). Another combination is that of the wind power plants with in the electric power plants, based on biomass or thermo (both with a certain capacity in terms of the output adjustment). The concept mentioned will above:

- that the wind power plants are grouped in order to smooth the power injected into SEN, the reduction of power in the large wind power plants and its control;
- the strengthening of distributed generation (DG) using biomass locally or regionally with wind or photovoltaic power plants;
- a correlation of the distributed renewable resources, to evaluate the excess of the energy produced, to determine the need for local storage capabilities etc.

3.3. A Proposed System for Managing the Clusters of Electric Power Plants Based on RES

We propose the adoption of the SEN control over the generation of electric power plants based on the RES by clusters of electric power plants with renewable sources basing on:

- A hierarchical management system;
- The OTS control the clusters to the needs of SEN;
- A Management System of Cluster based on renewable energy sources (SMCR), which contains an organizational structure and a hardware or software one, hierarchically on two levels (1 - Central Dispatch Renewable DEC / DCR , 2 - Centers of Dispatch of Clusters Renewable Plants DCCR).

Thus, the SMCR system management (Figure 2) will be in the DEC, helping the dispatchers in DEC's control room when each cluster should be operated separately, as SEN required.

For a better function (safely), both at SEN and at the energy transport networks should be followed some management strategies:

- the tension control, as in conventional electric power plants;
- the reducing of gradients at loading and unloading of the wind power plants;
- the photovoltaic and wind power plants must provide a reactive power as well as the conventional ones;
- the photovoltaic and wind power plants must provide a balancing power as well as conventional ones;
- a management of congestions in the transmission network;
- a programming of wind power and photovoltaic plants generation for the achievement of a safe operation for the power system planning.

The Figure 3 shows the implementation of Power Management Systems (PMS), generated by the electric power plants which composed a cluster. Using the cluster PMS, we can apply a set of management strategies:

- the providing of reactive power in an usually domain without depending on the characteristics of the wind for wind power plants or weather conditions if we talk photovoltaic plants.
- the generation programming must be configured (active power), to be followed by a given program for wind power plants, depend on wind, the photovoltaic plants depending on atmospheric conditions.

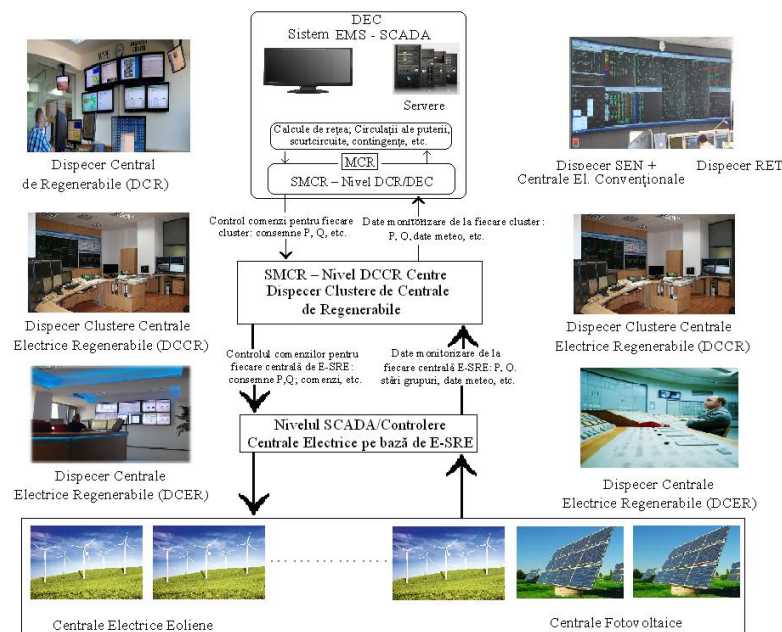


Figure 2 – The structure for monitoring and control SMCR system

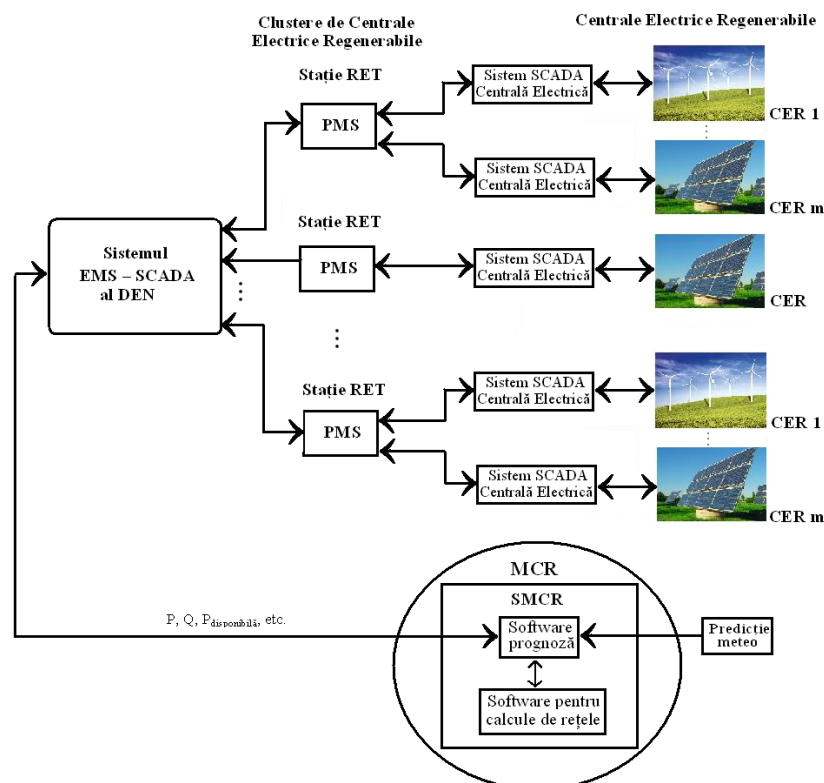


Figure 3 – The movement of data between SMCR, PMS and EMS SCADA for the Transmission Operator and System

According to figures 2 and 3, the SMCR subsystem found at DEC headquarters will receive data ($P_{product}$, $Q_{product}$, $P_{available}$) from each SMCR subsystem related. In turn, all SMCR subsystems related to the dispatcher cluster plants will receive instructions for

clusters from the SMCR subsystem located in DEC headquarters.

The day before, after receiving weather forecasts, MCR will estimate a forecast of the power that could be generated for each cluster the next day. This forecast is sent to DEN, as we can see in Figure 4.

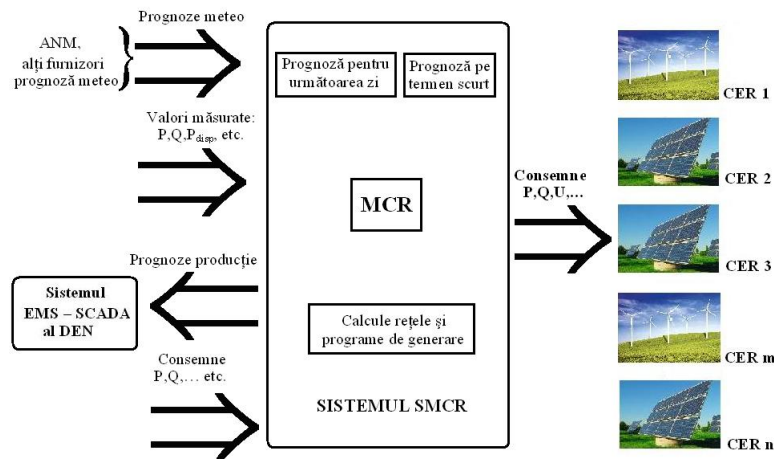


Figure 4 – The SMCR subsystem

Using this forecast in the next day programming of power which will be generated in SEN, the DEC / DEN are designed to calculate the circulations of the power transmission network, to detect the possible congestions, achieving a primary programming of power that will be generated each cluster in the next day, to balance the production and consumption in the SEN, this appointment being sent to MCR. The EMS SCADA system located in DEN will calculate the power requirements to a specific node of RET. Also, here are calculated the contingencies, the transfer capability of RET, the maximum power generated allowed in the network, the short circuit level, from DEN, for the evaluation of the SEN and RET safety. The corroboration of these calculations becomes active and reactive power requirements (P, Q) for the generation of RET nodes where the clusters are connected.

If necessary, MCR will recover the calculations, aiming DEN's compliance requirements referring to the programming of the power that will be generated the next day each cluster. Like this, the generated programs established for each power plant in part, to ensure that the cohesion of all power plants in clusters will lead to DEN requirements. Noteworthy is that the weather forecast for next day uses only like estimation of the generation by the power plants.

Throughout the operation of the MRC is able to more accurately estimate the power in each cluster can lead to, for time intervals of up to 4-6 hours, measuring and interpreting the current weather data.

Taking into account the current requirements regarding the power that each cluster must ensure, that are received every 15 minutes from EMS-SCADA to DEN, MCR will forecast power to be generated by each cluster for the next interval, for up to 4 hours, then the

generation programming of each power plant will be recalculated. Black lists will be referred from the SMCR subsystem of DEC to all SMCR subsystems related to the dispatch centers of clusters. Once received the Clusters requirements dispatch centers and the power plants that are in authority, they must execute them. The distribution of black lists for power plants will be conducted by the SMCR subsystems related to the dispatch centers of clusters.

In parallel with the existing control flow from the DEC Dispatch centers of clusters, we will find a flow monitoring data from the SMCR subsystems of the dispatch centers of clusters at the SMCR subsystem of DEC headquarters, thus allowing for the SMCR subsystem DEC to identify the current state of the cluster and the power plants, thus performing their own forecasts.

All these specific monitoring data allow us to know the current status of the cluster generation, so it is always necessary to have a way of communication between the levels (two in number) of SMCR system for a continue circulation of the information. Thus, we can use up the infrastructure communications SCADA system in order to move the required data of SMCR system.

IV. ELECTROMAGNETIC INTERFERENCE IN THE WIND FARMS

It is known that both radio waves and microwaves are used on a large scale in order to communicate. Generally any structure gauge which has moving parts will result in electromagnetic interference (Figure 5).

The turbine's blades causes interfaces reflecting electromagnetic signals, so that the handsets nearby will take direct and the reflected signal. Such signals are out of phase (the reflected one is delayed due both wavelength equivalent natural frequency of the blades and the blades due to rotation - Doppler effect).

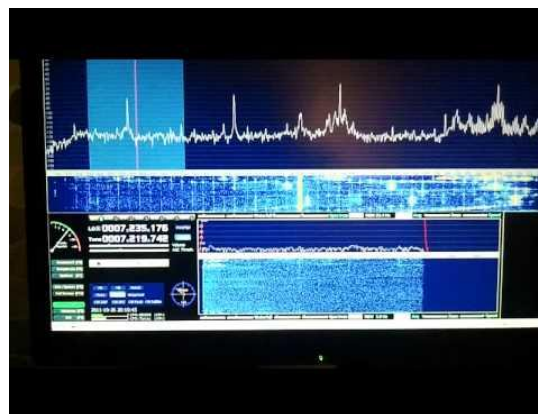


Figure 5 – Electromagnetic Interference in the Wind Farms

The metallic materials, highly reflected benefit by a more pronounced interference compared to wood or epoxy resins. The modern blades are made of a durable metal longeron,

dressed in polyester, reinforced with fiberglass, they are less transparent electromagnetic waves. The communication frequencies will not be visible altered if the wavelength of the transmitter will be 4 times greater than the height of the wind plant. The frequency limit is of 1.5 - 2 MHz (150-200 m), theoretically there is no upper limit.

The types of signals for civil and military communications, which may be subject to electromagnetic disturbances include: radio and TV signals, air or naval traffic control radar systems, mobile phone.

Occasionally there may be interference with a small number of TV receivers. It can suppress these problems, using multiple transmitters and / or receivers targeted or wired network.

To find technical beneficial solutions is necessary to require at the specialized organisms. Thus, we have previously analysed the placement of wind power plants installations, considering the transmitters and receivers nearness.

V. CONCLUSION

The article capture some aspects concerns the wind power plants penetrate the National Power System. The reasons to promote E-RES are: economic, social and environmental. The energy from renewable sources, particularly wind and solar, have certain special characteristics because they are intermittent and uncontrollable. Thus, it requires:

- the providing electrical power sources;
- the forecasting accurate, regularly updated and the control from both renewable energy and distributed generation sources.

It proposes a system for managing the clusters of the power plants based on RES.

All groups wind / solar / mixed related to a wind / solar / mixed power plant will be connected to a LAN (local area network), which in turn is connected to a remote control system involved in managing the collected data, in adjusting the settings of the wind groups, in warning, troubleshooting and reporting to the National Control Centre.

REFERENCES

1. **Kaltschmitt M., Streicher W., Wiese A.** – *Renewable Energy. Technology, Economics and Environment*. Springer-Verlag Berlin Heidelberg 2007.
2. **Ionela Negrea** - *Adaptability study of low-power wind turbines to the climatic conditions of Romania*, PhD thesis, Braşov, 2010.
3. **John Costin Coşoiu** – *Contributions to optimize the design and operation of wind generators*, PhD thesis, Bucharest, 2008.

4. **Iulian Munteanu** – *Contributions to the optimal management of wind energy conversion systems*, PhD thesis, Galați, 2006.
5. **Roman Baican** – *Energy regenrabile Publishing Grinta*, Cluj - Napoca, 2010.
6. **Mihai Octavian Popescu, Claudia Laurent Smith** – *Renewable Energy, Volume 1: Principles and Applications*, Electra Publishing, Bucharest, 2010.
7. **Victor Emil Lucian** – *Renewable resources and their conversion*, MatrixRom Publishing House, Bucharest, 2011.
8. **Troen I., Peterson E.L.** – *European Wind Atlas*, Riso National Laboratory, Roskilde Danmark.
9. **Thomas Ackermann** – *Wind Power in Power Szstems*, John Wiley&Sons. Ltd 2005.
10. **Burgers J., Van Ommne R., Verheij F.** – *System integration of distributed generation – renewable energy systems in different European countries*. KEMA Consulting, 2009, Leonardo Energy.
11. **CEI 61000-4-30:2008** – *Electromagnetic compatibility – Part 4: Testing and measurement techniques – Section 30: Power quality measurement methods*.
12. **CEI 61000-4-30:2008** – *Wind turbins – Part 21: Measurement and assessment of power quality characteristics of grid connected wind turbines*.
13. **Amaris H.** – *Power Quality Solutions for Voltage dip compensation at Wind Farms*, PESGM 2007, Tampa, Florida.
14. **Heier S.** – *Wind Energy Conversion Systems*, John Wiley&Sons. Ltd 2006.
15. **Lubosny Z.** – *Wind Turbine Operation in Electric Power Systems*, Springer, 2003.
16. **Blaabjerg F., Chen Z.** – *Power Electronics for Modern Wind Turbines*, Morgan&Cliaypool Publishers, 2006.
17. www.anre.ro
18. www.transelectrica.ro
19. www.ree.es
20. www.sier.ro

INSTRUCTIONS FOR AUTHORS

Name **SURNAME**¹, Name **SURNAME**², ...

¹ Affiliation of 1st author, ² Affiliation of 2nd author, ...

Email of 1st author, Email of 2nd author, ...(it is compulsory only for the first author)

Keywords: List 3-4 keywords (aligned to the left, 10 pt. bold; please choose keywords from [IEEE Approved Indexing Keyword List](#))

Abstract: Abstract of max. 120 words, justify, 10 pt. regular.

1. INTRODUCTION

The paper must be written in English. It shall contain at least the following chapters: Introduction, research course (mathematical algorithm); method used; results and conclusions, references.

Use DIN A4 Format (297 x 210 mm) MSWord format. Margins: top, bottom, left and right 2.5 mm each. The text should be written on one side of the page only. Use Times New Roman fonts, line spacing 1.3. The font formats are: paper title: 14 pt bold italic, capital letters, author's name(s): 12 pt italic for name and 12 pt. bold, italic for surname; Affiliation: 11 pt. italic; key words: 10 pt, bold; Abstract: 10 pt. italic, word Abstract in 10 pt. bold; chapter titles (do not use automatic numbering): 12 pt bold, capital letters; subtitles: 12 pt bold lower capitals; body text: 12 pt. regular. tables and figures caption: 11 pt. italic; references: author 11 pt. bold, title 11 pt. italic, year, pages, ... in regular.

The number of pages is not restricted.

2. FIGURES AND TABLES

Figures have to be made in high quality, which is suitable for reproduction and

printing. Don't include photos or color prints if there are not clearly intelligible in gray scale option. Place figures and tables at the top or bottom of a page wherever possible, as close as possible to the first reference to them in the paper. Use either *fig. 1* or *figure 1* when necessarily.

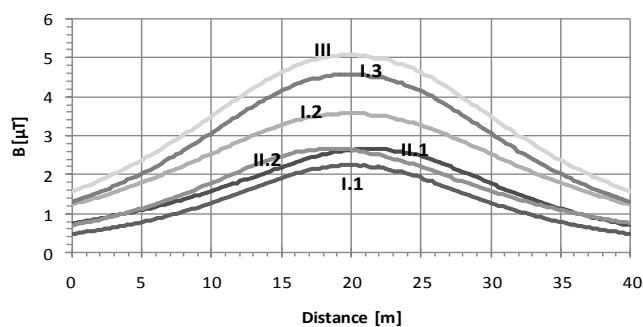


Fig. 4 - Magnetic flux density at 1 m above the ground

Table1. Transposing principle

		Circuit											
		I	2	I	2	I	2	I	2	I	2	I	2
1/3 line length		R	T	R	R	R	S	R	T	R	S	R	R
		S	S	S	T	S	R	S	R	S	T	S	S
		T	R	T	S	T	T	T	S	T	R	T	T
1/3 line length		T	S	T	T	T	R	T	S	T	R	T	T
		R	R	R	S	R	T	R	T	R	S	R	R
		S	T	S	R	S	S	S	R	S	T	S	S
1/3 line length		S	R	S	S	S	T	S	R	S	T	S	S
		T	T	T	S	T	S	T	S	T	R	T	T
		R	S	R	T	R	R	R	T	R	S	R	R
Name		I.1		I.2		I.3		II.1		II.2		III	

3. EQUATIONS

Equations are centred on page and are numbered in round parentheses, flush to right margin. In text respect the following rules: all variables are italic, constants are regular; the references are cited in the text between right parentheses: [1], the list of references has to be arranged in order of citation.

REFERENCES

- [1]. **International Commission on Non-ionizing Radiation Protection**, *Guidelines for limiting exposure to time-varying electric, magnetic and electromagnetic fields (Up to 300 GHz)*, Health Physics, vol. 74,no. 1, pp. 494-522, 1998.
- [2]. **A. Marincu, M. Greconici**, *The electromagnetic field around a high voltage 110 KV electrical overhead lines and the influence on the biological systems*, Proceedings of the 5th International Power Systems Conference, pp. 357-362, Timisoara, 2003.
- [3]. **Gh. Hortopan**, *Compatibilitate electromagnetica*, Ed. Tehnică, 2005.